Spring 5-15-2023

Zebrafish Swim Capacity, Gait, and Posture During Innate Spinal Cord Repair

Nicholas Oliver Jensen

WASHINGTON UNIVERSITY IN ST. LOUIS

Division of Biology and Biomedical Sciences
Computational and Systems Biology

Dissertation Examination Committee:
Mayssa H. Mokalled, Chair
Keith B. Hengen
Tao Ju
Robi D. Mitra
Zachary Pincus

Zebrafish Swim Capacity, Gait, and Posture During Innate Spinal Cord Repair

by

Nicholas Oliver Jensen

A dissertation presented to
Washington University in St. Louis
in partial fulfillment of the
requirements for the degree
of Doctor of Philosophy

August 2023
St. Louis, Missouri

Table of Contents

List of Figures iv
List of Tables vi
Acknowledgments vii
Abstract x
Chapter 1: Introduction 1
1.1 Zebrafish as a Model for Innate Spinal Cord Repair 1
1.1.1 Spinal cord injury 1
1.1.2 Metrics of functional recovery 2
1.2 Gait and Posture 6
1.3 Hypotheses and Aims 8
Chapter 2: Materials and Methods 10
2.1 Zebrafish Care and Assessment 10
2.2 Software 11
2.2.1 Video preprocessing 12
2.2.2 Automating posture annotation 15
2.2.3 Automating behavior annotation 16
2.2.4 External software dependencies 21
2.3 Classical Functional Metrics 22
2.4 Metrics from Posture and Gait 24
2.4.1 Metrics derived from posture 24
2.4.2 Metrics derived from gait 26
2.5 Trajectory Analysis 27
2.5.1 Cruise sonification 27
2.5.2 Cruise embedding 28
2.5.3 Tensor decomposition 28
2.5.4 Predicting 8 wpi regeneration groups at 2 wpi 30
Chapter 3: Comparing Functional Metrics 31
3.1 Classical Recovery in the Tracking Experiment 31
3.1.1 Results 31

3.1.2 Discussion 35
3.2 Posture-derived Metrics in the Tracking Experiment 36
3.2.1 Results 36
3.2.2 Discussion 42
3.3 Gait-derived Metrics in the Tracking Experiment 45
3.3.1 Results 45
3.3.2 Discussion 52
3.4 Metric Correlations at 8 wpi 54
3.4.1 Results 54
3.4.2 Discussion 59
3.5 Functional Metrics Outside Spinal Cord Transection Contexts 60
3.5.1 Introduction 60
3.5.2 Results 61
3.5.3 Discussion 66
Chapter 4: Recovery Trajectories 68
4.1 The Complexity of Posture Space 68
4.1.1 Results 68
4.1.2 Discussion 70
4.2 Cruise Exemplar Embedding 70
4.2.1 Results 70
4.2.2 Discussion 77
4.3 Tensor Decomposition 80
4.3.1 Results 80
4.3.2 Discussion 84
4.4 Predicting 8 wpi Regeneration from 2 wpi Function 86
4.4.1 Results 86
4.4.2 Discussion 93
Chapter 5: Conclusions 95
5.1 Conclusions and Significance 95
References 97

List of Figures

Chapter 2

Figure 2.1: Keypoint diagram for zebrafish posture and gait analysis. 15

Figure 2.2: Simple zebrafish behaviors. 17

Figure 2.3: Computationally predicted behaviors in three swim assays. 21

Figure 2.4 Visualization of the scoliosis score. 25

Figure 2.5: Rostral compensation measured as maximum distance or integrated area. 27

Figure 2.6: Parameter selection for tensor analysis of longitudinal measurements. 29

Chapter 3

Figure 3.1 Schematic of the SCI longitudinal tracking experiment. 32

Figure 3.2: Classic functional measurements of tracked male fish. 33

Figure 3.3: Classic functional measurements of tracked female fish. 34

Figure 3.4: Cellular regeneration outcomes for male and female fish. 35

Figure 3.5: Comparing centroid- and posture-derived burst frequency in still water (0 cm/s). ... 37

Figure 3.6 Assessment of lateral scoliosis among all 60 fish in the tracking experiment. 39

Figure 3.7: Comparing scoliosis to posture novelty. 41

Figure 3.8: Snapshots of cruise periods from control and 1 wpi assays. 45

Figure 3.9: Characterizing rostral compensation exhibited by injured male fish. 46

Figure 3.10: Characterizing rostral compensation exhibited by injured female fish. 47

Figure 3.11: Body oscillation frequency during cruise behavior. 49

Figure 3.12: Measurements of swim efficiency in still water (0 cm/s). 51

Figure 3.13: Tail beat frequency averaged over all flow speeds. 52

Figure 3.14: Pairwise comparisons of spinal cord regeneration metrics at 8 wpi (male fish in the tracking experiment). 56

Figure 3.15: Pairwise comparisons of spinal cord regeneration metrics at 8 wpi (female fish in the tracking experiment). 58

Figure 3.16: Uninjured *mstnb*$^{-/-}$ fish are not easily characterized by our functional metrics of spinal cord injury. 63

Figure 3.17: Fish with ablated neurons are not easily characterized by our functional metrics of spinal cord injury. 65

Chapter 4

Figure 4.1: Principal component analysis of angle poses observed in the tracking experiment. . 69

Figure 4.2: UMAP embedding of cruise behaviors for male fish with low scoliosis during SC regeneration..... 73

Figure 4.3: UMAP embedding of cruise behaviors for female fish with low scoliosis during SC regeneration..... 75

Figure 4.4: Control and 8 wpi cruises are significantly different in the first two UMAP components. 77

Figure 4.5: Rank-7 tensor component analysis of swim behavior for all tracked fish during SC regeneration..... 81

Figure 4.6: Average functional and cellular regeneration outcomes for five clusters of fish identified through tensor decomposition. 82

Figure 4.7: Rank-1 tensor component analysis reflects stereotypical recovery trends. 84

Figure 4.8: Predicting 8 wpi regeneration outcomes in the tracking experiment using measurements taken by 2 wpi. 87

Figure 4.9: Experimental validation for 8wpi outcome prediction. 88

Figure 4.10: Cellular regeneration measured in the validation experiment separated by sex. 89

Figure 4.11: Regeneration outcomes for prediction groups in the tracking and validation experiments separated by sex..... 90

Figure 4.12: Pairwise comparisons of spinal cord regeneration metrics at 8 wpi (male and female fish in the validation experiment). 92

List of Tables

Table 1.1: Published metrics of zebrafish swim function 3
Table 3.1: Numbers of fish that presented scoliosis above certain severity thresholds 38

Acknowledgments

Before any others, I must first acknowledge and especially thank my thesis mentors, Professors Mayssa Mokalled and Zachary Pincus. Their invaluable guidance helped me push through not only a graduate education but also the notorious pandemic lockdown in 2020. I thank Mayssa especially for supporting my preference to work from home with my family. Thanks to Zach for creating software libraries that jumpstarted this work. I also thank the rest of my thesis committee: Professors Keith Hengen, Robi Mitra, and Tao Ju. Every thesis update was thoroughly enjoyable, and I am sincerely grateful for your constructive feedback. I also thank the mentors who gave me experience and guidance in my first year at WashU: Professors Nancy Saccone, Celeste Karch, Kevin Black, and Thorold Theunissen. One of the things I have enjoyed most about the WashU community is a willingness to share ideas and discuss work outside the lab. For this, I particularly thank Professors Tim Schedl, Shamim Mollah, and Geoffrey Goodhill, and fellow student Thomas Darveniza. Thanks also to my undergraduate research mentor at Brigham Young University, Professor Seth Bybee, and to Anton Suvorov, Ph.D., who was then a graduate student in the Bybee Lab. From the time I spent as an undergrad working alongside him, Anton remains a treasured professional role model.

This work has all been possible because of the excellent animal care provided by the Washington University Zebrafish Facility and members of the Mokalled Lab. Thank you! I particularly wish to acknowledge Brooke Burris for enduring long hours swimming fish, Lili Zhou and Ryan McAdow for fish care, Lili especially for histological analysis and MTZ treatment, Dana Shaw for always giving the right advice during my lab updates, Vishnu Saraswathy for letting me use his *mstnb* fish, Hunter Yamada for histological analysis, and

Catrina Reyes for annotating 39,705 frames of fish behavior. Additionally, thanks to members of InPrint, a scientific communication network, for proofreading this document.

I'm thankful for financial support during this process and wish to acknowledge a few sources. This research was supported by grants from the NIH to my thesis mentor, Professor Mayssa Mokalled (R01 NS113915 and R01 NS123708). I also received entrepreneurship and leadership training and an internship stipend through the Skandalaris Center's Pivot 314 Fellowship. I thank everyone who made that experience possible. Moreover, I thank UNandUP, LLC for providing not only opportunity to work as an intern and consultant, but also one-on-one mentoring about research, leadership, and marketing in a cutting-edge biotech startup.

Lastly, I thank my family. I don't know when my dad started calling me Dr. Nick, but that's probably what made me start thinking about getting a PhD in the first place. He's been with me from the beginning, driving 1,300 miles with me when I moved to St Louis; and he has listened to my practice talks by video call before every thesis update. Dad's feedback always made my presentations clearer. Also, my mom has remembered every major event — my most important exams and presentations — and texted her support before each one. Thanks, mom! Many thanks to my older brother Andrew, a wizard of generative audiovisual art, for critical feedback on my zebrafish swim sonification videos: I love how it turned out. And I especially thank my wife, Jessica, who always offered an ear as I practiced my qualifying exam when we were dating, thesis proposal when we were newlyweds, thesis updates when we were new parents, and my thesis defense now that our little kiddo can point out a healthy zebrafish.

Nicholas Oliver Jensen

Washington University in St. Louis

August 2023

For Jessica and Levi, who endured with me.

ABSTRACT OF THE DISSERTATION

Zebrafish Swim Capacity, Gait, and Posture During Innate Spinal Cord

by

Nicholas Oliver Jensen

Doctor of Philosophy in Biology and Biomedical Sciences

Computational and Systems Biology

Washington University in St. Louis, 2023

Mayssa Mokalled, Ph.D. Chair

Adult zebrafish are capable of anatomical and functional recovery following severe spinal cord injury. Significant advances for understanding the cellular and molecular mechanisms of innate spinal cord repair are best supported by accurate assessment of swim function. This study introduces neuromuscular-associated measurements derived from gait and posture, compares new and classical functional measurements longitudinally, and provides a comprehensive correlative analysis of various functional and cellular regeneration outputs. It also explores trajectories of functional regeneration through tensor decomposition and demonstrates that swim function at 2 weeks post-injury can be used to predict 8-week regeneration outcomes. By establishing swim quality metrics which are both distinct from previous measurements and demonstrably more associated with glial bridging and axon regrowth, this study has the potential to accelerate discovery and reduce redundancy in future studies. Software for this study, featuring zebrafish swim quality analysis, is now freely available.

Chapter 1: Introduction

This chapter, and all subsequent chapters, contains data and text included in the following preprint manuscript authored by myself, Brooke Burris (BB), Lili Zhou (LZ), Hunter Yamada (HY), Catrina Reyes (CR), and Mayssa Mokalled (MM).

Jensen NO, Burris B, Zhou L, Yamada H, Reyes C, Mokalled MH. Functional trajectories during innate spinal cord repair. bioRxiv. doi: https://doi.org/10.1101/2023.01.31.526502

The manuscript is currently under review for publication. I retain the right, as author, to include this content in my dissertation according to Frontiers' (the publisher's) open access and copyright policies. Author contributions: BB, MM, and LZ performed animal husbandry and surgery. BB, LZ, and NJ performed swim behavior and exhaustion assays. BB, LZ, and HY performed histological analysis. NJ and CR annotated fish behaviors. NJ wrote code to process videos and quantify swim function. NJ performed the statistical analysis. NJ wrote the first draft of the manuscript, and MM provided polishing edits and guidance. All authors contributed to manuscript revision.

Because this dissertation contains content from our collaborative preprint manuscript in addition to unpublished work, I use the pronoun "we" rather than "I" throughout the text.

1.1 Zebrafish as a Model for Innate Spinal Cord Repair

1.1.1 Spinal cord injury

Humans do not recover well from spinal cord (SC) injury. In the US, it is estimated that 299k people are currently living with SC injury, 18k new cases occur each year, and less than 1% of new cases completely recover by hospital discharge (1). Although mammals do not spontaneously

recover from the sensory and motor deficits caused by SC injury (2,3), some aquatic and amphibious animals including zebrafish (*Danio rerio*) do functionally regenerate, even after complete SC transection (4–7). By studying model organisms that have greater innate ability to recover than humans, researchers aim to discover neuroprotective, neuroplastic, and regenerative treatments (8).

As vertebrates with elevated regenerative potential, adult zebrafish are an excellent model for innate SC repair. After complete SC transection, pro-regenerative responses involving the immune system, neurons, and glia contribute to functional regeneration (9). Prompted by a host of injury-induced, regeneration-promoting factors, glial and axonal bridges reconnect the lesioned tissue, neurons regenerate proximal to the lesion, and swim capacity is restored, all within 6–8 weeks post-injury (wpi) (10). Due to the remarkable ability of adult zebrafish to reverse paralysis, recovery of swim function is an ultimate metric and a central readout of SC repair. Although the operation causes paralysis caudal to the injury, paralyzed zebrafish can still swim using muscles rostral to the lesion (4,11). Swim function, therefore, must be accurately measured.

1.1.2 Metrics of functional recovery

Functional measurements of swim ability may be classified into two broad categories: swim capacity, which represents the amount or extent of swimming a fish can perform under specific conditions; and gait quality, which reflects the quality of a swim bout and the healthiness of a fish during active swimming. For a comprehensive list of functional measurements that have been applied to zebrafish SC injury, see Table 1.1.

Table 1.1: Published metrics of zebrafish swim function. The following functional metrics are listed in chronological order according to when each was first published. Each metric was used to assess adult fish unless indicated with "larvae only" beside the metric name. All studies, according to a thorough literature search, that used the metric to assess zebrafish functional ability in SC injury context (transection, hemi-section, or crush) are cited, along with a simplified description of the assay and a classification: whether it measures capacity or quality of locomotor function. This table includes metrics published from 1997 to 2022.

Metric	Year Introduced	Assay Condition	Citations	Classification
Binary swim recovery (recovered / not recovered)	1997 (4)	Swim quality after startle (visual assessment)	(4)	Quality
Time to exhaustion	1998 (12)	Increasing flow speed	(10,12–20)	Capacity
Swim distance (2D, one camera)	2004 (21)	Open tank	(15,17,21–42)	Capacity
Swim distance (3D, two cameras)	2012 (43)	Open tank	(43)	Capacity
Perceived quality on an integer scale (1 to 5, 1 to 6)	2012 (44)	Open tank	(35,44)	Quality
Binary response recovery (larvae only)	2014 (45)	Touch stimulus at various anatomical locations	(45)	Capacity
Swim distance after touch (larvae only)	2016 (46)	Touch stimulus	(46–49)	Capacity
Binary swim recovery	2020 (50)	Swim activity (visual assessment)	(50)	Capacity
Maximum speed at exhaustion	2021 (51)	Increasing flow speed	(11,51,52)	Capacity
Free swimming speed	2021 (52)	Open tank	(11,42,52)	Capacity
Body angle (larvae only)	2021 (49)	Open tank	(49)	Quality

Power Spectral Densities (larvae only)	2021 (53)	Moving light/dark gradient projected beneath the larva	(53)	Quality
Burst frequency	2021 (17)	15-minute swim assay with 0 cm/s, 10 cm/s, 20 cm/s flow	(17,19,20)	Capacity
Time active	2021 (17)	15-minute swim assay with 0 cm/s, 10 cm/s, 20 cm/s flow	(17,19)	Capacity
Time swimming against the flow	2021 (17)	15-minute swim assay with 0 cm/s, 10 cm/s, 20 cm/s flow	(17)	Capacity
Time spent in each quadrant	2021 (17)	15-minute swim assay with 0 cm/s, 10 cm/s, 20 cm/s flow	(17)	Capacity
Mean Y: average position in the axis of flow	2021 (17)	15-minute swim assay with 0 cm/s, 10 cm/s, 20 cm/s flow	(17,19,20)	Capacity
Centerline kinematics (larvae only)	2022 (54)	Static or flow	(54)	Quality
Tail beat frequency and amplitude	2022 (11)	Open tank	(11)	Quality
Roaming/Exploration (observations, no quantifications)	2022 (42)	Open tank	(42)	Quality

Early assays, such as the 1997 startle assay, evaluated swim function in zebrafish as binary quality, “recovered” or “not recovered”, assigned by an observer (4). In the startle assay, fish that respond to a stimulus and appear to swim using mostly their tail instead of their head are labeled as “recovered”. Based on these and other criteria, swim quality scoring systems on 1 to 5 and 1 to 6 scales have also been developed (35,44). Two capacity measurements were subsequently introduced: time to exhaustion in 1998 (12) and swim distance in a static tank in 2004 (21). These offered several advantages: they are less subjective, provide continuous scale measurements, and are scalable for longer assays using computational tools. Consequently, swim distance and time to exhaustion have been widely applied to SC regeneration studies between 1997 and 2020. Since 2020, the toolkit to quantify swim function has rapidly expanded and diversified. As more functional metrics continue to be developed, methods to compare and benchmark them are increasingly pertinent.

Classical and recently described measurements of swim capacity include swim endurance as quantified by time to exhaustion against increasing water current velocities, maximum speed either against increasing water current velocities or in a static tank, swim distance, time active, time swimming against flow, burst frequency, and average position of the fish against a water flow axis (mean y). Although new quality measurements have been developed for larval fish including body angle, power spectral densities, and centerline posture kinematics, published quality measurements for adult fish are limited to manual scoring of perceived swim ability, tail beat frequency, and tail beat amplitude. Moreover, manually assigned scores are subjective and do not scale well for higher throughput. Thus, behavioral tests to quantify gait quality in adult zebrafish are less developed, yet much needed for accurate assessment of musculoskeletal function and neural regeneration.

1.2 Gait and Posture

Gait analysis offers a scalable approach to quantify swim quality. Prior applications of gait analysis, such as dorsal centerline posture and tail beat kinematics, supported the model that functional recovery emerges directly from structural recovery among ray-finned fishes (11,54,55). These studies revealed stepwise recovery of specific gait features in correlation with axon regeneration from V2a interneurons (11,56). These findings suggested that formerly paralyzed zebrafish may regain the ability to swim in a preinjury-like manner after neural regeneration. Yet, further analysis of swim gait metrics, including posture and behavior, is required to confirm this hypothesis.

The first step in gait analysis is usually to annotate elemental components of gait: posture and behavior. Automated pose and behavior annotation tools for model organisms are increasingly accessible. While traditional computational methods for zebrafish pose annotation include thresholding and skeletonization (57,58) or template-fitting (59,60), many newer, cross-species methods prioritize deep learning. Such tools include DeepLabCut (61), DeepPoseKit (62), OptiFlex (63), and SLEAP (64). In terms of zebrafish with SC injury, the dorsal centerline is an appropriate representation of body posture. Despite its limitations in measuring vertical position, body deformity in the dorso-ventral axis, or pectoral fin motion, dorsal centerline quantification has been applied to larval and adult locomotion analysis (11,57,58) and lateral tail beating has been noted as the source of most swim propulsion (65). Moreover, certain injury-induced gait alterations are known to manifest in the dorsal centerline (11). Similar to recent pose annotation methods, automated behavior annotation is often performed through machine learning either by clustering in a latent space (57,58,66), such as B-SOiD (67), or through deep learning, such as

DeepBhvTracking (68) or DeepEthogram (69). As a maturing field, pose and behavior classification tools are generally well developed.

Despite advances in pose and behavior annotation, methods to compare episodes of the same zebrafish behavior, either between animals or between recovery timepoints, are underdeveloped. Nonetheless, comparing multiple episodes of the same behavior is a critical component of gait quality analysis for injury-recovery models. One viable option is novelty detection, a branch of machine learning which classifies data points as inliers or outliers relative to a control distribution. Another option is posture parameter quantification, which has been used to assess SC injury in larval zebrafish (54). Overall, there is no standard way to computationally describe the quality of an adult zebrafish's gait.

Posture and gait parameter quantification is well established in human and mouse studies, however (70–73). Tools employed for collecting these parameters range from observation to exoskeleton devices, and even to game consoles. One such system is the Basso, Beattie, and Bresnahan (BBB) locomotor scale for mice, which is based on frequencies of observed gait features, e.g., toe clearance while stepping (74,75). Interscorer variability prompted the development of the Basso Mouse Scale for Locomotion (BMS) (76). Automated scoring was also developed based on foot-to-surface contact for fixed-distance walks, CatWalk (77), and continuous measurement, TreadScan (78). A scale, highly correlated with BBB, based on quantitative gait features (e.g., step height) was developed using a robotic mouse harness (79). Human research similarly applies posture and gait quantification. Robotic exoskeletons are used clinically to both assess injury and assist rehabilitation training (80). Non-invasive analyses have even been developed using posture-tracking entertainment devices to score the rehabilitation of fine motor control (81) and limb

movement (82). In summary, translational and clinical research is concerned with the quality of locomotion, which is generally measured through gait and posture analysis.

One possible reason a BBB- or BMS-like scale has not yet been established for zebrafish is that zebrafish locomotion is extremely different from that of mice and humans. For example, a fish does not contact a surface as it swims, and fish propulsion does not originate primarily from limbs. Moreover, mechanical harnesses for fish are impractical, so swim analysis must rely on a non-invasive tool, like computer vision. Creating a set of scorable parameters for zebrafish gait is less intuitive and more challenging to score. Therefore, as swim quality is proposed to be a more direct readout of SC function and musculoskeletal wellness than swim capacity, recovery metrics based on posture and gait are much needed and have the potential to become standards for functional assessment of zebrafish.

1.3 Hypotheses and Aims

Given the recent diversification of swim capacity and gait quality measurements for zebrafish, this study compares various established and novel functional recovery metrics and describes their correlations with anatomical regeneration. To this end, we tracked swim function before injury and weekly between 1 and 8 wpi. Fish identities were tracked throughout the experiment, and cellular regeneration parameters were measured at 8 wpi. For the purposes of this study, we define cellular regeneration at the lesion as axon regrowth, measured by anterograde tracing, and glial bridging, measured by histological staining for glial fibrillary acidic protein (Gfap). We hypothesize that swim gait quality is a more direct readout of spinal cord wellness than swim capacity (e.g., swim distance). Rostral compensation is established as a new gait feature that highly correlates with functional recovery. For comprehensive analysis of multiple functional metrics, we also describe recovery trajectories using tensor decomposition of longitudinal recovery data. By

observing correlations between established swim capacity, new gait analysis metrics, and cellular regeneration features, we propose and validate a strategy for predicting 8 wpi recovery outcomes using 1 and 2 wpi swim function parameters. This study establishes new measurements of neuromuscular health that are derived from posture and swim gait, provides a comprehensive correlative analysis of various functional and cellular regeneration outputs, and provides software that calculates various classical and novel functional measurements given posture annotations as input. These results will help reduce measurement redundancy in future studies.

Chapter 2: Materials and Methods

2.1 Zebrafish Care and Assessment

This section details animal care and methods that we used to injure the fish, record swim function, and measure cellular regeneration.

Zebrafish

Adult zebrafish of the Ekkwill and AB strains were maintained at the Washington University Zebrafish Core Facility. All animal experiments were performed in compliance with institutional animal protocols. Male and female animals 4 months of age and ~2–2.5 cm in length were used.

SC transection

Zebrafish were anaesthetized using MS-222. Fine scissors were used to make a small incision that transects the spinal cord 4 mm caudal to the brainstem region. Complete transection was visually confirmed at the time of surgery. Injured animals were also assessed at 2- or 3-days post-injury (dpi) to confirm loss of swim capacity post-surgery.

15-minute swim behavior assay

Two fish at a time were placed in a 5 L swim tunnel device (Loligo, cat# SW100605L, 120V/60Hz). A customized physical divider was secured in the center of the swim chamber parallel to the flow, separating the tunnel into 2 chambers to enable individual tracking of each fish. A camera was placed directly above the tunnel and recorded videos at 70 frames per second. Each 15-minute assay included three 5-minute periods of increasing water current velocity at 0, 10, and 20 cm/s.

Swim endurance assay

The swim endurance assay, applied only in the validation experiment at 8 wpi, was performed as previously described (18). Briefly, zebrafish were exercised in groups of 8–12 fish. After 10

minutes of acclimation inside the enclosed tunnel, water current velocity was increased every two minutes and fish swam against the current until they reached exhaustion. Exhausted animals were removed from the chamber without disturbing the remaining fish. Swim time and current velocity at time of exhaustion were recorded.

Histological assessment of glial bridging

Glial bridging was measured at 8 wpi using Gfap immunohistochemistry on serial transverse sections as previously described (18). The cross-sectional area of glial tissue at the lesion and the area of the intact SC rostral to the lesion were measured using ImageJ (Fiji) software (83). Glial bridging was calculated as a ratio of these measurements.

Histological assessment of proximal and distal axon regrowth

Axon regrowth was measured using anterograde axon tracing (18). Fish were anaesthetized using MS-222 and fine scissors were used to transect the cord 4 mm rostral to the lesion site. Biocytin-soaked Gelfoam Gelatin Sponge was applied at the new injury site (Gelfoam, Pfizer, cat# 09-0315-08; Biocytin, saturated solution, Sigma, cat# B4261). Fish were euthanized 6 hours post-treatment and Biocytin-labeled axons were histologically detected using Alexa Fluor 594-conjugated Streptavidin (Thermo Fisher, cat# S-11227). Biocytin-labeled axons were quantified using the "threshold" and "particle analysis" tools in the Fiji software. Four sections per fish at 0.5 (proximal) and 2 (distal) mm caudal to the lesion core, and 2 sections 1 mm rostral to the lesion, were analyzed. Proximal and distal regrowth were calculated as ratios of these measurements.

2.2 Software

This section highlights our computational methods, including video processing, pose and behavior classification, and software dependencies.

Code availability

Code written for this study, including methods to standardize videos, compute functional metrics from pose annotations, and predict regeneration outcomes as described in our preprint manuscript, are publicly available in a GitHub repository (https://github.com/MokalledLab/SwimFunction). It is primarily written in python and has a defined virtual environment that includes necessary dependencies (.yaml file for Anaconda). It accepts pose annotation files in the format of DeepLabCut outputs (either .csv or .h5) as minimal required input and normalized video files as supplemental input. Its outputs include functional metrics as .csv files and figures like many in this manuscript. Its installation, inputs, outputs, and usage are described in greater detail in the README.md markdown document located in the repository's top-level directory.

2.2.1 Video preprocessing

After taking videos according to our established protocol (17), two preprocessing techniques were used for downstream efficiency and accuracy: normalization and automated region-of-interest (ROI) cropping. For brevity, the descriptions below do not include all runtime optimizations in the code, so the actual implementation differs slightly from what is written.

Normalization protocol

Normalization is an essential step in most computer vision pipelines. We normalized videos in the following manner:

1. Calculated the pixel-wise median image for each video.
2. Calculated a normalizing factor for each video as the median pixel intensity for an arbitrary reference median frame divided by the median pixel intensity for the video's median image.
3. Normalized all frames by multiplying all pixels by this normalizing factor.

4. Subtracted the video's normalized median frame from all other frames, converting values to 8-bit unsigned integers by clipping to the range [0, 255].
5. Grayscaled the resulting frames using RGB weights (0.2125, 0.7154, 0.0721).

ROI cropping protocol

In parallel with these normalizing steps, our software also used thresholding to detect the fish and crop to the surrounding area. It stored the corner of the cropped area in a log file for later reference. In greater detail, our code performed the following:

1. For each fish in the video, a log file was created with metadata including video dimensions, total number of frames in the original video, cropped video dimensions, and corners.
2. For each frame, we:
    a) Applied the frame normalization protocol.
    b) Thresholded the image.
    c) Labeled objects in the binarized image using `label` in the scipy.ndimage package.
    d) Identified putative fish labels based on an expected size. If more putative fish are found than the number (N) in the movie, we took the N largest putative fish.
    e) Found centroids for each fish object using `center_of_mass` from the scipy.ndimage package on its label mask.
    f) For each fish object:
        i. Cropped to the 400 x 400 region such that the center of the crop area is the center (centroid) of the fish object. We buffered the image with

the max-value (255 for 8-bit image) to keep the crop dimensions exact, even if the fish is close to an edge.

ii. Obtained a corresponding crop from the grayscale frame using the label mask. Wherever the label mask was not the fish of interest or the background (label 0), we assigned pixels as max-value (255 for 8-bit image). This occluded all other fish and dark floating objects (e.g., drifting fish waste).

g) Found the pairwise distances from all fish object centroids in the previous frame and the centroids observed in the current frame.

h) Used `linear_sum_assignment` from the scipy.optimize package to match each fish's center in the current video with the fish that most likely matches it in the previous frame.

i) Wrote each cropped image as the next frame in the corresponding fish's video file and stored the frame number and corner coordinate in the corresponding log file.

Consequentially, each fish had its own normalized, cropped video where it is always centered in the frame, and a matching log file that mapped keypoint coordinates in the cropped-area back to full-video coordinates. The code was written to operate on videos that contain multiple fish swimming together, but fish identities are not perfectly maintained during collisions and occlusions. For this reason, almost all the analysis in this dissertation is performed on videos with two fish separated by a physical divider (the one exception is the *huc*:mCherry-NTR neuron ablation experiment in Chapter 3 section 3.5). For videos where two fish were physically divided,

the code performed a simplified version of the above protocol by operating on the two halves of the video separately and tracking one fish in each half-video.

2.2.2 Automating posture annotation

We trained a DeepLabCut (61,84) model to identify ten points on the dorsal centerline, from the head to the base of the tail fin, and a point near the tip of the tail fin (Figure 2.1). After raw keypoint coordinates were annotated by DeepLabCut, we cleaned the annotations and calculated angle poses as described in this subsection.

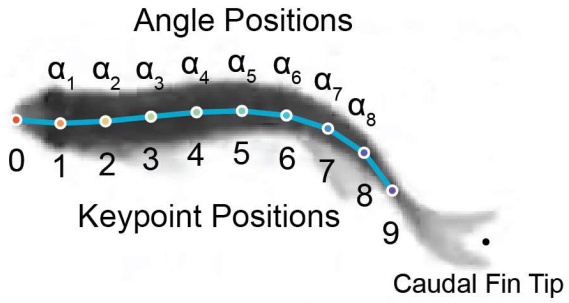

Figure 2.1: Keypoint diagram for zebrafish posture and gait analysis.
A diagram showing keypoint and angle positions labeled on a fish's dorsal centerline. These keypoints were used to develop posture and gait quality quantifications. A DeepLabCut model was trained to identify the keypoints, then the curvature between three adjacent keypoints were calculated at each angle position. The rostral region of the fish corresponds to angle positions α_1 to α_5. We defined the body region of the fish as angle positions α_2 to α_8.

Coordinate pose cleaning

To smooth the poses, we fit cubic splines to each computer-annotated pose and resampled ten evenly spaced points from the spline. In rare cases, the resulting spline created impossibly long or short fish centerlines, which were computationally filtered using the average head-to-tail distance. In such an event, we returned to the original frame and used thresholding and skeletonization to approximate a more accurate centerline. If the centerline was still impossibly long or short, the original DeepLabCut annotation was kept without smoothing. After smoothing, we filtered away poses that were likely incorrectly annotated according to the following criteria: DeepLabCut likelihood score (required >0.5 at all keypoints), total pose length (required within 8 median

absolute deviations from the median length), pose curvature (required z-score < 8 at each angle position), and whether the pose was too far from annotated poses in adjacent frames (required movement within 45 pixels at all keypoints). This reduced annotation error, which was often due to mistakenly annotating a body keypoint on a piece of floating debris or failure to detect a keypoint when the fish was partially or fully out of frame.

Angle pose calculation

We calculated angles between triplets of adjacent keypoints along the centerline. We called this sequence of angles (α_1, α_2, … α_8) the angle pose (Figure 2.1). Specifically, from keypoint positions 4, 5, and 6, the angle α_5 is how far the line drawn by keypoints 4-to-5 must rotate to be parallel to the line drawn by keypoints 5-to-6. In this manner, each pose of ten coordinate keypoints was reduced to an angle pose with eight measured angles. Eight angle positions have been shown to be sufficient to capture ordinary variation in zebrafish posture (11). Although other studies have used different methods to convert keypoints to angle poses, we chose this representation because the summed angle pose for a resting non-scoliotic fish is close to zero.

2.2.3 Automating behavior annotation

We annotated many episodes of simplified behaviors: rest (1,355 episodes), cruise (3,243), and clockwise (128) and counterclockwise (165) turns (Figure 2.2). For this study, we defined "cruise" as a forward swim with at least three body oscillations.

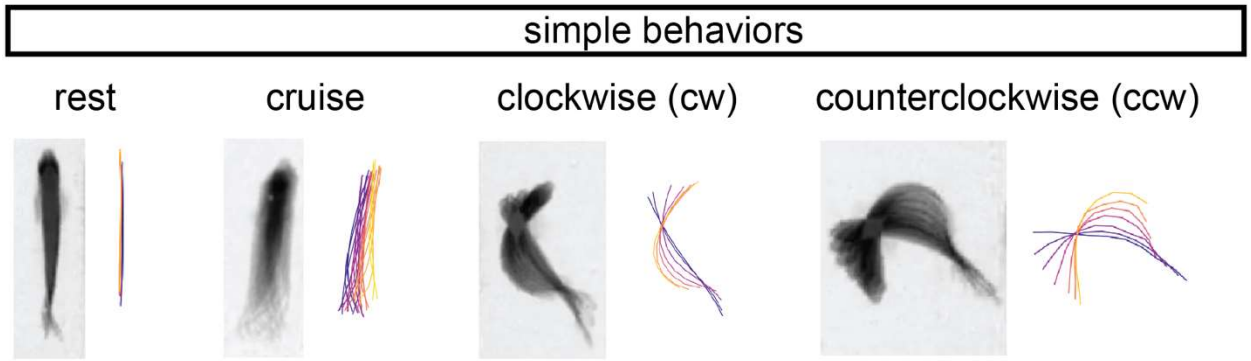

Figure 2.2: Simple zebrafish behaviors.
These are examples of four simple behaviors: rest, cruise, clockwise turn, and counterclockwise turn. For each example, overlayed snapshot frames are shown on the left with corresponding dorsal centerlines on the right.

Where possible, we annotated three cruises per flow speed for every fish's control, 1 wpi, 3 wpi, and 6 wpi assays. We annotated cruises in the same manner for all nine assays of 34 fish. We also annotated several cruises from 2, 4, 5, 7, and 8 wpi assays selected randomly. Although we focused our analysis on cruise and rest behavior, we annotated and classified turns so the model would not mistakenly classify every non-rest behavior as cruise. Annotations included a nearly equal representation by sex (51% female). Representation by wpi was weighted to include more uninjured behaviors (control: 26%, 1: 14%, 2: 6%, 3: 15%, 4: 4%, 5: 7%, 6: 14%, 7: 6%, 8: 8%).

To prepare the data for classification, episodes were split into frames. Each annotated frame's angle pose was concatenated with the six angle poses before and the six angle poses after to create a larger vector, a temporal "pose window", labeled with the middle frame's annotated behavior. We withheld 25% of the annotated data for validation. Because cruises were overrepresented in our annotations, we oversampled the train and validation datasets such that all behaviors were equally represented. To do this, we used Synthetic Minority Over-sampling Technique (SMOTE) (85) with k=20 as the k-nearest neighbors parameter.

We fit a UMAP (86) model (2 components, 50 nearest neighbors) to all pose windows in the training set, then fit a random forest classifier (87) to the UMAP-transformed windows for final classification. Finally, because some assays contained unusually high numbers of rest frames incorrectly classified as active behaviors, particularly for severely scoliotic fish, we applied a posture change threshold: if an angle pose differed no more than a certain threshold from either the previous or the next pose, it was labeled as "rest". We optimized this threshold using the same training set. Classifying and thresholding as described resulted in a high number of correctly classified cruises (94.8% training, 94.8% validation) and rests (96.5% training, 95.8% validation). We used this model to assign behavior labels to all frames with high-quality posture as described.

Quality control for behavior classification

To further assess the classifier's accuracy, we plotted predicted behavior episodes and inspected them for quality. First, we looked at behaviors throughout full assays by creating images where each pixel represents a frame, colored according to the behavior in that frame. Three representative full-assay behavior images are shown in Figure 2.3A-C. From these assay-behavior images, we noticed behavioral differences between fish. For example, some fish prefer to cruise for long periods of time against moderate (20 cm/s) flow (Figure 2.3C), but others prefer to swim back-and-forth against the flow with cruises separated by turns and rests (Figure 2.3A). The assay-behavior images allowed us to quickly check the classifier's output, visualizing each fish's behavior patterns, over many 62000-frame assays.

Beyond behavior frequency and duration, it was important to check that the automatically classified behaviors were believable. Withholding part of the training data for testing performed part of this function. We also validated the model by visualizing predicted behavior episodes using principal component analysis (PCA), comparing the visualized behaviors to expected shapes. It is

known that uninjured zebrafish behaviors can be identified using decomposition of angle poses (57). Simple behaviors have a characteristic manifestation in PCA: forward locomotion (cruise) as a toroid, turns as loops in opposite directions, and rest as a cluster relatively close to the origin. We used this knowledge to check whether poses with annotated behaviors appeared correctly labeled when decomposed using PCA. For visualization, we connected adjacent poses with lines and colored the lines according to the predicted behavior. Manually annotated adult behaviors manifested in this PCA pose space similarly to those seen in previous studies of larvae (57). Predicted behaviors from three full assays are shown in Figure 2.3D-F, mimicking the shapes observed in the training set and in previous studies. As expected, rest episodes of highly scoliotic fish were centered away from the origin around a point in space corresponding to its average body curvature (results not shown). We plotted behaviors in posture space for all assays, confirming that behavior shapes were roughly similar to the expected shapes while allowing for variation due to injury and body shape. These quality control plots provided evidence that the computationally classified behaviors, particularly cruises and rests, were accurate.

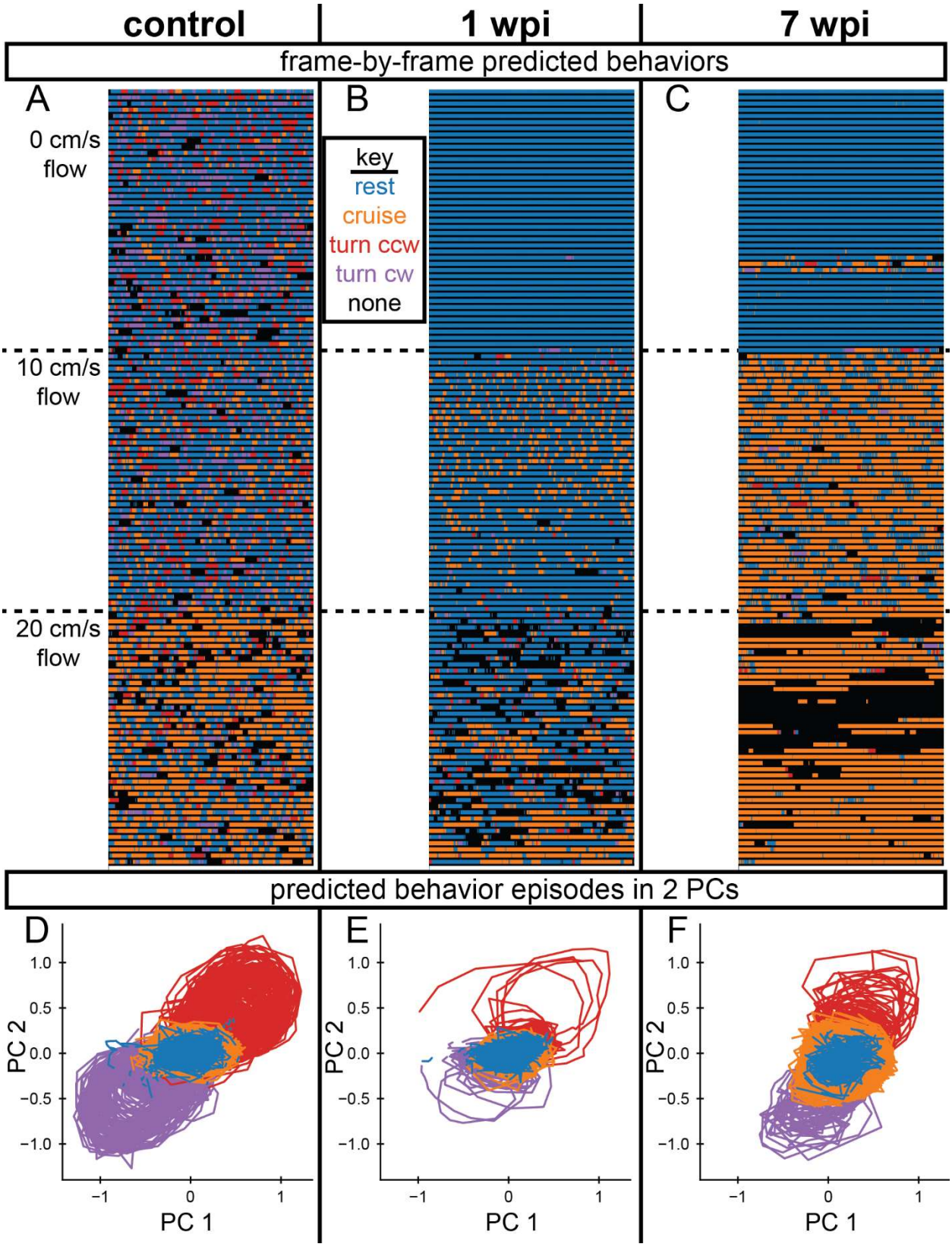
control
1 wpi
7 wpi
frame-by-frame predicted behaviors
A
B
C
0 cm/s flow
10 cm/s flow
20 cm/s flow
key
rest
cruise
turn ccw
turn cw
none
predicted behavior episodes in 2 PCs
D
E
F
PC 2
PC 1
1.0
0.5
0.0
−0.5
−1.0
−1
0
1

Figure 2.3: Computationally predicted behaviors in three swim assays.
(A-C) Frames from full assays plotted like text (left to right, top to bottom) colored according to the predicted behavior. Thin black lines separate rows to make them more visually distinct. Colors: rests are blue, cruises are orange, counterclockwise turns are red, clockwise turns are purple, and frames that could not be classified are black. Some frames could not be classified due to low-quality posture annotation. Generally, this meant that the fish was partially or completely out of frame. Assays in panels A-C were selected from fish that swam well against flowing water primarily to demonstrate automated behavior annotation, but also to show fish that swam with different behavior patterns. Note that one fish preferred to swim back and forth against the flow (A), another rested frequently (B), and the third cruised for longer periods without resting or turning (C). **(D-F)** Tracks of poses from behavior episodes decomposed into two principal components and colored according to the predicted behavior. For each assay, predicted behaviors manifested as similar shapes in PC space, as expected.

2.2.4 External software dependencies

Statistical analysis and data visualization

For comparing individual metrics within groups and between timepoints, Brown-Forsythe and Welch's ANOVA tests and Dunnett's T3 multiple comparisons tests were performed in GraphPad Prism (https://www.graphpad.com). To compare glial bridging and axon regrowth between outcome prediction groups, we used independent t-test in SciPy (88) version 1.7.3. Metric cluster significance was tested using R (89) version 4.0.4 and sigclust2 (90,91) version 1.2.4. Plots were generated using Matplotlib (92) version 3.4.3 and Seaborn (93) version 0.12.1 and were compiled and stylized using Adobe Illustrator.

Third-party software

All video and swim function analyses were performed in Python (https://www.anaconda.com) version 3.7.3, except cluster statistics calculated in R (89) version 4.0.4. The primary packages used for our analyses include NumPy (94) version 1.21.5, pandas (95,96) version 1.2.4, tensortools (97) version 0.3, scikit-learn (87) version 1.0.2, SciPy (88) version 1.7.3, dtw-python (98) version 1.1.12, umap-learn (86) version 0.4.2, DeepLabCut (61,84) version 2.1.6.2, Matplotlib (92) version 3.4.3, Seaborn (93) version 0.12.1, sigclust2 (90,91) version 1.2.4, and FFmpeg (https://ffmpeg.org) version 4.3.2. We also used open-source code created by the Zachary Pincus Lab (https://github.com/zplab).

2.3 Classical Functional Metrics

One purpose of this study was to generate new functional metrics. However, we also quantified several classical metrics for comparison. Perceived swim quality was scored using criteria similar to published methods (35,44). We calculated mean y, distance, activity, burst frequency, and time against flow nearly identically to our previously published protocol (17). In this study, however, we did not down-samples videos to 30 frames per second (fps) but kept the videos at the original framerate (70 fps). Appropriate corrections were calculated for frame-to-frame pixel-change thresholds as needed. This section describes each of these classical functional metrics in detail.

Perceived Swim Quality

This score was assigned by observation on a scale from 1 (low quality) to 5 (high quality). We first found the best and worst fish, then scored all fish compared to these. We focused our observation on the first few minutes when the flow started (5 min) and when the flow accelerated (10 min). Our criteria were as follows:

> **5:** Fish's swimming pattern looked normal and mostly used tail movement, not its head, to swim. No scoliosis.
>
> **4:** Fish appeared to swim at the same rate and speed as those categorized as 5. Slight scoliosis. Slightly less tail movement than 5 and slightly more head movement or "wiggling".
>
> **3:** Fish could not swim as effectively as 4. Equal head and tail movement. Scoliosis looked "bent" at about a 45-degree angle.
>
> **2:** Fish had some tail movement and could rotate its body, but it could not swim forward effectively. Severe scoliosis with tail movement. No swimming once flow started.

1: Fish had no tail movement. Severe scoliosis was observed. No swimming once flow started.

We treated the above criteria as guidelines because not all fish had all the features as described. For example, a fish could score "3" due to excessive head movement without significant scoliosis.

Mean Position in the Flow Axis (Mean Y)

"Mean y" was defined as the average centroid position along the water flow axis in the swim tunnel. Higher mean y was closer to the flow source. It was assumed that exhausted fish would be pushed backward by the flow and have a lower mean y. We reported mean y only for periods of the behavior assay when water was flowing (10, 20 cm/s).

Distance

Swim distance was measured as the sum of frame-to-frame centroid displacement in pixels. In this study we did not adjust distance according to water flow velocity, and we measured during the entire assay at all flow speeds.

Activity

Activity was defined as the sum of frames where centroid displacement (see Distance) was above a certain threshold, divided by the total number of frames. In this study we did not adjust activity according to water flow velocity, and we measured during the entire assay at all flow speeds.

Centroid Burst Frequency

We defined a centroid burst as an uninterrupted period of at least two active frames (see Activity). Centroid burst frequency was the number of centroid bursts per minute. We reported this measurement only for periods of the behavior assay when water was not flowing (0 cm/s).

Time Against Flow

Time against flow was defined as the sum of frames where centroid displacement (see Distance) was above a certain threshold in the direction of the flow, allowing 45-degree deviation in either

direction, divided by the total number of frames where water is flowing. Accordingly, time against flow was only calculated for periods of the behavior assay when water was flowing (10, 20 cm/s).

Endurance or Time to Exhaustion

We defined endurance, or time to exhaustion, as the duration of time that a fish swam against flowing water until exhausted. Fish were allowed to acclimate in calm water, then the flow speed was increased periodically. When the fish could no longer pull away from a barrier at the back of the tunnel, it was removed from the tunnel without disturbing the other fish and the time was recorded.

2.4 Metrics from Posture and Gait

This section describes metrics that were derived from pose and behavior annotation: pose burst frequency, lateral scoliosis, posture novelty, cruise rostral compensation, cruise body frequency, and tail beat frequency. Of the six metrics derived from posture and gait that we analyzed, only cruise body frequency and tail beat frequency were previously applied to SC injury in adult zebrafish (11). “Pose burst frequency” is a variation on the previously described burst frequency (17), which we call “centroid burst frequency”. The scoliosis score, posture novelty, and rostral compensation were newly described for this study.

2.4.1 Metrics derived from posture

Pose Burst Frequency

Pose burst frequency was the number of posture bursts per minute. Like centroid burst frequency, a burst was defined as an uninterrupted period of at least two active frames. For this metric, however, active frames were defined as those with active posture. Such frames had a high-quality pose annotation, implying that the fish was fully visible in frame and was not classified as “rest” by our behavior classifier. Although this definition of “active” did not depend on flow velocity, we only reported this value for periods without water flow (0 cm/s) to be comparable with our

reported centroid burst frequency. Note that at the frame rate of our videos (70 fps), bursts of posture movement occur faster than the human eye can track. Our previously published protocol for behavior analysis reduced video framerate to 30 fps and calculated burst frequency based on the centroid, called "centroid burst frequency" in this study. Although 30 fps was previously shown to adequately measure body centroid displacement, we used full framerate (70 fps) videos to calculate both centroid and pose burst frequency in this study.

Lateral Scoliosis

For each period of rest, or inactive posture, we calculated the average sum of each angle pose, then took the weighted average of these values over the entire swim where weights are the length of the rest periods. Although the calculation would have been essentially equivalent for non-scoliotic fish, we chose to analyze each rest bout separately and average their results rather than taking the average posture over the entire swim because some fish with severely poor recovery could not control their dorsal-ventral orientation. For example, when a scoliotic fish flipped to its back, its posture was inverted; and repeated flipping led to an artificially lower scoliosis score when posture was averaged over the entire swim. Hence, each period of rest was analyzed separately, then values for all rest periods were averaged as described. Representative frames taken from fish at rest in the tracking experiment are shown in Figure 2.4.

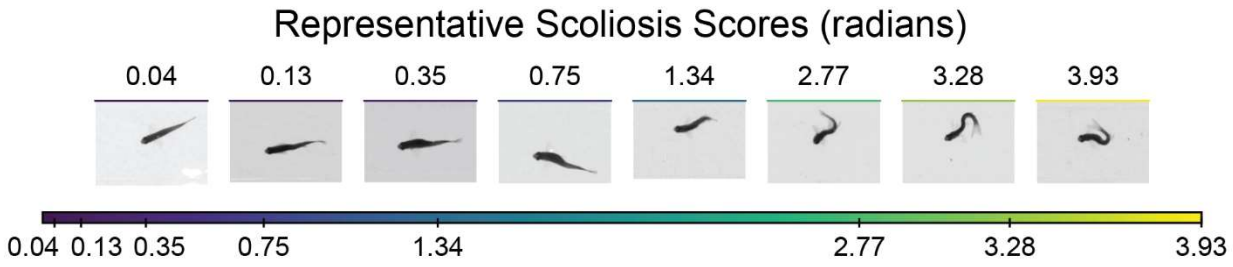

Figure 2.4 Visualization of the scoliosis score.
The scoliosis score is the sum of curvature measured at angle positions on the centerline at rest. To demonstrate how this score relates to body curvature, frames were taken from representative assays identified using k-medoids clustering of scoliosis scores of all assays.

Posture Novelty

As an alternate measure of posture wellness including both resting and active posture, we used novelty detection to calculate the proportion of poses in each assay that were significantly different from those seen in control assays. To do this, we trained a Local Outlier Factor (LOF) model using sampled uninjured control poses, then used the model to perform novelty detection on all assays. An assay's posture novelty score was calculated as the number of poses identified as "novel" by LOF divided by the total number of poses in the assay. We created a representative training set by sampling 1,200 poses from each control assay: 100 poses from 12 k-mean clusters. K-means clustering was performed separately for each assay.

2.4.2 Metrics derived from gait

Cruise Rostral Compensation

First, we calculated average angular amplitudes at each angle position along the dorsal centerline during episodes of cruise behavior. We called this a cruise curvature profile. We calculated a control profile as the average profile of uninjured fish. Note that angular amplitudes measure curvature extrema at centerline positions, not Euclidean displacement. To account for drift in swimming trajectories and body shape deformities, amplitudes were determined by comparing oscillation extrema to the moving mean. We defined rostral compensation as the maximum absolute difference between an assay's cruise curvature profile and the control profile at rostral angle positions α_1 to α_5 (Figure 2.1). We compared two methods for quantifying the difference between cruise curvature profiles — maximum absolute difference and integrated area (Figure 2.5A) — and discovered that these methods were strongly correlated (Figure 2.5B). Therefore, we were satisfied to define rostral compensation using the maximum absolute difference between rostral positions of the cruise curvature profiles.

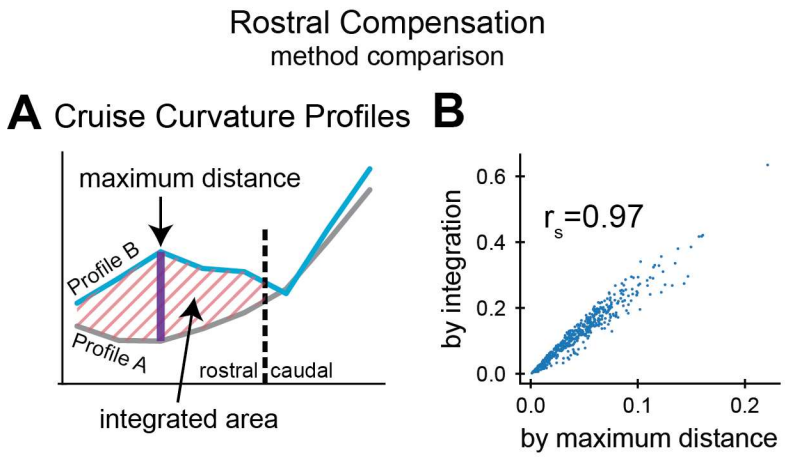

Figure 2.5: Rostral compensation measured as maximum distance or integrated area.
(A) Demonstrating two ways to quantify rostral compensation. The difference between cruise curvature profiles could be determined either by the maximum distance between them (purple line), or by the integrated area between them (pink shaded area). **(B)** Both strategies were calculated for every assay in the tracking experiment then plotted against each other. Spearman rank correlation (r_s) shows a strong correlation between them, indicating that they are nearly equivalent.

Cruise Body Frequency

Cruise body frequency is the number of posture oscillations per second while swimming forward.

For average cruise frequency measurements over full assays, we computed cruise body frequency for each body angle position along a fish's centerline, then averaged all frequencies in the cruise. Frequency values for all cruises in the assay were then averaged get a single assay score.

Tail Beat Frequency

To quantify tail beat frequency, we used an annotated point near the tip of the caudal fin to measure lateral displacement oscillation extrema, then calculated frequency using those measurements.

2.5 Trajectory Analysis

We tracked individual fish as they recovered from SC transection. This section explains our methods for exploring this unique longitudinal data.

2.5.1 Cruise sonification

Each angle position on the fish's centerline was assigned a pitch on the C harmonic series: C2, C3, G3, C4, E4, G4, C5, and E6. Slowed to 19 frames per second, each angle position's note played on its local maxima, or the peaks of the oscillatory waveform. If the waveform's amplitude was

higher than the average control amplitude, the pitch of the note was shifted down (flat) proportionally. Therefore, fish with unusually high angular amplitude, e.g., high rostral compensation, sounded flat: the more extreme, the more flat. An accompanying video was created in which the position on the fish displayed a dot when the tone sounded.

2.5.2 Cruise embedding

Taking all annotated cruise episodes in each assay, we performed a 5-principal component decomposition on the angle poses, and then created a pairwise distance matrix for these cruise episodes using dynamic time warping (DTW). From each distance matrix, we used affinity propagation to select exemplars, or cruises that are most representative of the fish's general behavior. If affinity propagation failed to converge, we randomly sampled at most 16 cruises from the assay. To calculate the embedding for several assays, we calculated a pairwise DTW distance matrix for all exemplar cruises from the assays, then fed the distance matrix into UMAP (86) using 20 as the k-nearest neighbors parameter, which is consistent with published work (58). We omitted fish with scoliosis scores higher than 0.35.

2.5.3 Tensor decomposition

Tensor decomposition, also called tensor component analysis (TCA), can be conceptualized as an extension of PCA (97). Whereas PCA operates on a rank-2 tensor (subjects, measurements), TCA can operate on a rank-3 tensor (subjects, measurements, time). A rank-3 tensor was created by concatenating all fish with their measurements in all assays (sorted temporally) in the tracking experiment. We standardized each measurement type first by multiplying its values by -1 if its average was increased at 1 wpi compared to controls so that higher values were always associated with control (these measurements were scoliosis, posture novelty, rostral compensation, tail beat frequency). Then we scaled all measurements to comparable ranges using StandardScaler from

scikit-learn (87). We omitted 6 fish that died before 8 wpi and 10 fish that did not perform a measurable cruise at every assayed week. Tensor component analysis was performed using the tensortools python library (97). Unlike PCA, tensor decomposition is not deterministic, so multiple models had to be trained and compared.

TCA model selection

We compared ranks from 1 to 90 for three varieties of canonical polyadic (CP) tensor decompositions: unconstrained by alternating least squares (cp_als), nonnegative by block coordinate descent (ncp_bcd) and nonnegative by hierarchical alternating least squares (ncp_hals). After comparing model error (Figure 2.6A) and replicate similarity (Figure 2.6B) for 4 replicates of each rank and model, our chosen combination was rank-7 CP decomposition by alternating least squares.

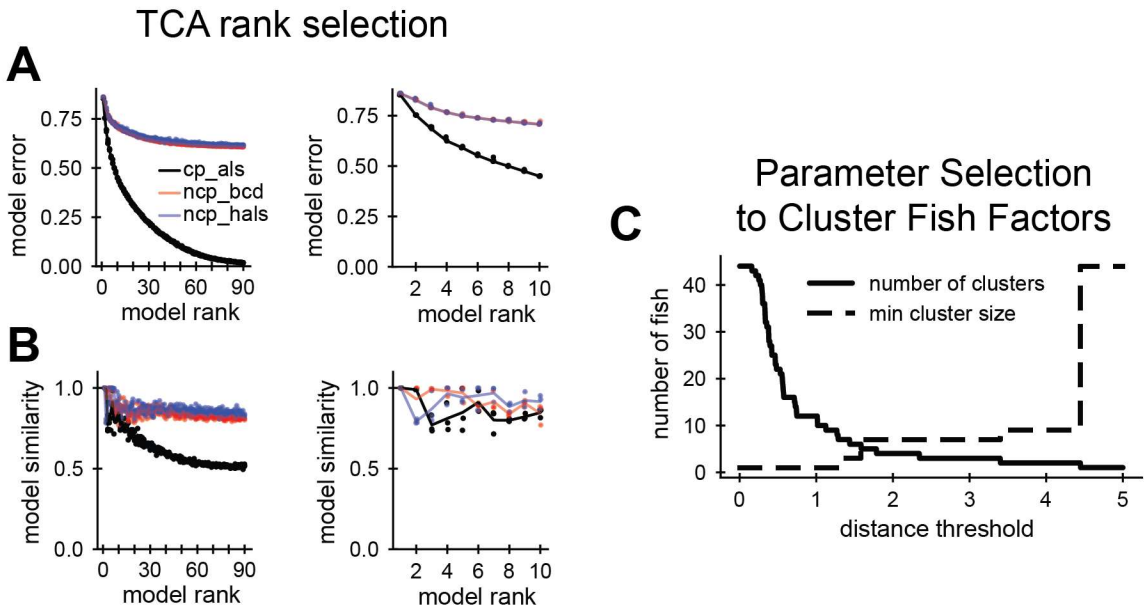

Figure 2.6: Parameter selection for tensor analysis of longitudinal measurements.
Unlike PCA, TCA is not deterministic, so multiple models were fit and compared. Three model types are shown. To achieve an optimal balance between low model error and high model similarity, we chose a rank-7 canonical polyadic decomposition by alternating least squares (cp_als). After decomposition, we clustered fish according to their factor values from the seven components. **(A)** Model error for various ranks. Four replicate models were fit for each rank. **(B)** Model similarity for various ranks. **(C)** Selecting an appropriate distance threshold for clustering. We clustered fish according to their TCA factors using agglomerative clustering. To maximize the number of clusters while keeping a high minimum cluster size, we chose 1.7 as our distance threshold with five clusters identified.

Fish factor clustering

We clustered fish according to their factor values using agglomerative clustering with a distance threshold of 1.7 using scikit-learn. This distance threshold was chosen by comparing the number of clusters to the minimum cluster size for 1,000 threshold values spaced evenly from 0.001 to 5 (Figure 2.6C).

2.5.4 Predicting 8 wpi regeneration groups at 2 wpi

Prediction method

We divided groups of fish in half, with one group predicted to regenerate more successfully than the other, according to the following method. The average distance swum and rostral compensation between assays 1 wpi and 2 wpi were calculated (e.g., for distance swum, add the distance swum at 1 wpi and 2 wpi together, then divide by two). Fish were ranked according to both averages, a rank from high to low for distance swum and a rank from low to high for rostral compensation, then the two ranks were added together. Fish were divided in half across median of this value. In this manner, the group that was predicted to regenerate well contained fish that were ranked high in distance swum and low in rostral compensation compared to the other fish in their cohort. Male and female fish were ranked and divided separately according to the sex group's calculated median. All caregivers were blinded to the predictions.

Chapter 3: Comparing Functional Metrics

3.1 Classical Recovery in the Tracking Experiment

3.1.1 Results

A longitudinal study of spinal cord regeneration parameters

To develop and compare functional metrics, we devised a longitudinal study that allowed us to record and track swim function in individual animals for 8 weeks of spinal cord (SC) regeneration (Figure 3.1). Sixty wild-type fish of the Ekkwill/AB strains (30 males and 30 females) were housed separately from each other with physical dividers for the duration of the study. Swim behavior was recorded for each fish before injury and weekly between 1 and 8 wpi. At each time point, fish were placed in an enclosed swim tunnel and a dorsally placed camera was used to capture swim behavior at 70 frames/s for a total of 15 min, divided into three sequential 5-min periods with water current velocities of 0 cm/s, 10 cm/s, and 20 cm/s. At 8 wpi and following swim behavior recording, axon tracing experiments and glial bridging measurements were performed to assess cellular regeneration metrics. Most fish survived to the end, however six fish (3 male, 3 female) died during the course of the experiment: two females after surgery and before 1 wpi, one male and one female between 3 and 4 wpi, one male between 5 and 6 wpi, and one male between 6 and 7 wpi. Overall, 90% of the fish (54 out of 60) survived until the 8 wpi experimental endpoint.

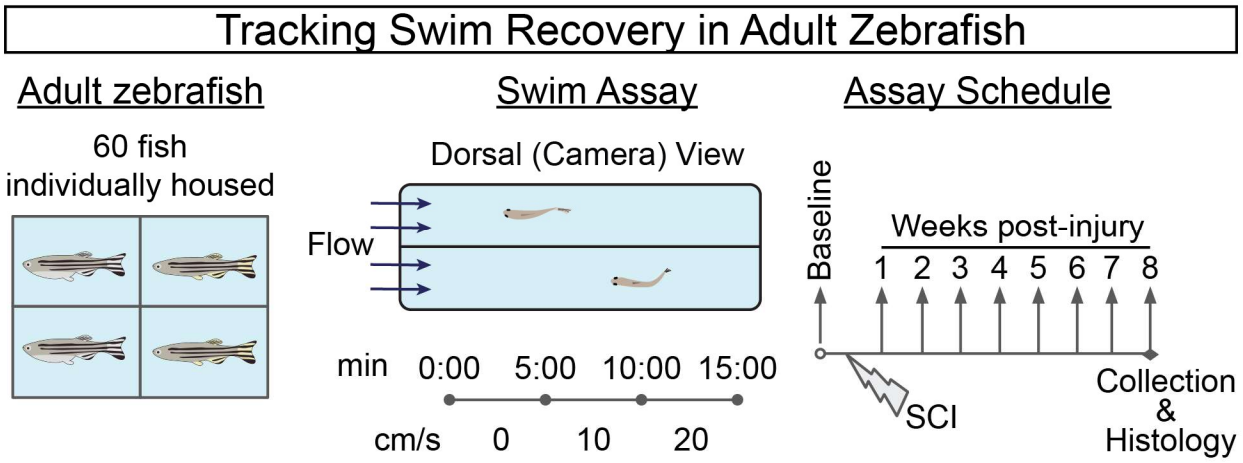

Figure 3.1 Schematic of the SCI longitudinal tracking experiment. This experiment tracked individual zebrafish from a preinjury control assay through eight weeks of spontaneous recovery from spinal cord injury (SCI). A total of 60 fish (30 males and 30 females) were housed separately throughout the entire experiment to allow for longitudinal tracking of individual fish. In each swim behavior assay, fish were video recorded in a swim tunnel for fifteen minutes. Fish first acclimated in calm water for 5 min (0 cm/s), then water current velocity was increased to 10 cm/s for the next 5 min and to 20 cm/s in the final 5 min. Swim behavior was recorded before SC transection and weekly between 1 and 8 wpi. After the 8 wpi swim, spinal cords were collected for histology.

Classical regeneration metrics

To begin to assess SC regeneration parameters in this study, we first calculated previously described swim behavior measurements from the captured swim videos, including five capacity measurements (Figure 3.2A-E; Figure 3.3A-E) and one quality measurement (Figure 3.2F; Figure 3.3F). These measurements provided a baseline against which newly developed metrics could be compared. Functional measurements indicated that zebrafish are still capable of recovery from SC transection while isolated from other fish.

Swim distance, centroid time active, and time against flow were significantly disrupted by injury for both sexes (Figure 3.2A-C, Figure 3.3A-C), as was centroid burst frequency in calm water for female fish (Figure 3.2E). Significant recovery between 1 wpi and 8 wpi was observed only for male fish centroid time active (Figure 3.3B), although most swim capacity measurements for both sexes were no longer significantly different from control by 8 wpi. Similarly, the proportion of fish that swam healthily, according to perceptually assessed swim quality, decreased after injury

and increased through recovery (Figure 3.2F, Figure 3.3F). We noted that male fish exhibited this stereotypical recovery trend more strongly than females in this experiment. Overall, the female fish in this experiment regenerated poorly (Figure 3.3F) and were less energetic both before and after injury, which is not necessarily typical of zebrafish (42). For this reason, data from male and female fish are plotted separately.

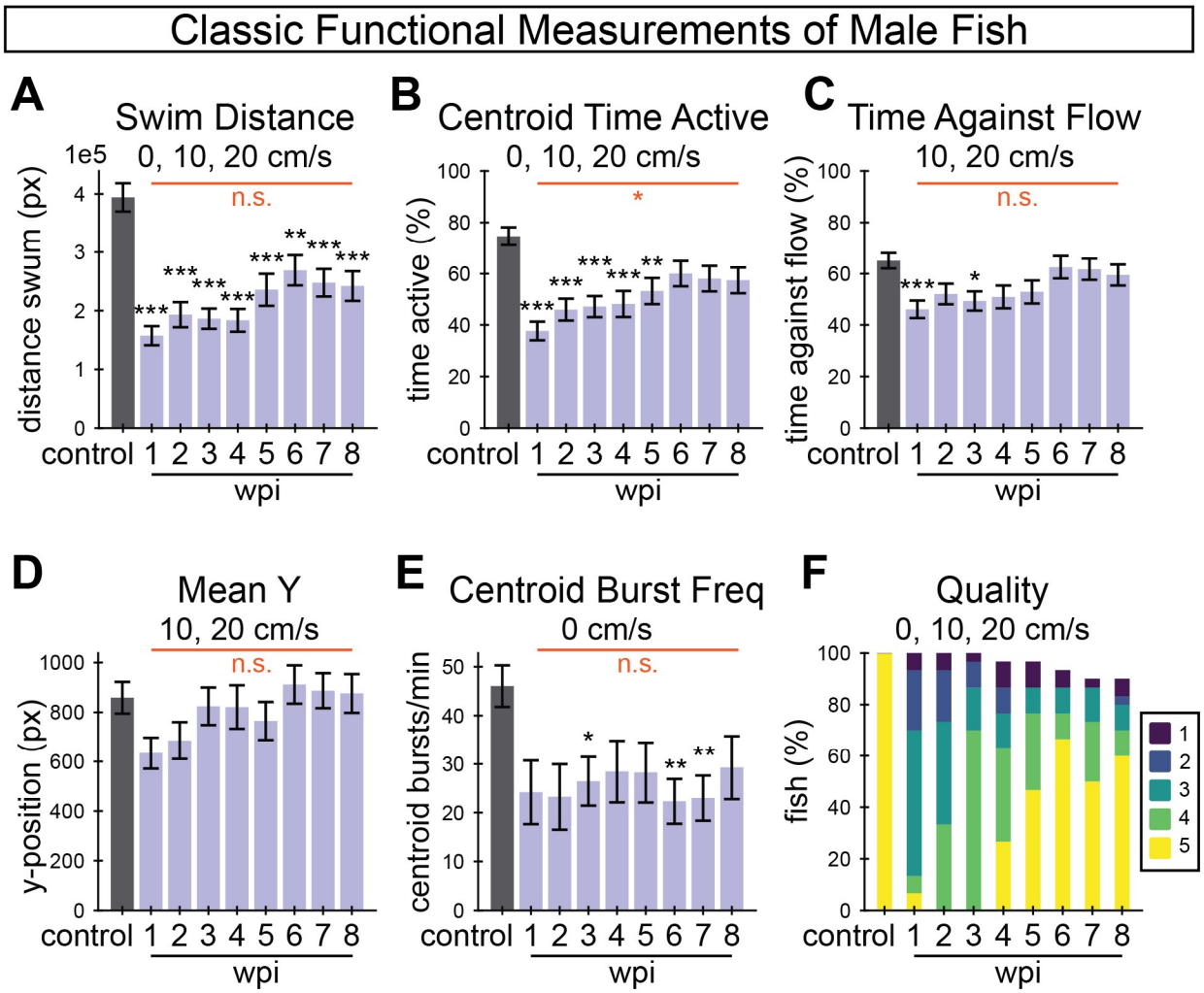

Figure 3.2: Classic functional measurements of tracked male fish.
A suite of established functional measurements was used to assess swim recovery for male fish following SC transection. Swim distance **(A)**, activity as measured by centroid movement **(B)**, time swimming against the flow **(C)**, mean position in the axis of flow (mean y) **(D)**, and burst frequency as measured by centroid movement **(E)** represent swim capacity measurements. **(F)** Perceived swim quality scores. The height of each bar represents the number of fish that survived to that time point as a percentage of 30 total male fish. This figure includes 30, 30, 30, 30, 29, 29, 28, 27, 27 fish at control, 1, 2, 3, 4, 5, 6, 7, 8 wpi assays, respectively. Error bars depict SEM and statistical significance was determined by Brown-Forsythe and Welch's ANOVA tests with Dunnett's T3 multiple comparisons tests. p-value

markers in black represent comparisons between each time point post-injury relative to control measurements before injury. Red horizontal bars and p-values marked in red show significance between 1 wpi and 8 wpi. ***P<0.001; **P<0.01; *P<0.05; ns, P>0.05.

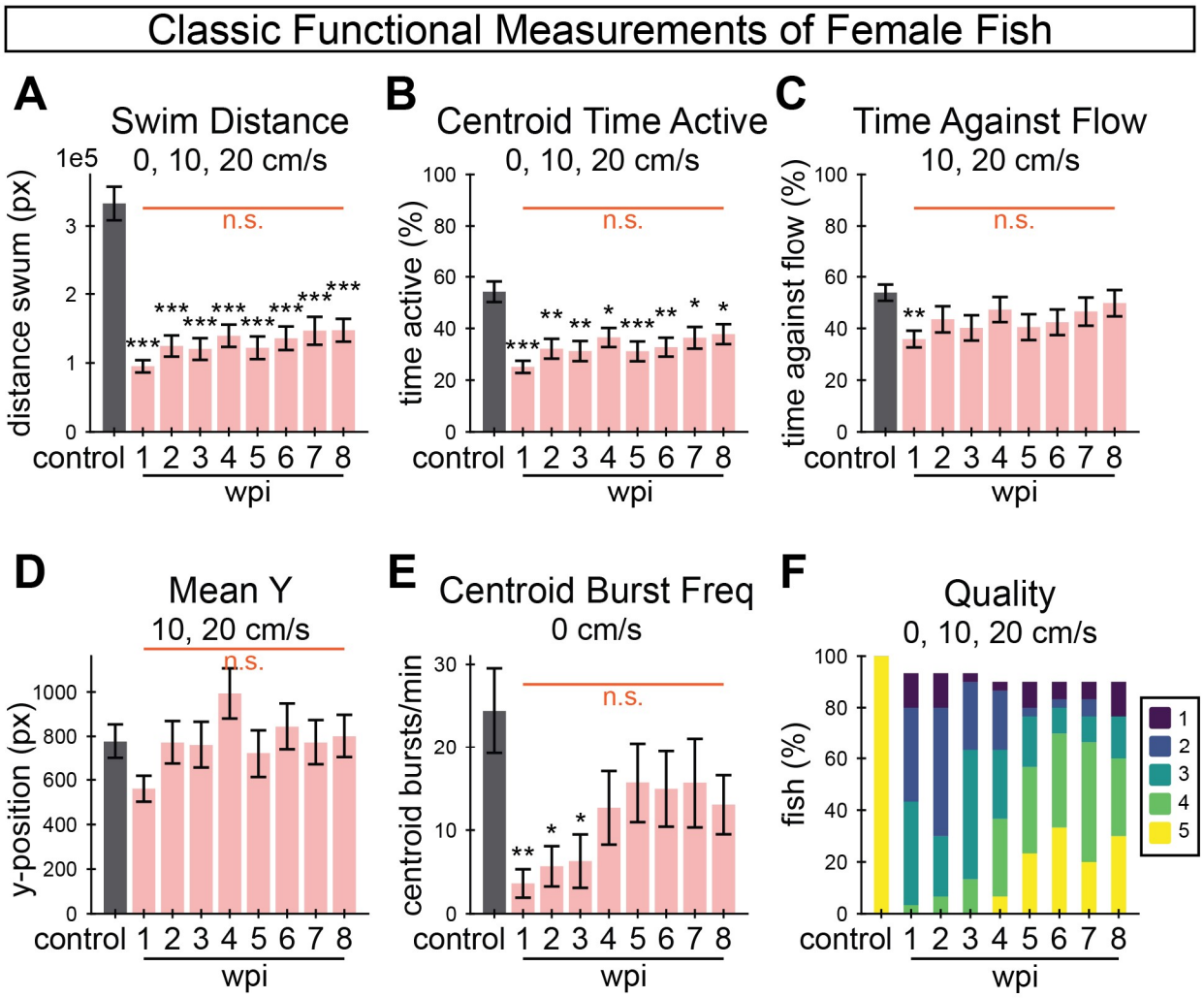

Figure 3.3: Classic functional measurements of tracked female fish.
A suite of established functional measurements was used to assess swim recovery for female fish following SC transection. Swim distance **(A)**, activity as measured by centroid movement **(B)**, time swimming against the flow **(C)**, mean position in the axis of flow (mean y) **(D)**, and burst frequency as measured by centroid movement **(E)** represent swim capacity measurements. **(F)** Perceived swim quality scores. The height of each bar represents the number of fish that survived to that time point as a percentage of 30 total female fish. This figure includes 30, 28, 28, 28, 27, 27, 27, 27, 27 fish at control, 1, 2, 3, 4, 5, 6, 7, 8 wpi assays, respectively. Error bars depict SEM and statistical significance was determined by Brown-Forsythe and Welch's ANOVA tests with Dunnett's T3 multiple comparisons tests. p-value markers in black represent comparisons between each time point post-injury relative to control measurements before injury. Red horizontal bars and p-values marked in red show significance between 1 wpi and 8 wpi. ***P<0.001; **P<0.01; *P<0.05; ns, P>0.05.

In terms of cellular regeneration, measured as glial bridging and axon regrowth, the male fish regenerated significantly more glial tissue and axons proximal to the lesion in this experiment

(Figure 3.4D). Distribution histograms suggest that this significant difference between the sexes was not driven by outliers (Figure 3.4A-C).

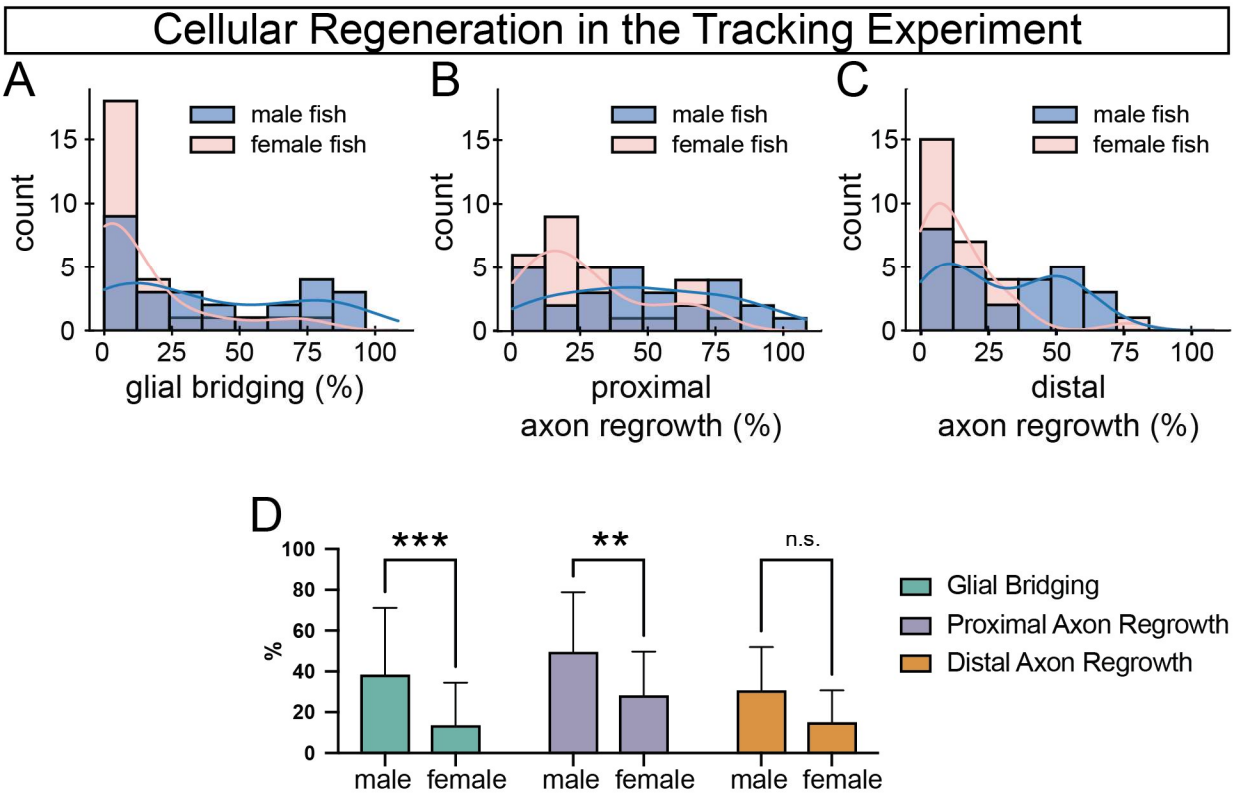

Figure 3.4: Cellular regeneration outcomes for male and female fish.
Results summarizing n=27 female fish and n=27 male fish. **(A-C)** In the tracking experiment, male fish appeared to have regenerated more successfully than female fish in terms of glial bridging, proximal axon regeneration, and distal axon regrowth. Measurements for each sex are presented as histograms with kernel density estimates. **(D)** Two-way ANOVA with Šídák's multiple comparisons test indicated that male fish regenerated significantly more glial tissue at the lesion and more proximal axon projections. ***P<0.001; **P<0.01; *P<0.05; ns, P>0.05.

3.1.2 Discussion

This study explored connections between functional and cellular regeneration measurements during SC regeneration in adult zebrafish. Fish were individually housed to enable their longitudinal tracking for 9 weeks. In comparison with alternative methods of tracking fish identities such as fin clipping, dye injection, passive integrated transponder tagging or skin pattern recognition, physical separation was the method of choice to avoid introducing additional injuries or imaging steps to our experimental pipeline (99).

It is important to note that, compared to the well-known elevated regenerative capacity of zebrafish SC tissues, regeneration efficiency was reduced in this cohort of 60 fish, with female fish recovering particularly poorly. Recovery of these measurements appeared to stop around 6 wpi (Figure 3.2A-D, Figure 3.3D-E). It should also be noted that even in such conditions where functional recovery is expected to continue to 8 wpi, some fish experienced negligible functional improvement after 6 wpi (4). Regarding male and female recovery, one other study has reported differential recovery patterns between the sexes (42), but it is generally assumed in the literature that male and female fish recover equally well in standard conditions, such as group housing. Although it remains to be determined whether physical separation negatively impacts SC regeneration in a sex-specific manner, we propose that our previously established injury and post-operative standards, including group housing, support optimal regeneration conditions (18,19). However, our purpose was not to demonstrate SC regenerative capacity in zebrafish, but to compare traditional and new functional measurements and their associations with structural recovery. Our fish exhibited significant recovery up to 6 wpi, thus irrespective of whether housing conditions for this study were detrimental to recovery, the broad range of regeneration observed in this study was not only well suited, but also retrospectively ideally tailored, for our purposes.

3.2 Posture-derived Metrics in the Tracking Experiment

3.2.1 Results

We measured three attributes of fish posture: pose burst frequency, lateral scoliosis, and posture novelty. Pose burst frequency is a variation on the classical metric “burst frequency,” which we call “centroid burst frequency.” Lateral scoliosis and posture novelty are introduced in this study.

Centroid and pose burst frequencies are compared

We define a burst as a period when the animal is active. Activity is traditionally defined in terms of centroid movement, which has been the standard method to quantify swim behavior since "swim distance" was introduced as a functional metric in 2004 (Table 1.1). An alternate, more computationally intensive approach is to define swim activity in terms of body undulations. We, therefore, calculated burst frequency in the classical manner using a frame-to-frame centroid change threshold (centroid burst frequency) and in a pose-informed manner using computationally classified behaviors (pose burst frequency). To identify pose bursts, any high-quality pose that was not classified as "rest" was considered active. In the tracking experiment, we calculated these values only in calm water (0 cm/s flow velocity) during the first five minutes of the behavior assays. Mean centroid burst frequency, measured for male and female fish, both decreased significantly after injury, but only pose burst frequency significantly increased by 8 wpi (Figure 3.5). On the other hand, mean pose burst frequency at 8 wpi was still significantly different from control. The two measurements were highly correlated (Spearman r_s = 0.91), but pose burst frequency usually measured much higher than centroid burst frequency.

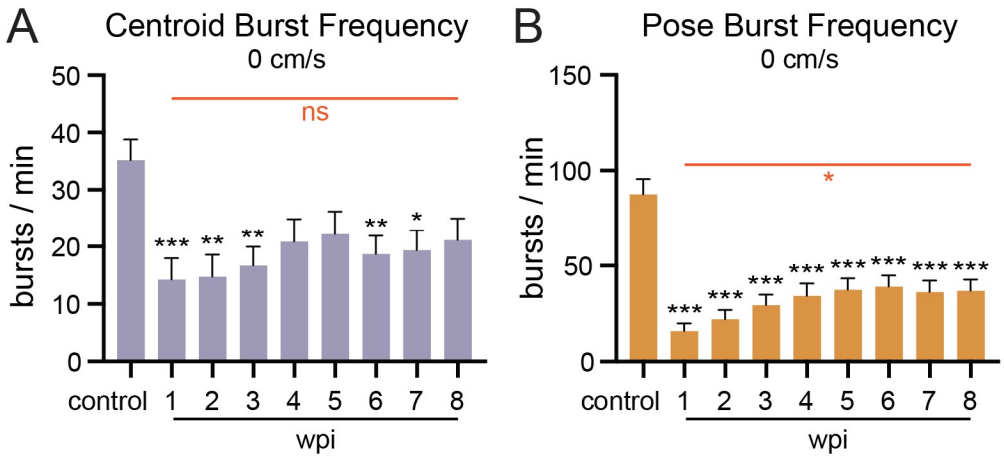

Figure 3.5: Comparing centroid- and posture-derived burst frequency in still water (0 cm/s).
(A) Average centroid burst frequency and **(B)** pose burst frequency measured in the tracking experiment. Both panels in this figure include 60, 58, 58, 58, 56, 56, 55, 54, 54 fish at control, 1, 2, 3, 4, 5, 6, 7, 8 wpi assays, respectively. Error bars depict SEM and statistical significance was determined by Brown-Forsythe and Welch's ANOVA tests with Dunnett's T3 multiple comparisons tests. p-value markers in black represent comparisons between each time

point post-injury relative to control measurements before injury. Red horizontal bars and p-values marked in red show significance between 1 wpi and 8 wpi. ***P<0.001; **P<0.01; *P<0.05; ns, P>0.05.

Postoperative scoliosis is irreversible by 2 weeks post-injury

The first novel measurement of posture that we devised was a scoliosis score. Although all fish in the experiment appeared healthy before injury, fish sometimes develop abnormal body curvature, or lateral scoliosis, sometime after injury. Depending on the degree of scoliosis, body shape deformities can significantly affect other measurements of posture and gait. To determine which fish were most likely to influence such measurements, we devised a scoliosis index based on dorsal centerline body curvature during periods of inactivity. We quantified scoliosis for each fish at each time point as the summed curvature at eight angle positions along the fish's dorsal centerline (Figure 2.1) averaged over all rest periods in an assay. To provide an intuition about the scale of these scores, representative fish with their scoliosis scores are shown in Figure 2.4. Our analysis indicated that of the 30 male and 30 female fish, 4 male fish and 4 female fish presented scoliosis scores >1.34 (Table 3.1).

Table 3.1: Numbers of fish that presented scoliosis above certain severity thresholds. Of the eight fish that were severely misshapen (>1.34), five scored above 2.77. Of those five, three scored above 3.28.

Scoliosis	Number of male fish	Number of female fish
>1.34	4	4
>2.77	2	3
>3.28	1	2

Pairwise comparisons of scoliosis scores between time points, using Spearman correlation, showed that relative scoliosis rankings stabilized after 2 wpi (Figure 3.6A). Fish did not exhibit noticeable scoliosis at 1 wpi, nor did scoliosis scores at 1 wpi correlate with the following weeks. Scores at pre-injury and 1 wpi weakly correlated with subsequent time points since the fish were all straight-bodied at the beginning of the experiment and had not developed scoliosis by 1 wpi. The

randomness of scoliosis rankings at 1 wpi and stability of rankings after 2 wpi are presented in Figure 3.6B using trendlines for each fish colored by the fish's rank at a specific point in recovery. As an alternative, unsupervised posture-driven recovery measurement, we used a nearest-neighbors approach to quantify postural abnormality for each assay. Taken as a ratio compared to representative posture observed in preinjury assays, we called this measurement "posture novelty." Posture novelty was closely associated with scoliosis scores. Pairwise rank correlations of scoliosis scores suggest that injury-induced scoliosis is irreversible by 2 wpi, and these results altogether revealed that scoliosis is an important factor in the variation of poses observed in the experiment at 8 wpi (Figure 4.1D-E).

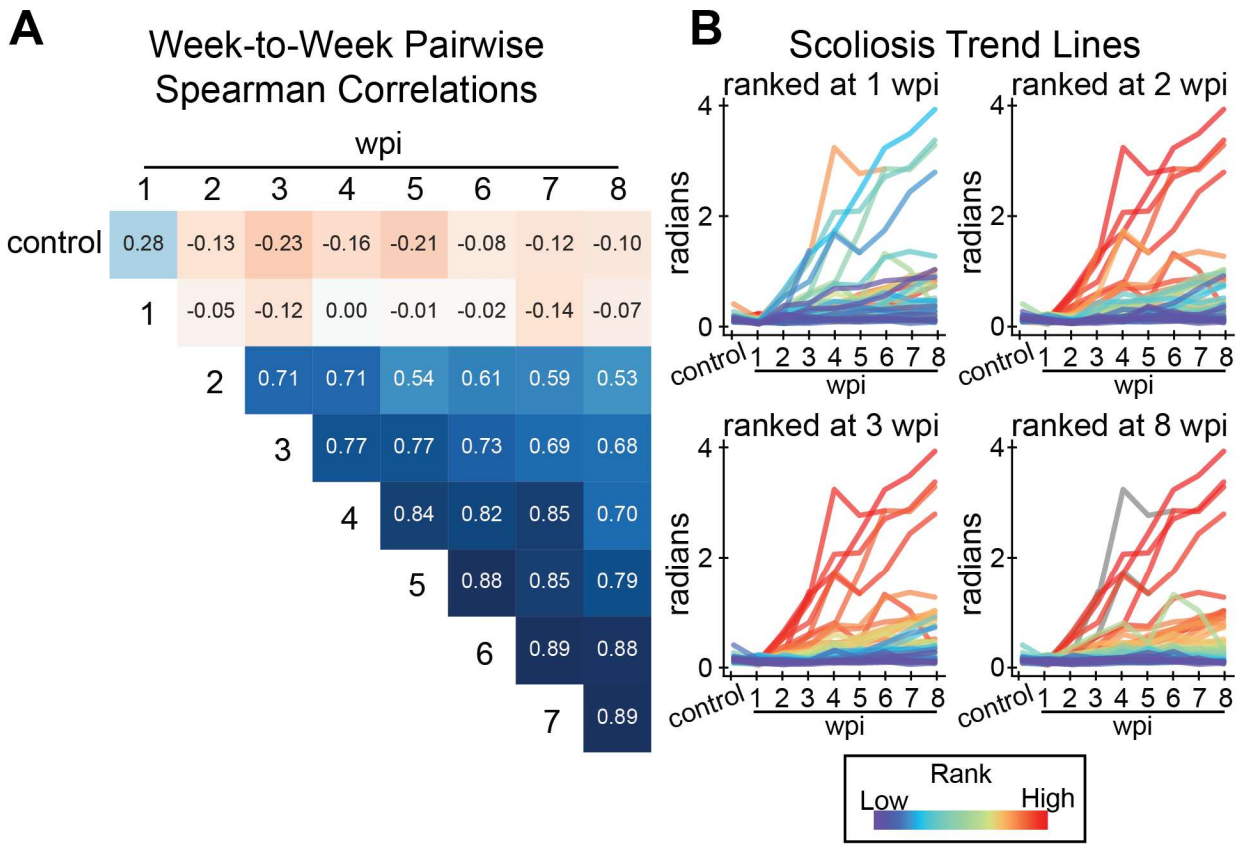

Figure 3.6 Assessment of lateral scoliosis among all 60 fish in the tracking experiment.

Scoliosis manifests with irreversible trajectories by 2 wpi. (A) Pairwise comparison of scoliosis scores between weeks by Spearman's rank correlation. Scoliosis scores correlate weakly between control and 1 wpi to other assays. Scores are most strongly correlated from 2 wpi onward. (B) A demonstration that scoliosis ranks stabilize after 2 wpi. Scoliosis trend lines for individual fish are plotted over all assays (x-axis), colored by rank at 1, 2, 3, and 8 wpi (top-left to bottom-right). Fish scoliosis trend lines are colored on a rainbow scale from red (most severe) to violet (least), and colored gray if the fish did not survive to the ranked week. This figure includes 60, 58, 58, 58, 56, 56, 55, 54, 54 fish at control, 1, 2, 3, 4, 5, 6, 7, 8 wpi assays, respectively.

Posture novelty is heavily influenced by scoliosis

Next, we sought to describe differences between fish in a less biased fashion. Centroid burst is more a measure of behavior than posture, and the scoliosis score depended on computationally annotated rests, but we wanted a measurement that did not depend on extra assumptions or post-processing beyond basic posture annotation quality control. We took inspiration from novelty detection, a subfield of machine learning that seeks to define which observations would be considered outliers in a reference distribution. We created a reference distribution using randomly sampled poses from control assays and trained a local outlier factor model on that distribution. Using that model, we identified novelties in all assays. Conceptually, a "novelty" is a pose that healthy fish are unlikely to present in our assay conditions. We thus defined "posture novelty" per assay as the percent of novelties measured in the assay.

We hypothesized that scoliosis and posture novelty would measure low before injury, then high after injury. Scoliosis was hypothesized to increase, measuring higher at 8 wpi than at 1 wpi, and this was observed (Figure 3.7A). Posture novelty was hypothesized to measure highest at 1 wpi and decrease over time as fish recover, assuming fish recover control-like gait. Contrary to expectation, mean posture novelty did increase at 1 wpi but did not decrease over time (Figure 3.7B). Rather, posture novelty increased as scoliosis became more pronounced after 2 wpi. Including all sixty fish, both those that developed severe scoliosis and those that did not, these measurements were moderately correlated (Spearman $r_s = 0.60$). When we limited the analysis to seventeen fish with high glial bridging (>20%) and low scoliosis in all assays (<0.35), both

measurements reported trends closer to expectation: scoliosis showed no significant change, and posture novelty was only significantly different from control at 1 wpi (Figure 3.7C-D). However, for this subset of relatively well-regenerated fish, mean posture novelty after 1 wpi showed an unusual trend, not decreasing, and was measured with relatively high variance.

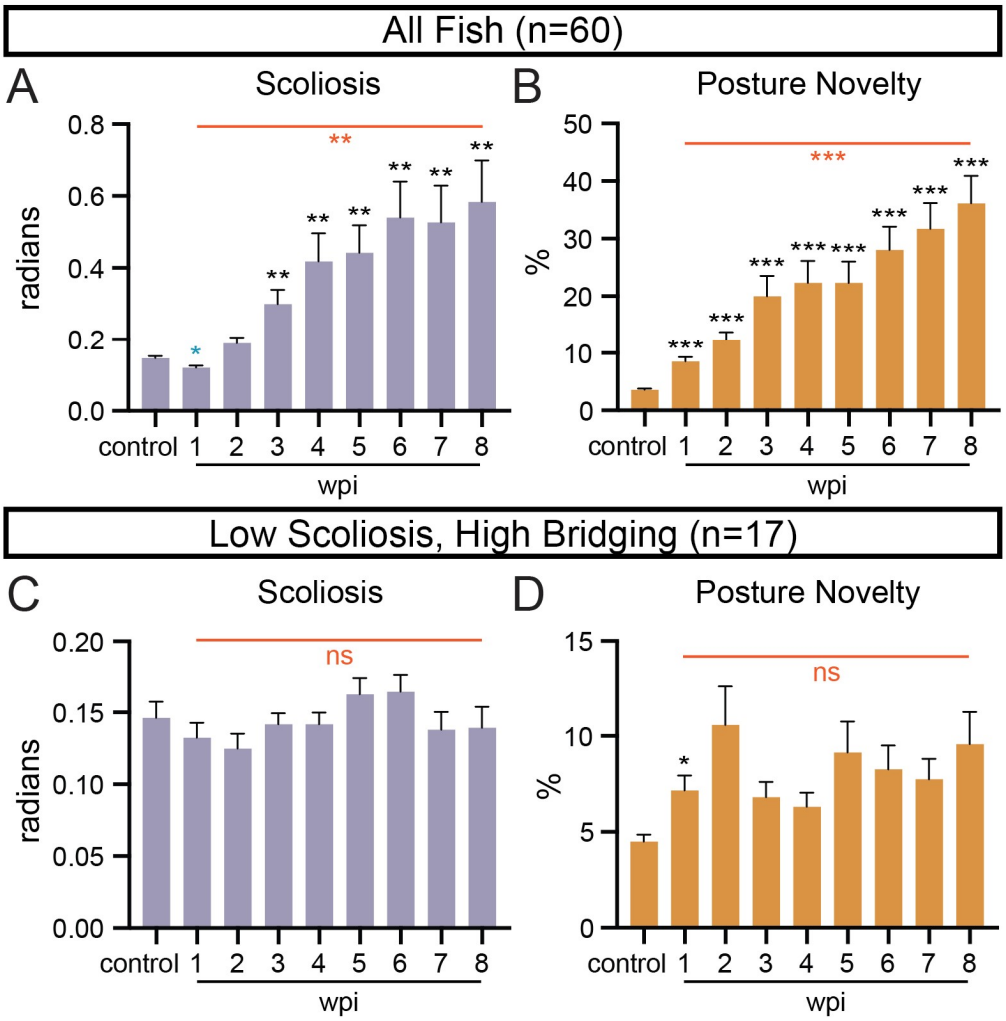

Figure 3.7: Comparing scoliosis to posture novelty.
Scoliosis and posture novelty were measured across all assays in the tracking experiment. (A-B) Measurements taken from all sixty fish (30 male, 30 female). (C-D) Measurements taken from the 17 fish (14 male, 3 female) that regenerated at least 20% glial tissue and never presented scoliosis greater than 0.35. Error bars depict SEM and statistical significance was determined by Brown-Forsythe and Welch's ANOVA tests with Dunnett's T3 multiple comparisons tests. p-value markers in black represent comparisons between each time point post-injury relative to control measurements before injury. The blue marker in panel A at 1 wpi indicates that mean scoliosis was measured significantly lower than control at 1 wpi. Red horizontal bars and p-values marked in red show significance between 1 wpi and 8 wpi. ***P<0.001; **P<0.01; *P<0.05; ns, P>0.05.

3.2.2 Discussion

Pose burst frequency

Classical functional metrics discussed in this study, except for endurance and perceived quality, were quantified using fish centroids. As we compared and analyzed these measurements, we discovered that burst frequency is somewhat problematic to quantify, and we eventually divided it into two types: centroid and pose.

Burst frequency is defined differently in other contexts, but for this study, we defined burst frequency as the number of active bouts per minute. Activity was measured using a pixel-change threshold from frame to frame. The limitation here is that adult zebrafish, having sufficient inertia due to high body mass relative to surface area, coast as they swim (100); but this definition of burst frequency, sometimes called episodes per minute (101), is more commonly applied to larvae which perform distinct, stereotyped bouts of movement separated by longer periods of rest (102). Water is more viscous to a small, light larva than to a grown adult zebrafish, and this is reflected in their locomotion (102). Consequentially, active posture equates with pixel change thresholds more accurately for larvae than for adult fish. Therefore, despite an overall high correlation between the two measurements, we recommend deriving burst frequency using active posture rather than centroid change for adult zebrafish.

Postoperative scoliosis

After spinal cord injuries in humans, some patients develop scoliotic deformities, especially younger patients (103). Two weeks after surgery, we noticed that some fish also began to exhibit scoliosis deformities (Figure 3.6B). As a direct measurement of posture abnormality, our scoliosis score correlated strongly with posture novelty, a quality measurement that accounts for all observed poses during a swim assay (Figure 3.7, Figure 3.14A, Figure 3.15A, 4.11A). It is not surprising that scoliosis may reduce a fish's motor coordination, range of body swing, and

perception of flowing water, all of which would reduce a fish's measured swim capacity. In the tracking experiment, higher scoliosis was not only associated with poor swimming ability but also less successful SC regeneration (Figure 3.14A, Figure 3.15A).

As for its etiology after spinal cord injury, there are several possibilities. One hypothesis is postoperative spinal malunion (27). Although this hypothesis was stated in a protocol for adult zebrafish spinal cord injury, to our knowledge it has never been experimentally confirmed. Drawing upon scoliosis research for humans, injury-induced spinal deformities are more likely to develop in people who experience traumatic injury before the adolescent growth spurt (104). Thus, another hypothesis is that the degree of scoliosis after injury could be associated with how much the fish grew in length during the period of recovery. We eliminated this hypothesis by calculating fish length using centerline keypoint poses and finding a negative correlation between fish growth and change in body curvature ($R=-0.73$, $p=3e-11$). Another possible cause is asymmetric muscle tension or relaxation after spinal cord injury, which likely contributes to idiopathic scoliosis in humans (105). Of these hypotheses, we consider the latter most probable.

We hypothesize that post-injury scoliosis in these zebrafish is neuromuscular rather than skeletal in origin. If the degree of muscle tension or relaxation is asymmetrical, the muscles on the relatively tense side will continue to pull the spine toward the ipsilateral curve, and long-term unilateral muscle pulling will eventually lead to scoliosis. This pull would be more pronounced when the muscles are exerting than at rest, and we did observe that when scoliotic fish swim in high-speed currents the lateral curvature is more pronounced. Because our quantification for scoliosis was based on rest posture, the scoliosis score was not well-suited to capture this observation. We observed no preference for scoliosis to develop toward the left or the right side. Moreover, some scoliotic fish appeared straighter after they were euthanized in tricaine (MS-222)

at the early stage during spinal cord regeneration (data not shown). From this, we hypothesize that injury-induced scoliosis may be more neuromuscular than skeletal in origin, but experimental confirmation is beyond the scope of this study. Scoliosis is an unavoidable problem during regeneration after spinal cord injury, and it is associated with poor glial and axon regeneration, so discovering and resolving the mechanism would improve zebrafish neuromotor recovery after spinal cord injury.

Posture novelty

We formulated posture novelty to have less supervision, or human bias, than our other posture-derived measurements. In contrast to pose burst frequency and lateral scoliosis, both of which required accurate rest behavior annotation, posture novelty accepted all high-quality poses as input. The obvious tradeoff here is that by ignoring behavior, the measurement is affected greatly by the fish's inherent motivation or capacity to move. For example, a recently injured fish (1 wpi) would show no signs of postoperative scoliosis (Figure 3.7A), so it would not present novel poses during periods of rest. If the fish swims no more than a few short bursts in the 15-minute assay, most of the observed posture would be indistinguishable from that of control fish. Consequentially, its novelty score would be low, within the range of healthy fish. Given this limitation, we considered using only active, non-rest, poses instead. The two major limitations of active-only posture novelty would have been that it breaks our intention of defining an unsupervised posture metric and that any fish that rests for the entire assay could not be measured. Based on our observations, the unsupervised approach for scoring posture novelty measured similarly to lateral scoliosis (Figure 3.7A-B) and showed a weak recovery-like trend for non-scoliotic fish which regenerated well (Figure 3.7D). It also assigns low, healthy-like scores to non-scoliotic fish with the least motivation or capacity to swim, whether healthy or impaired. Given these results, the

supposed limitations of active-only posture novelty may be strengths. We recommend active-only posture novelty for future consideration.

3.3 Gait-derived Metrics in the Tracking Experiment

3.3.1 Results

Rostral compensation

While established measurements of swim behavior captured the recovery of swim capacity after SCI, our swim videos showed even more pronounced swim gait differences. Comparing one period of oscillatory forward swim behavior (cruise) before injury (Figure 3.8A) and at 1 wpi (Figure 3.8B), we found that acutely injured fish swim using more motion in the rostral portion of their body.

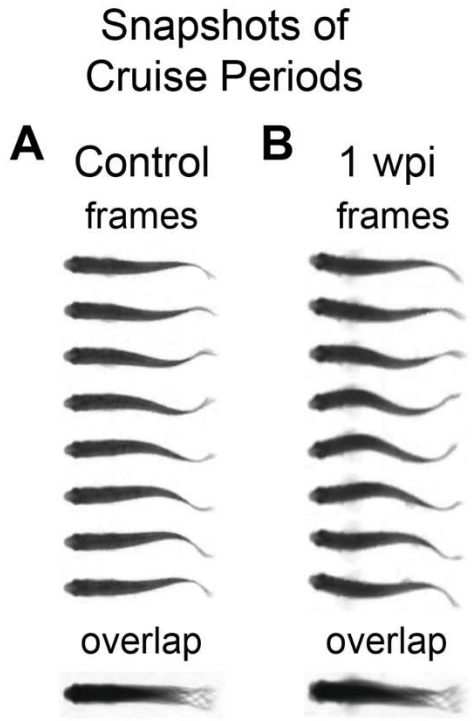

Figure 3.8: Snapshots of cruise periods from control and 1 wpi assays.
Each cruise period shows a fish swimming against a current velocity of 10 cm/s. Overlayed swim forms shown below the separate frames highlight defective caudal movement after SC transection. **(A)** Snapshots of swim behavior before injury. **(B)** Snapshots of swim behavior at 1 wpi.

We thus postulated that a scalable quantification of gait healthiness would provide a markedly improved functional regeneration parameter compared to established swim capacity metrics and manually assigned quality scores. To perform high-throughput gait analysis, we began by annotating dorsal centerline posture (Figure 2.1). After training DeepLabCut (61,84) to annotate keypoints on the centerline, we filtered and processed the poses, then trained a classifier to annotate simplified behaviors including rest, turn, and cruise. For simplicity, we defined a cruise as a forward swim with at least five measured extrema, or approximately three body oscillations.

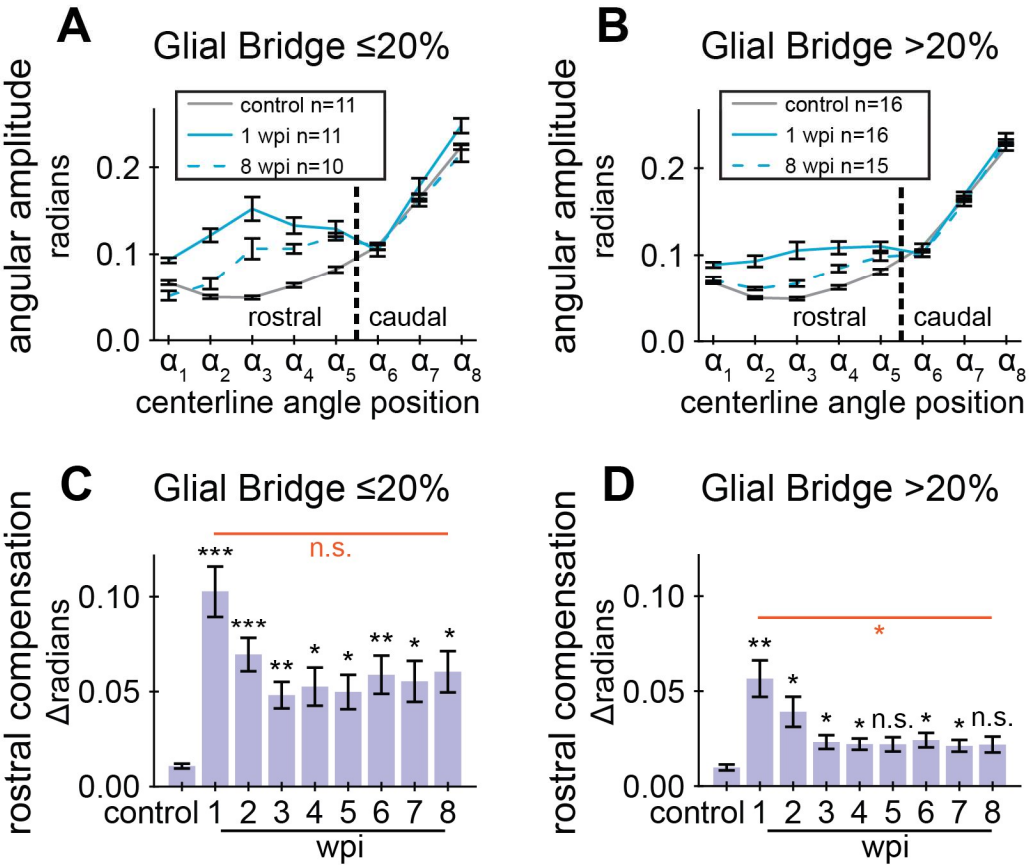

Figure 3.9: Characterizing rostral compensation exhibited by injured male fish.
We measured center-to-peak (half of peak-to-peak) curvature amplitude at all angle positions during cruise oscillations, then quantified the exaggerated rostral movement of injured fish. **(A)** Cruise curvature profiles for male fish that regenerated less than 20% of the glial tissue at the lesion site. Profiles are plotted for fish before injury, acutely injured fish at 1 wpi, and recovered fish at 8 wpi. Each cruise curvature profile represents the mean lateral angular amplitude along the dorsal centerline while cruising. The vertical dotted line separates rostral and caudal positions, demonstrating that acutely injured fish swim with markedly elevated curvature in the rostral portion of their body. **(B)** Cruise curvature profiles (control, 1wpi, and 8wpi) for male fish that regenerated more than 20% of the glial

tissue at the lesion site. **(C)** Quantification of rostral compensation in male fish that regenerated less than 20% of the glial tissue at the lesion site. This quantifies the displacement between cruise profiles: it is the maximum distance, on the vertical axis, between rostral positions of a cruise profile from the control profile. Angle positions α_1 to α_5 were used to define the rostral region (Figure 2.1). **(D)** Rostral compensation scores for male fish that regenerated more than 20% of the glial tissue at the lesion site. Panels A and C include 11, 5, 4, 5, 6, 7, 9, 9, 8 fish at control, 1, 2, 3, 4, 5, 6, 7, 8 wpi assays, respectively. Panels B and D include 16, 9, 9, 13, 11, 14, 12, 12, 13 fish at control, 1, 2, 3, 4, 5, 6, 7, 8 wpi assays, respectively. Error bars depict SEM and statistical significance was determined by Brown-Forsythe and Welch's ANOVA tests with Dunnett's T3 multiple comparisons tests. p-value markers in black represent comparisons between each time point post-injury relative to control measurements before injury. Red horizontal bars and p-values marked in red show significance between 1 wpi and 8 wpi. ***P<0.001; **P<0.01; *P<0.05; ns, P>0.05.

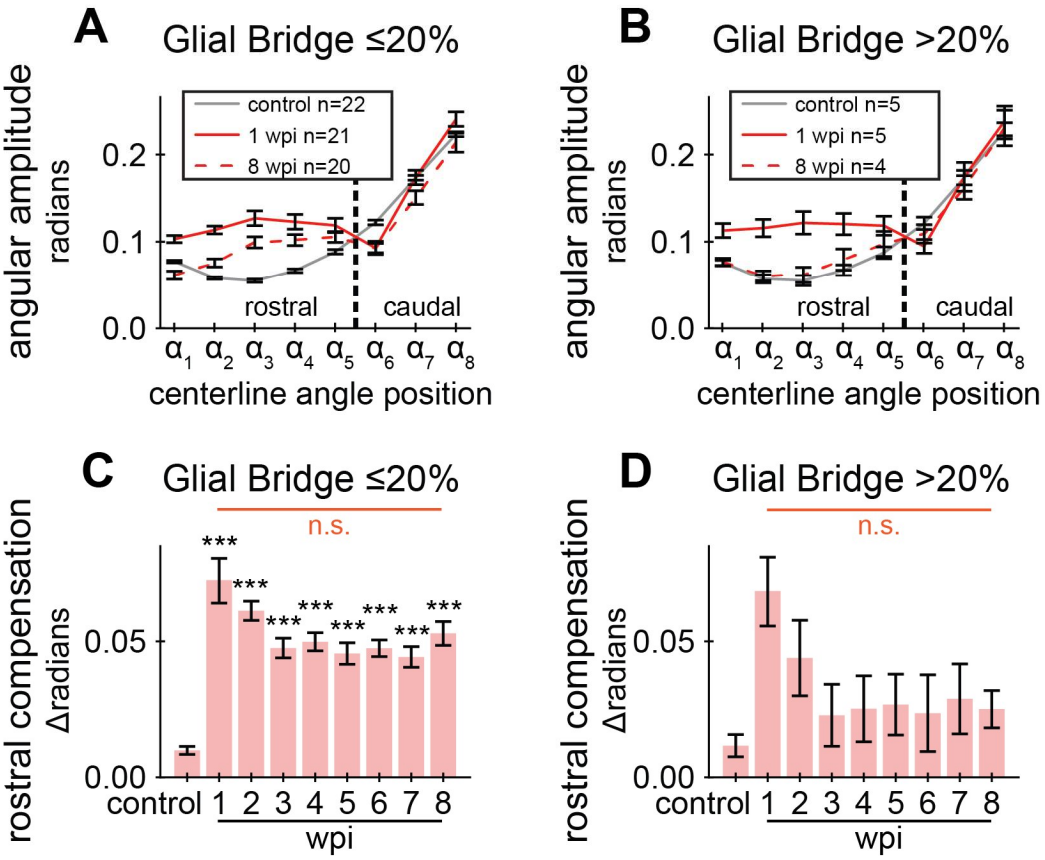

Figure 3.10: Characterizing rostral compensation exhibited by injured female fish.
We measured center-to-peak (half of peak-to-peak) curvature amplitude at all angle positions during cruise oscillations, then quantified the exaggerated rostral movement of injured fish. **(A)** Cruise curvature profiles for female fish that regenerated less than 20% of the glial tissue at the lesion site. Profiles are plotted for fish before injury, acutely injured fish at 1 wpi, and recovered fish at 8 wpi. Each cruise curvature profile represents the mean lateral angular amplitude along the dorsal centerline while cruising. The vertical dotted line separates rostral and caudal positions, demonstrating that acutely injured fish swim with markedly elevated curvature in the rostral portion of their body. **(B)** Cruise curvature profiles (control, 1wpi, and 8wpi) for female fish that regenerated more than 20% of the glial tissue at the lesion site. **(C)** Quantification of rostral compensation in female fish that regenerated less than 20% of the glial tissue at the lesion site. This quantifies the displacement between cruise profiles: it is the maximum distance, on the vertical axis, between rostral positions of a cruise profile from the control profile. Angle positions α1 to α5 were used to define the rostral region (Figure 2.1). **(D)** Rostral compensation scores for female fish that regenerated more than 20% of the glial tissue at the lesion site. Panels A and C include 22, 22, 21, 20, 20, 20, 20, 19, 20 fish at control, 1, 2, 3, 4, 5, 6, 7, 8 wpi assays, respectively. Panels B and D include 5, 5, 5, 4, 4, 5, 4, 4, 4 fish at

control, 1, 2, 3, 4, 5, 6, 7, 8 wpi assays, respectively. Error bars depict SEM and statistical significance was determined by Brown-Forsythe and Welch's ANOVA tests with Dunnett's T3 multiple comparisons tests. p-value markers in black represent comparisons between each time point post-injury relative to control measurements before injury. Red horizontal bars and p-values marked in red show significance between 1 wpi and 8 wpi. ***P<0.001; **P<0.01; *P<0.05; ns, P>0.05.

Using cruise episodes annotated by the machine learning classifier, we measured body curvature amplitudes and frequencies at each measured angle position. The curvature at each angle position was calculated using the corresponding keypoint position and two adjacent keypoint positions (Figure 2.1). We measured center-to-peak (half of peak-to-peak) curvature amplitude at all angle positions during cruise oscillations. Cruise amplitudes along the centerline were plotted for control, 1 and 8 wpi (Figure 3.9A-B, Figure 3.10A-B). At 1 wpi, we observed a significant change in angular amplitude at angle positions 1 to 5 compared to uninjured controls. Cruise amplitudes appeared closer to control values at 8 wpi. These findings indicate that acutely injured fish compensate for paralysis using the rostral portion of their body and that compensation is less pronounced after cellular regeneration.

Hypothesizing that fish swim more naturally if they regenerated well, we separately plotted cruise amplitudes for fish that regenerated at least 20% of their glial tissue at the lesion core (Figure 3.9B, Figure 3.10B). Well-regenerated fish appeared to swim using amplitudes closer to control values. These results were also observed for female fish, although fewer female fish, 5 females versus 16 males, recovered more than 20% of their glial tissue at the lesion. We quantified maximal rostral compensation and noted that this swim gait feature recovers toward control levels (Figure 3.9C-D, Figure 3.10C-D). Fish with more regenerated SC tissue recovered healthier gait on average, indicated by lower rostral compensation at 8 wpi (Figure 3.9D, Figure 3.10D). Individual recoveries were more pronounced: 17 fish at 8 wpi exhibited rostral compensation lower than 3 standard deviations above the control mean, and these fish had high average cellular regeneration:

59% glial bridging, 57% proximal axon regrowth, and 34% distal axon regrowth. All fish with compensation scores lower than 0.025 (2.49 standard deviations from the control mean) regenerated at least 20% at the glial bridge. These results indicate that rostral compensation is most pronounced during earlier stages of SC regeneration and that stronger cellular regeneration is associated with higher physiological swim quality.

Cruise Body Frequency

In addition to angular amplitude, we also measured cruise frequency, defined as the number of complete oscillations at each angle position per second. Regardless of injury, the rate of movement during cruises was nearly uniform along the fish's body (Figure 3.11A). Like amplitude, average body cruise frequency was also disrupted by injury and improved over time (Figure 3.11B). Although functional abilities appeared different between the sexes according to established functional metrics, there was no evidence that rostral compensation differs between males and females at 1 wpi (Student's t-test p-value = 0.6), suggesting that SC transection affects the gait of both sexes equally and independently of swim capacity differences.

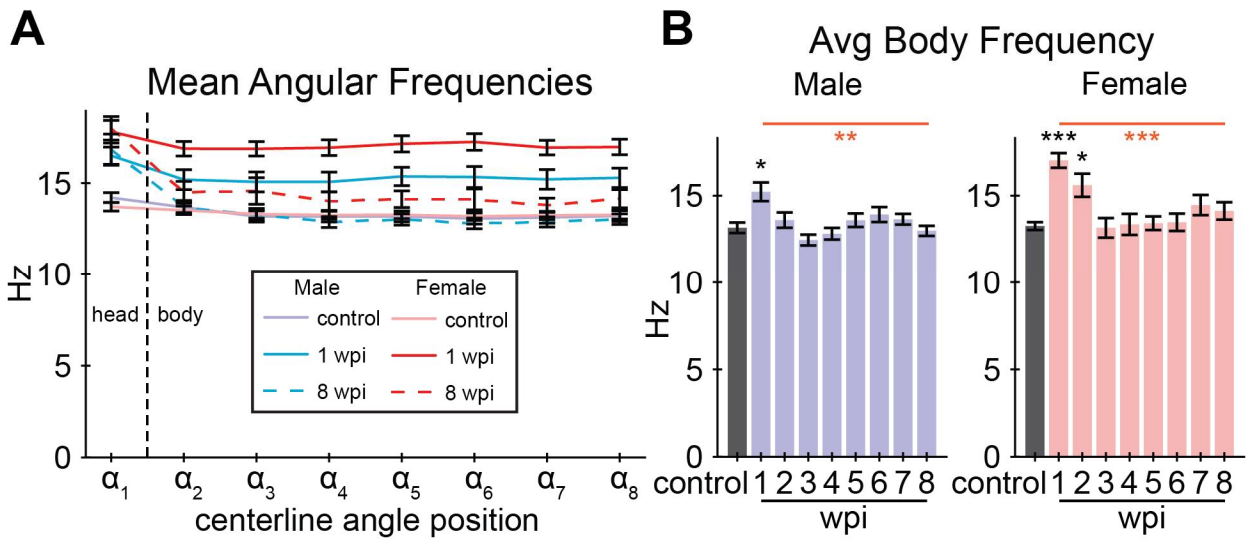

Figure 3.11: Body oscillation frequency during cruise behavior.
We measured cruise angular frequency as the number of complete oscillations at each angle position per second. The body of the fish corresponds to angle positions α_2 to α_8. This figure includes 30, 30, 29, 28, 26, 27, 26, 26, 26 male fish and 30, 28, 26, 24, 24, 25, 24, 23, 24 female fish at control, 1, 2, 3, 4, 5, 6, 7, 8 wpi assays, respectively. **(A)** Mean

angle frequencies at each angle position on the centerline (x-axis) measured during cruise episodes, plotted for control, 1 wpi, and 8 wpi. Frequency was stable along the body of the centerline regardless of injury. **(B)** Average angular frequency along body positions for each assay and separated by sex. Error bars depict SEM and statistical significance was determined by Brown-Forsythe and Welch's ANOVA tests with Dunnett's T3 multiple comparisons tests. p-value markers in black represent comparisons between each time point post-injury relative to control measurements before injury. Red horizontal bars and p-values marked in red show significance between 1 wpi and 8 wpi. ***P<0.001; **P<0.01; *P<0.05; ns, P>0.05.

Tail beat frequency and swim efficiency

Cruising zebrafish produce thrust by ejecting vortices of water behind them (65). Strouhal number (St) is a unitless value related to vortex shedding mechanics and is defined as tail beat frequency times the peak-to-peak amplitude of the tail tip divided by the speed of forward motion. Cross-species research has concluded that St between 0.2 and 0.4 are most physiologically efficient (106). We calculated tail beat frequency for fish swimming in static water (0 cm/s flow velocity) and did not observe a significant change after injury (Figure 3.12A-B). Using displacement amplitude of the caudal fin, fin flick frequency, and swim speed during cruises, we calculated St for all cruises during the first five minutes (0 cm/s flow velocity) of the swim assay. Average St was within or near the efficiency limits throughout the experiment (Figure 3.12C-D).

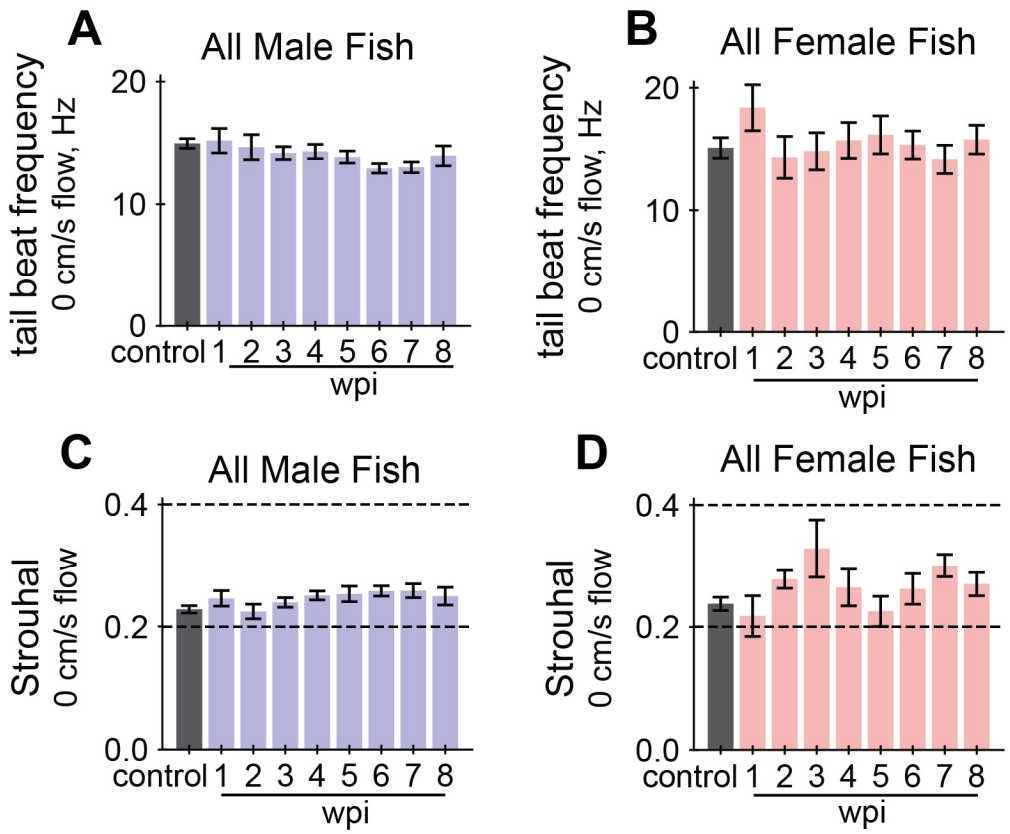

Figure 3.12: Measurements of swim efficiency in still water (0 cm/s).
Strouhal number is a unitless value related to vortex shedding mechanics and is defined as tail beat frequency times the peak-to-peak amplitude of the tail tip divided by the speed of forward motion. To avoid complications measuring the speed of forward motion against flowing water, Strouhal was calculated only for the first five minutes of video (0 cm/s flow velocity). **(A-B)** Tail beat frequency of male and female fish at each assayed week in still water. **(C-D)** Strouhal numbers of male and female fish at each assayed week in still water. ANOVA was not significant for A-D. Panels A and C include 30, 16, 14, 18, 17, 22, 21, 21, 21 male fish at control, 1, 2, 3, 4, 5, 6, 7, 8 wpi assays, respectively. Panels B and D include 20, 7, 7, 5, 10, 12, 11, 11, 14 female fish at control, 1, 2, 3, 4, 5, 6, 7, 8 wpi assays, respectively. Error bars depict SEM and statistical significance was determined by Brown-Forsythe and Welch's ANOVA tests with Dunnett's T3 multiple comparisons tests. ANOVA was not significant for these data.

However, we also measured tail beat frequency throughout full assays (0, 10, and 20 cm/s flow velocity) and did observe significant effects at 1 wpi, and this measurement recovered by 3 wpi for both male and female groups (Figure 3.13A-B). We did not measure cruise speed during 10 and 20 cm/s flow velocity periods, so we could not calculate Strouhal numbers for full assays.

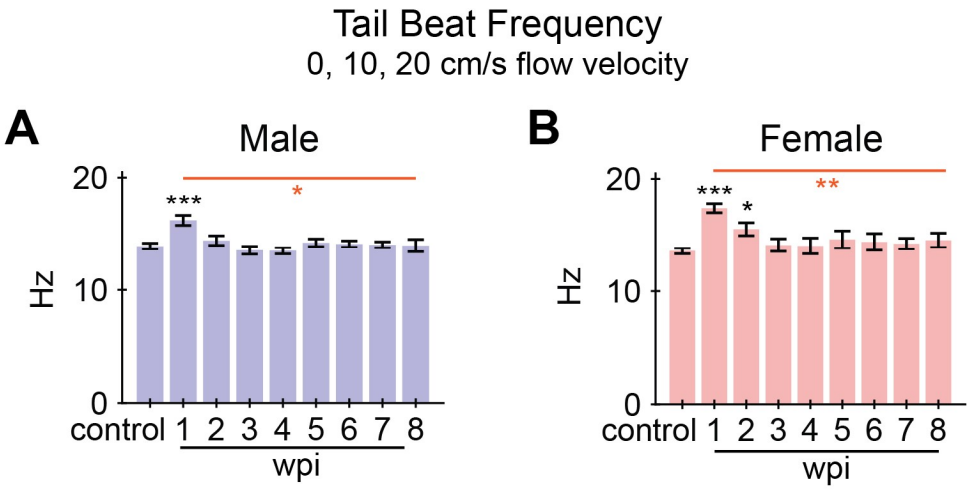

Figure 3.13: Tail beat frequency averaged over all flow speeds.
This figure includes 30, 30, 29, 28, 26, 27, 26, 26, 26 male fish and 30, 28, 26, 24, 24, 25, 24, 23, 24 female fish at control, 1, 2, 3, 4, 5, 6, 7, 8 wpi assays, respectively. **(A-B)** Mean tail beat frequency measured throughout each 15-minute swim assay including all three periods of flow velocity, plotted for each assay and separately for males (A) and females (B). Unlike tail beat frequency measured in the absence of flow (0 cm/s), when we measured tail beat frequency throughout the entire assay the measurement was significantly disrupted by injury, and its recovery plateaued by 3 wpi like other gait-related metrics described in the study. Error bars depict SEM and statistical significance was determined by Brown-Forsythe and Welch's ANOVA tests with Dunnett's T3 multiple comparisons tests. p-value markers in black represent comparisons between each time point post-injury relative to control measurements before injury. Red horizontal bars and p-values marked in red show significance between 1 wpi and 8 wpi. ***P<0.001; **P<0.01; *P<0.05; ns, P>0.05.

Given that we observed Strouhal measurements within a range that is associated with high efficiency and that the tail beat frequency associated with those Strouhal numbers was not significantly different from control after injury, these results suggest SCI does not preclude efficient swim thrust, likely due to compensatory movement in the rostral portion of the body during periods of active cruising.

3.3.2 Discussion

Rostral compensation

Our study introduces a rostral compensation score as a scalable quantification for gait quality. The calculation of rostral compensation was entirely automated after training a classifier to annotate cruise behaviors from centerline posture. It is a viable candidate to replace manually assigned

perceived quality scores as a premiere metric of swim quality, at least in the context of SC transection.

As a recovery metric in the tracking experiment, average rostral compensation scores showed nearly full recovery at 8 wpi for fish that regenerated at least 20% glial tissue at the lesion. Notable and significant changes in rostral compensation occurred by 3 wpi, suggesting a threshold of cellular regeneration may be required for healthy functional outcomes and that cellular regeneration beyond 3 wpi has a diminished effect on functional recovery. Although male and female fish regenerated SC tissue to different degrees (Figure 3.4D), and swim capacity in terms of distance and activity was measured lower for females than for males at all time points (Figure 3.2A-B, Figure 3.3A-B), we saw no evidence that the cruise gait of males and females were affected differently by SC transection, as measured by rostral compensation scores at 1 wpi (Student's t-test, p-value = 0.6). These results suggest both that all fish received a comparable injury, and that the rostral compensation score is less influenced by a fish's motivation to move, unlike classical swim capacity measurements. Overall, our findings show that rostral compensation is a neural health-associated measurement that recovers earlier than swim capacity.

Body and tail beat frequency

Tail beat frequency, as a coefficient in the Strouhal number, is related to swim efficiency. Interestingly, in calm water (0 cm/s) no significant difference in tail beat frequency was found between the control assay and assays after SC transection. These results support our hypothesis that extreme rostral movement after injury is a compensatory behavior. Tail beat frequency averaged over full assays, including periods of water flow, was significantly affected by injury (Figure 3:13A-B). However, because we calculated locomotor speed in terms of pixel change without correcting for flow velocity, we could not calculate Strouhal numbers for full assays to

test the compensation hypothesis in the presence of flow. Cruise body frequency and tail beat frequency averaged across all three periods of flow speed were strongly correlated (Spearman r_s = 0.92). Given this tight relationship, we felt that using both measurements in the downstream metric-to-metric comparative analysis would be redundant. Therefore, we chose tail beat frequency instead of body frequency for later comparisons.

3.4 Metric Correlations at 8 wpi

3.4.1 Results

Selected functional measurements correlate with cellular repair at 8 weeks post-injury

We next explored relationships between the full array of functional and cellular regeneration metrics at 8 wpi. We measured Spearman correlations between all 8 wpi measurements, pairwise, then performed hierarchical clustering on the correlation matrix (Figure 3.14A). For the sake of meaningful clustering, values for each measured attribute were multiplied by -1 if that measurement's average was increased at 1 wpi compared to controls (these measurements were scoliosis, posture novelty, rostral compensation, and tail beat frequency). While not all measurements correlated well with cellular regeneration metrics, some did, including quantifications of capacity, behavior, and gait. Selected measurements of these classes were plotted against glial bridging: swim distance, a swim capacity measurement (Figure 3.14B); burst frequency quantified using active posture, a behavior measurement (Figure 3.14C); and rostral compensation, a gait quality measurement (Figure 3.14D). Percent glial bridging correlated strongly ($r_s > 0.6$) with both proximal and distal axon regrowth (Figure 3.14E). Assays could only be included in the pairwise correlative analysis if the fish exhibited every measurable attribute, and because two fish did not cruise in the 8 wpi swim assay, their data was omitted from the heatmap in Figure 3.14A. There were also three male and three female fish that did not survive to

the end of the experiment. Hence correlations differ slightly between Figure 3.14A and Figure 3.14B-E.

Comparing pairwise correlations at 8 wpi, swim capacity and behavior measurements generally correlated strongly with one another and resided in a swim capacity-associated cluster that we labeled Cluster 2 (Figure 3.14A). Such measurements include distance, activity, pose burst frequency, and time swimming against the flow. Mean y correlated moderately with time swimming against the flow, but weakly with the other swim capacity measurements. Most, but not all, capacity measurements were at least moderately ($r_s > 0.3$) correlated with glial bridging and axon regrowth. At 8 wpi, tail beat frequency, which did not change significantly after injury or through recovery when measured in calm water (Figure 3.12A-B) and recovered by 3 wpi when measured in full assays including water flow (Figure 3.13A-B), did not correlate well with any other functional, structural, or cellular measurement. A separate cellular regeneration-associated cluster, labeled Cluster 1, contained all cellular regeneration measurements, rostral compensation, perceived swim quality, scoliosis, and posture novelty. Unlike the swim capacity-associated cluster, all metrics in Cluster 1 were at least moderately and positively correlated with each other. Of all functional metrics, rostral compensation correlated most strongly with perceived quality and percent glial bridging, and with axon regrowth to the same extent as posture novelty. Together, this analysis showed that not all the swim capacity metrics we measured were representative of the SC's condition at 8 wpi, and that rostral compensation is a neurologically associated measurement of gait quality.

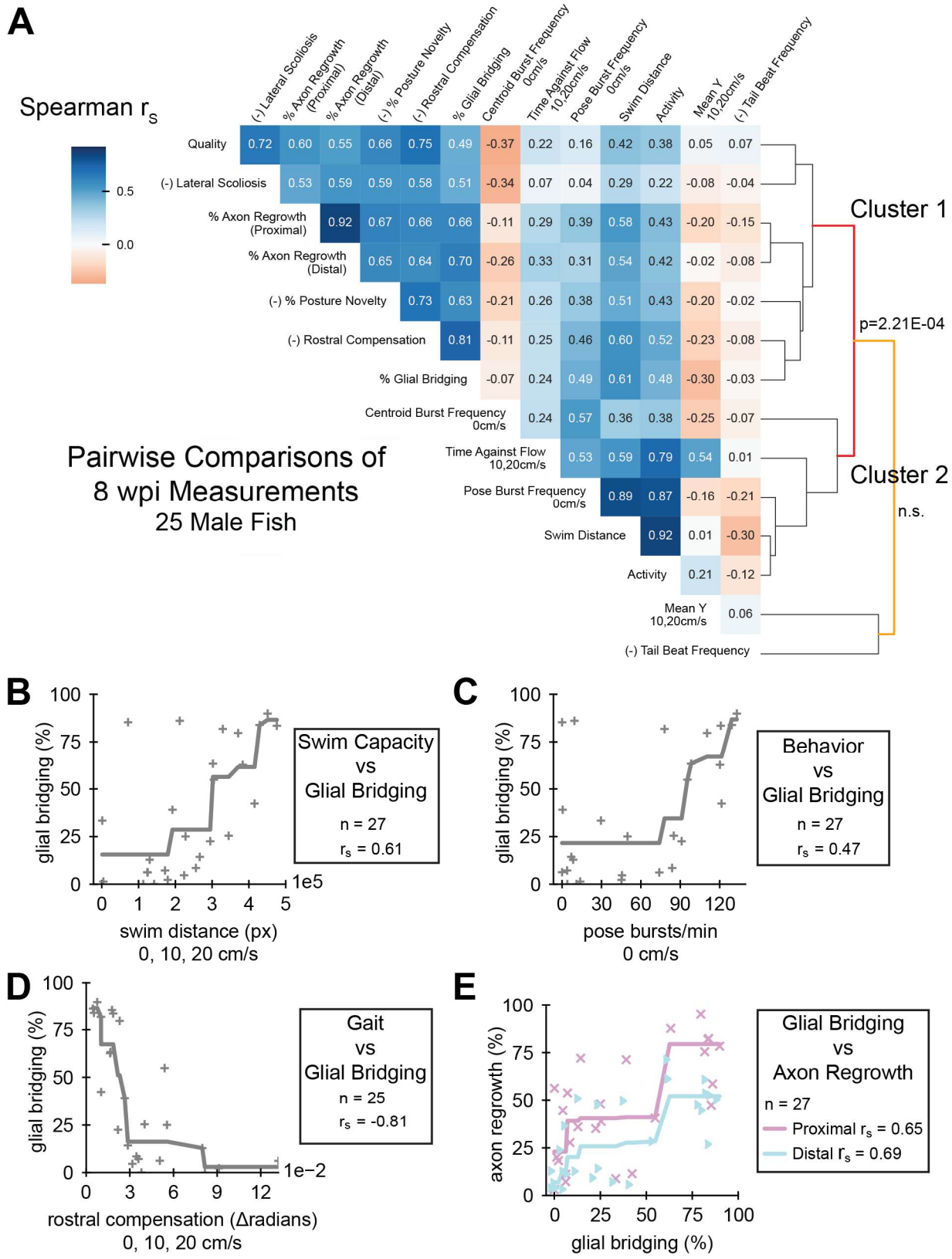

Figure 3.14: Pairwise comparisons of spinal cord regeneration metrics at 8 wpi (male fish in the tracking experiment).

(A) Heatmap of Spearman's rank correlations (r_s) between cellular and functional measurements. Regeneration metrics include swim capacity, swim quality, structural, and neurological measurements. A dendrogram representing similarities between correlation patterns of measurements is shown. Twenty-five male fish at 8 wpi were analyzed. Five fish that could not be measured in all attributes due to lack of activity (2) or death (3) were omitted. Correlations are reported regardless of p-value. For the sake of meaningful clustering, a measured attribute was multiplied by -1 if its average was increased at 1 wpi compared to controls. These attributes are marked with the prefix "(-)" on the label. (n=25) **(B-D)** One metric each of swim capacity (swim distance), behavior (burst frequency), and gait (rostral compensation) were plotted against glial bridging to demonstrate their correlation. Because the Spearman correlation operates on ranked values, we fit monotonic splines to plots where r_s were significant ($p < 0.05$) to visualize possible associations. (Panels B-C: n=27; panel D: n=25) **(E)** Scatter plot showing a strong association between the size of regenerated glial tissue and axon regrowth, proximal and distal. (n=27)

As previously described, female fish in this experiment regenerated more poorly than male fish. Nonetheless, a similar clustering of 8 wpi measurements from female fish yielded similar correlation patterns and clusters (Figure 3.15A). Spearman rank correlation of swim distance, pose burst frequency, rostral compensation, and axon regrowth with glial bridging did not reach statistical significance for female fish (Figure 3.15B-E).

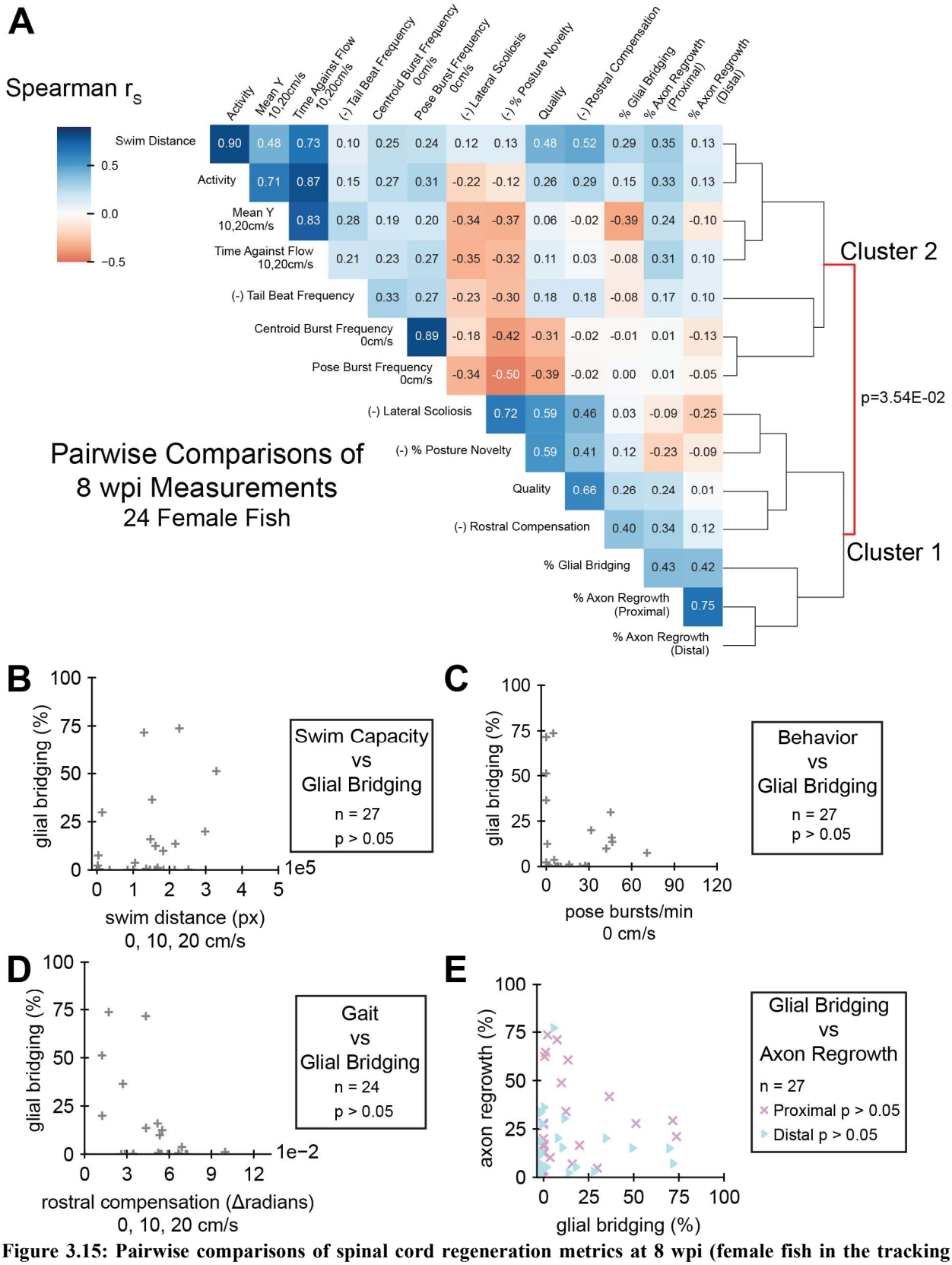

Figure 3.15: Pairwise comparisons of spinal cord regeneration metrics at 8 wpi (female fish in the tracking experiment).

(A) Heatmap of Spearman's rank correlations (r_s) between cellular and functional measurements. Regeneration metrics include swim capacity, swim quality, structural, and neurological measurements. A dendrogram representing similarities between correlation patterns of measurements is shown. Twenty-four female fish at 8 wpi were analyzed. Six fish that could not be measured in all attributes due to lack of activity (3) or death (3) were omitted. Correlations are reported regardless of p-value. For the sake of meaningful clustering, a measured attribute was multiplied by -1 if its average was increased at 1 wpi compared to controls. These attributes are marked with the prefix "(-)" on the label. (n=24) **(B-D)** One metric each of swim capacity (swim distance), behavior (burst frequency), and gait (rostral compensation) were plotted against glial bridging to demonstrate their relationship, though the correlation p-values were not significant. (Panels B-C: n=27; panel D: n=24) **(E)** Scatter plot showing a non-significant association between the size of regenerated glial tissue and axon regrowth, proximal and distal. The size of regenerated glial tissue plotted against proximal and distal axon regrowth. r_s were not significant for Panels B-E, likely because most female fish in this experiment exhibited compromised glial regeneration. (n=27)

3.4.2 Discussion

This experiment allowed us to perform comprehensive correlative analyses of recovery metrics over a wide range of regeneration parameters. We found that glial and axon bridging were highly correlated and that all three measurements of cellular regeneration showed similar correlation patterns with examined functional and structural metrics. Rostral compensation correlated more highly with glial bridging than any other measurement at 8 wpi. The strong correlations we observed between rostral compensation and cellular regeneration measurements support a model in which unusually high rostral movement is a manifestation of compensatory effort that paralyzed fish make to produce sufficient thrust to move. In terms of efficiency, tail beat frequency did not correlate with cellular regeneration measurements. Given that tail beat frequency and Strouhal number in 0cm/s flow were not affected significantly by injury (Figure 3.12A-D), whether fish optimize their efficiency neurologically through learning to adjust the required amount of rostral compensation (Figure 3.9D, Figure 3.10D) or whether the optimal parameters are physiologically enforced by the natural elasticity of a fish's body (107) remains to be explored.

As previously discussed, pose burst frequency is a more appropriate measurement for adult zebrafish than centroid burst frequency. Although centroid and pose burst frequency measurements were highly correlated for all assays collectively, at 8 wpi these values were only

moderately correlated with each other and did not share the same metric-to-metric correlation patterns when the data were separated by sex (Figure 3.14A, Figure 3.15A). The way these two measurements correlate with others provides evidence that pose burst frequency is a more appropriate metric for recovery than centroid burst frequency. Using glial bridging as proxy for neurological regeneration, other functional measurements such as swim distance and rostral compensation were more representative of overall health than either variety of burst frequency.

3.5 Functional Metrics Outside Spinal Cord Transection Contexts

3.5.1 Introduction

Besides spinal cord injury and repair, zebrafish are used to model other movement-associated phenotypes, for example, muscle development (108), epilepsy (109), and balance (110). Functional assessment can sometimes be tailored to a specific context by choosing an observable phenotype to quantify, as we did when developing the rostral compensation score for spinal cord transection. If a previously established functional measurement is sufficient to measure phenotype, however, then research may proceed more rapidly. We chose to apply classical swim capacity and gait and posture to two different experiments to explore whether these measurements could extend well into other, supplemental contexts besides spinal cord transection.

The first supplemental context involves fish bearing a mutation in the *mstnb* gene, $mstnb^{bns5}$(111). These fish were acquired by the lab for a recent lab publication (19). The zebrafish *mstnb* gene is homologous to human and mouse Myostatin, which negatively regulates skeletal muscle growth (112). Like other animals, $mstnb^{-/-}$ fish appear hypermuscular (111). One may hypothesize that a muscular phenotype would correspond with functional differences. Interestingly, time-to-exhaustion swim endurance has not been shown to significantly differ between $mstnb^{-/-}$, $mstnb^{+/-}$,

and wild types (19). Whether *mstnb* loss of function has any effect on swim gait, posture, or other aspects of swim capacity has not been described.

The second supplemental context involves fish with ablated neurons. These fish bear a transgene, *huc*:mCherry-NTR, which produces a Nitroreductase (NTR) enzyme driven by a neuron-specific promoter, HuC (113). NTR converts the drug Metronidazole (MTZ) into cytotoxins, which induces cell death (114). Thus, neurons are selectively ablated by treating the fish with a drug. If a large dose of MTZ is given to the transgenic animals, too many neurons are ablated, and the animal dies. A small dose, however, will ablate only the most susceptible neurons and the animal survives. Lili Zhou, a staff scientist in the Mokalled Lab, performed the work to titrate a non-lethal MTZ dosage and treat the fish in the experiment described below. As an unpublished transgenic line, we did not know which neurons would be most susceptible to MTZ treatment, nor which functional phenotype to expect.

3.5.2 Results

Swim function of *mstnb* mutants

Swim behavior assays were recorded for ten *mstnb* fish (n=10) and twelve wild types (n=12) according to the same 15-minute swim protocol that we used in the spinal cord repair tracking experiment. We plotted cruise amplitude and frequency profiles for both groups ("control" and "*mstnb*$^{-/-}$") compared to uninjured control assays ("EKAB") from the tracking experiment (Figure 3.16A-B). Both experimental groups appeared to cruise with similar amplitude and frequency, with some possible difference in amplitude near the tip of the tail. We measured many of the same functional attributes as we did in the tracking experiment (Figure 3.16C-M). Instead of calculating rostral compensation we calculated summed caudal amplitude because the amplitude trace looked slightly lower for *mstnb* fish, and we hypothesized that the bulkier bodies were less flexible, and

the caudal part of the fish would bend less during cruises (Figure 3.16C). However, we did not observe significant differences between mutant or wild types in terms of any of these measured attributes. These results are inconclusive for assigning swim capacity, gait, and posture phenotypes to *mstnb* fish.

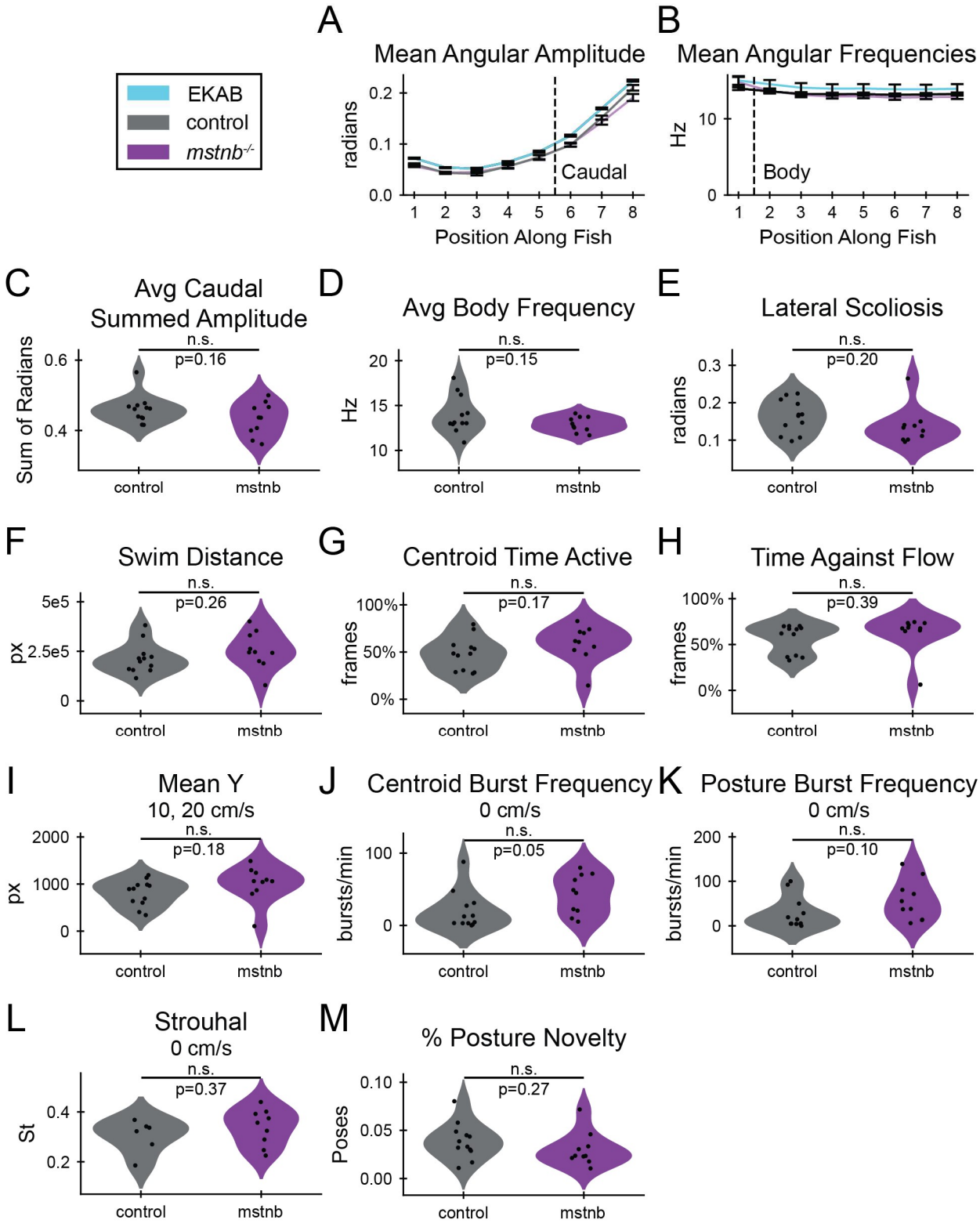

Figure 3.16: Uninjured *mstnb*$^{-/-}$ fish are not easily characterized by our functional metrics of spinal cord injury. Swim ability of ten mstnb fish (n=10) and twelve wild type siblings (n=12) were compared. **(A-B)** Cruise gait waveform features amplitude and frequency measured along the dorsal centerline. Three groups were plotted: *mstnb* fish, wild type siblings, and uninjured control measurements from the tracking experiment. **(C-M)** Various functional

measurements from the SCI tracking experiment but applied to *mstnb* fish and their wild type siblings. Significance between groups was tested using Student's t-test.

Swim function of fish with ablated neurons

huc:mCherry-NTR transgenic (R+) fish were treated with a non-lethal dose of MTZ to ablate neurons. Three controls were also assayed for comparison: untreated R+ fish and treated/untreated non-transgenic (R-) fish. By visual assessment we knew the R+ fish were affected by the treatment because they exhibited impaired balance after MTZ treatment: treated R+ fish would occasionally roll sideways and then swim briefly to correct their orientation. Eight fish (n=8) from each control group were assayed. Twelve fish (n=12) were included in the treated transgenic group in case some did not survive the treatment, yet all treated fish did survive. Fish were recorded in the same 15-minute behavior assay as used in the spinal cord repair tracking experiment with one difference: instead of swimming two fish at a time separated by a divider, fish swam in groups of four without dividers and we modified our video preprocessing code to split each video into sub-videos each cropped to a single fish. Significant differences were observed between R+ fish before and after treatment in terms of swim distance (decreased), scoliosis (decreased), time against flow (increased), and centroid burst frequency (increased). For swim distance, scoliosis, and centroid burst frequency, at least one control group also significantly changed in the same direction between treatments. The treated R+ fish were only different from all control groups in time swimming against the flow. These results suggest that the metrics we chose for spinal cord regeneration studies do not generalize well to this type of neurological phenotype.

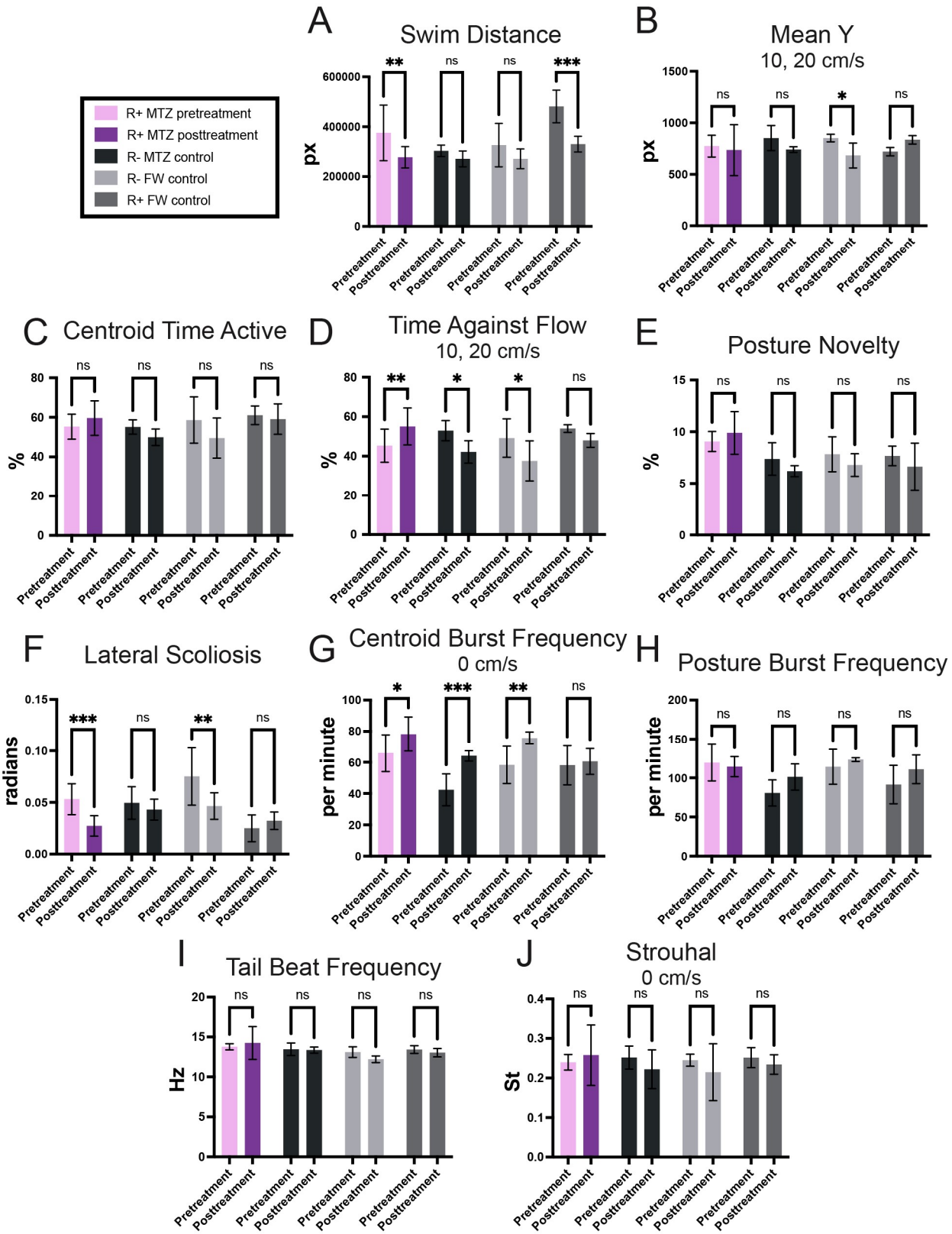

Figure 3.17: Fish with ablated neurons are not easily characterized by our functional metrics of spinal cord injury.

(A-J) Various functional measurements from the SCI tracking experiment but applied to a neuron ablation experiment. This experiment included fish of two genotypes: R+ (transgenic) and R- (wild type control). For each genotype, there were two treatment subgroups: MTZ (Metronidazole treated) and FW (fish water control). In combination, this produced three controls and one experimental group: R- FW (untreated WT control, n=8), R- MTZ (treated WT control, n=8), R+ FW (untreated transgenic control, n=8), R+ MTZ (treated transgenic, n=12). The experimental group, R+ MTZ, was colored purple. Error bars depict SEM and statistical significance was determined by Brown-Forsythe and Welch's ANOVA tests with Dunnett's T3 multiple comparisons tests. p-value markers represent comparisons between pre- and post-treatment means for each group. ***P<0.001; **P<0.01; *P<0.05; ns, P>0.05.

3.5.3 Discussion

Although these functional measurements significantly captured differences between control and injured fish in the tracking experiment, they did not clearly distinguish fish with ablated neurons or *mstnb*$^{-/-}$ fish from their controls. The main caveat of these results is that groups contained at most 12 fish, so detecting more subtle effects was not possible due to low statistical power. While we believed that effect size would have been larger given the experimental conditions, we found more modest phenotypes. Therefore, we can only offer preliminary interpretations of trends. In the case of *mstnb*$^{-/-}$ fish, power analysis power analysis recommended at least 10 fish per group to detect significance in terms of scoliosis, cruise body frequency, and cruise summed caudal amplitude. Although we did have ten fish in each group, p-values were still above the 0.05 significance threshold. With a larger sample, we expect that *mstnb*$^{-/-}$ fish would measure lower scoliosis if higher body muscle mass reinforces symmetry, lower body frequency if bulkier bodies take more effort to move, and lower summed caudal amplitude if their bodies are less flexible.

Regarding the neuron ablation experiment, the primary phenotype of MTZ-treated *huc*:mCherry-NTR fish was occasional loss of balance while resting, which none of the functional measurements could capture. Before the experiment, we could not predict what the phenotype would be because we did not know which neurons would be ablated. Similarly, as not all fish neural networks have been mapped to functional pathways, linking neural ablation to phenotype *a priori* was not feasible. One significant difference after treatment was in terms of body curvature. While scoliosis

was measured significantly lower after treatment for some groups in the *huc*:mCherry-NTR experiment, this is likely a calculation quirk, not a true change in body curvature. We calculated scoliosis by averaging body curvature over episodes of rest, weighted by the rest's duration. It can be difficult to determine when one behavior ends and another begins, so the beginning and end of behavior episodes are classified with the least confidence. It follows that shorter rest episodes contain proportionally more low-confidence poses. Therefore, fish that rest for shorter periods may have artificially higher scoliosis scores because there are proportionally more active, curvy poses accidentally included in the calculation. This happened in the tracking experiment, where scoliosis was also measured significantly higher before injury when they were more active than at 1 wpi when they were more lethargic. In terms of function more generally, our results suggest that the neurons most susceptible to MTZ treatment are less likely to be involved in swim capacity or gait quality measured by the dorsal centerline. However, this experiment also had low n-numbers and was thus underpowered to detect subtle phenotypes. Follow-up experiments were not pursued because these experiments were only supplemental to the aims of this dissertation.

Chapter 4: Recovery Trajectories

4.1 The Complexity of Posture Space

4.1.1 Results

Our first approach to probe recovery trends beyond individual recovery metrics was to examine posture variation in healthy and injured animals, regardless of behavior, at different timepoints. To this end, we used PCA to decompose all poses where the fish was not near a wall. PCA was performed for all fish and all assays (Figure 4.1A), separately for males (Figure 4.1B) and females (Figure 4.1C), and at control and recovery endpoints 1 and 8 wpi per sex group (Figure 4.1D-E). In this analysis, each PC corresponds to a dorsal centerline pose, which is called an "eigenfish" when plotted. Exploring the principal components of control poses, three components were required to explain as much as 98% of the variance in both groups, with the third component contributing minimally. Four components were required to capture 98% of the variance in a PCA of poses from 1 wpi assays. At the end of 8 weeks in recovery, as many as five components were required to capture 98% of the variance. Likewise, scree and eigenfish plots show that the third and fourth components consume more variance at 1 wpi than control, and more at 8 wpi than 1 wpi (Figure 4.1D-E). Finally, we compared variance explained by each PC to a distribution of variances created by shuffling the data (115). We set a significance threshold of two standard deviations above the mean. This test indicated that one PC captured a significant amount of variance for a PCA poses from control fish, but two PCs captured significant amounts of variance for most PCAs that included poses from injured fish (Figure 4.1A-E). These results indicated that centerline posture increased in complexity after injury and throughout recovery.

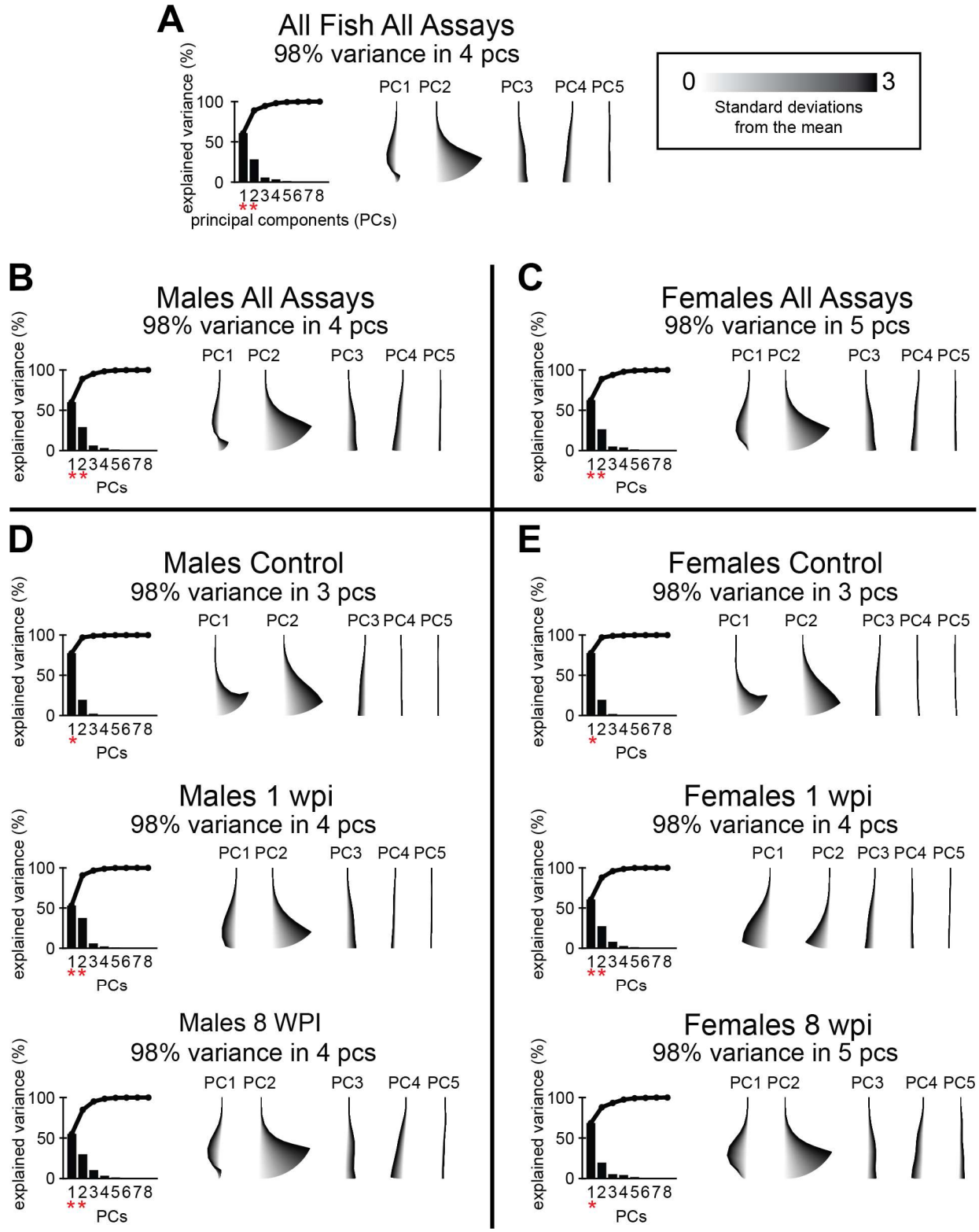

Figure 4.1: Principal component analysis of angle poses observed in the tracking experiment.
On the left side of each PCA is a scree plot showing the percentage of variance captured by each PC. PCs that captured significant amounts of variance are indicated by a red asterisk. On the right side of each PCA are the first five components plotted as "eigenfish" by adding multiples of each PC to the mean pose. **(A)** A general representation of

the posture space, and its complexity, for both healthy and injured fish. PCA of poses from all fish, all assays. **(B)** PCA of poses from all assays, male fish only. **(C)** PCA of poses from all assays, female fish only. **(D)** Posture space for male fish using poses taken from control, 1 wpi, and 8 wpi assays (top to bottom). **(E)** Posture space for female fish using poses taken from control, 1 wpi, and 8 wpi assays (top to bottom). Posture space is similarly complex whether separated by sex or taken altogether. At control, 1, 2, 3, 4, 5, 6, 7, 8 wpi assays, panel A includes 60, 58, 58, 58, 56, 56, 55, 54, 54 fish; panels B and D include 30, 30, 30, 30, 29, 29, 28, 27, 27 fish; and panels C and E include 30, 28, 28, 28, 27, 27, 27, 27, 27 fish, respectively.

4.1.2 Discussion

The observation of increased posture complexity over the course of recovery is easily explained. At 8 wpi, the fish manifested significant variation in terms of cellular regeneration (Figure 3.4A-C) and scoliosis (Figure 3.7A). These measurements had much lower variation before injury—where fish had intact SCs, no scoliosis, and swam in a characteristically healthy way—and at 1 wpi—where fish had recently transected SCs and mostly swam in a characteristically paralyzed way. Our model proposes that cellular regeneration enables functional recovery, the primary evidence being that variation in cellular and functional metrics correlate (Figure 3.14D). Therefore, with relatively high variation in SC connection and scoliosis at 8 wpi, fish are expected to display a greater variety of posture when poses from many fish are combined for a single PCA. A more interesting direction for future research would be to explore the posture complexity of individual fish at different points in recovery to characterize intra- and inter-variability. In other words, future research would determine whether the complexity we observed from many fish collectively comes from differences between individuals, each swimming with relatively low posture complexity in any given assay.

4.2 Cruise Exemplar Embedding

4.2.1 Results

Sonification suggests that a certain fish recovered healthy gait by 4 weeks post-injury

The field of astronomy has enjoyed public engagement and even a few discoveries by representing data through sound (116), so we took inspiration from such studies to create sonic representations

of specific cruises. One 40-frame cruise segment from each assay of two fish were chosen for sonification to demonstrate how gait changes during successful and unsuccessful regeneration. These fish were selected because they had rostral compensation scores between 0.07 and 0.1 at 1 wpi, but at 8 wpi they displayed divergent outcomes. At 8 wpi, one fish showed rostral compensation of 0.025 with 23% glial bridging, while the measured compensation of the other fish remained above 0.05 with no glial bridge (0.0005%). Each video included 40 frames of one cruise from each assay from left to right: control, 1 wpi, 2 wpi, …, 8 wpi. At the end of each video, the control assay's cruise was repeated for comparison. Please view the videos at the following URLs.

Fish that recovered well:

https://github.com/MokalledLab/SwimFunction/blob/main/example_figures/cruise_sonification_M8_well_recovered.mp4

Fish that recovered poorly:

https://github.com/MokalledLab/SwimFunction/blob/main/example_figures/cruise_sonification_F6_poorly_recovered.mp4

Sonification explicitly captured the following attributes of angle positions during cruises: the timing of curvature peaks (coded as rhythm), position on the centerline (coded as pitch), and amplitude (coded as intonation). The accompanying videos showed dots on the centerline when its associated tone played. The sounds produced from cruises of control fish were all in tune, as expected. Likewise, cruises at 1 wpi sounded unpleasantly out-of-tune. Finally at 8 wpi, the well-recovered fish sounded more in tune than the poorly recovered fish. The well-recovered fish begins to sound more in tune as early as 2 wpi, with noticeable intonation improvement in the 4 wpi sound

segment. These results demonstrate that sonification is a satisfactory supplement to our cruise waveform analysis and suggest that healthy-like gait can recover by 4 wpi.

Gait recovery plateaus around 3 weeks post-injury

Because our rostral compensation score is just one feature of complex locomotion, we next set out to comprehensively analyze cruise gate recovery by embedding cruise episodes into a latent space. To reduce the effects of body shape on gait, we omitted fish with a scoliosis score greater than 0.35 at 8 wpi. For computational efficiency, we performed embedding on representative cruise episodes, exemplars, sampled from each assay. To explore the data in posture space, we decomposed poses using PCA. Cruise traces in posture space manifested as ellipses, similar to previously described traces for larval zebrafish (57,58). We noted that 1 wpi cruise traces are both distinct from preinjury cruises and visually similar for different animals at the same time point (Figure 4.2A).

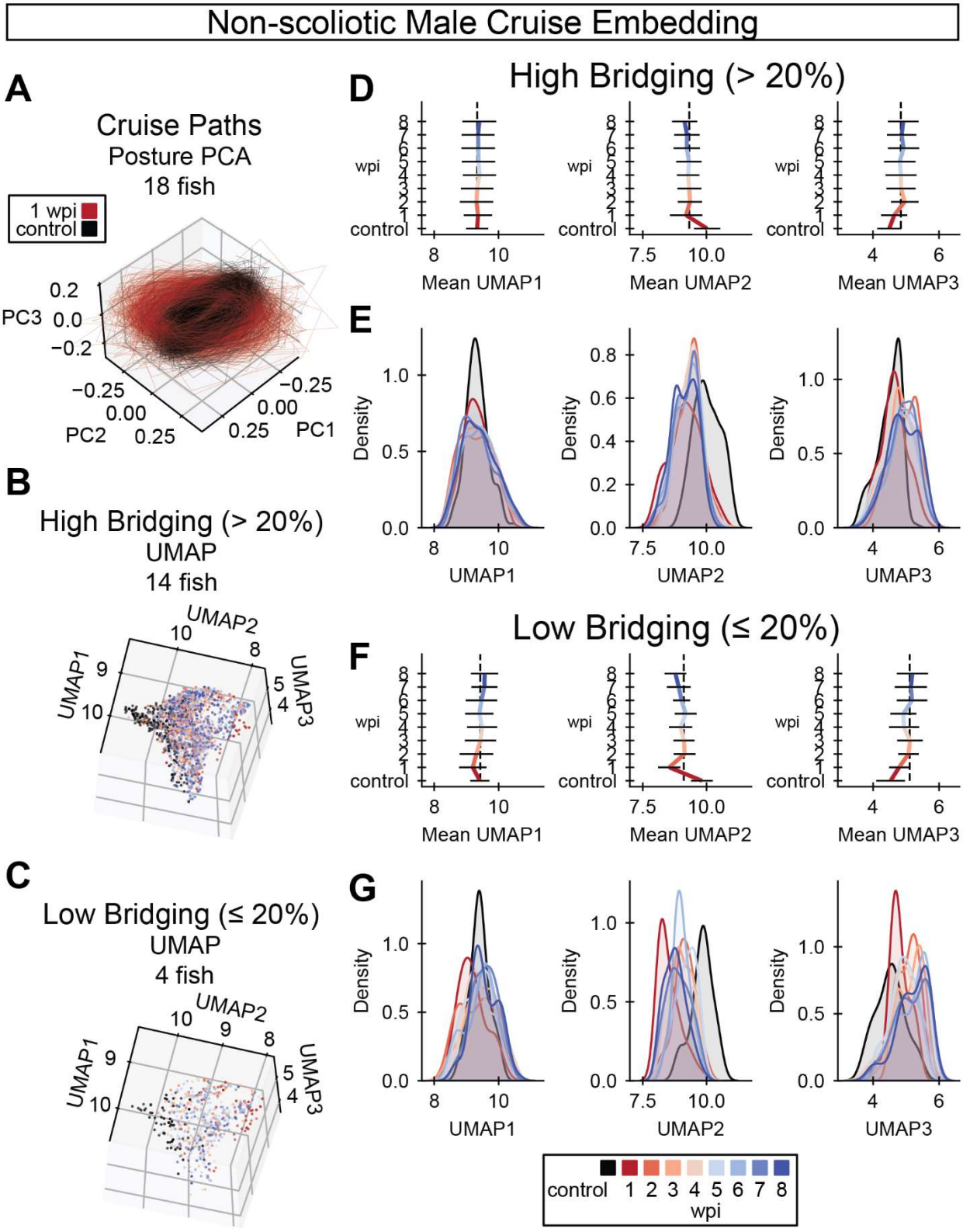

Figure 4.2: UMAP embedding of cruise behaviors for male fish with low scoliosis during SC regeneration.

(A) Cruise poses from control (black) and 1 wpi (red) male zebrafish were decomposed using PCA. Male fish with scoliosis score < 0.35 at 8 wpi are shown. In this posture space, cruise trajectories from acutely injured fish at 1 wpi are markedly distinct from control fish trajectories. (n=18 fish) **(B-C)** Cruise poses were embedded using UMAP with precomputed dynamic time warping (DTW) distances. Cruise poses were analyzed for fish that regenerated well (glial bridging > 20%) in B and for fish with compromised cellular regeneration (glial bridging < 20%) in C. (Panel B: n=14 fish, panel C: n=4 fish) **(D)** Gait recovery trendlines in UMAP 1, 2, and 3 (left to right) for fish that regenerated well. Colored bars indicate the mean trend of each UMAP component. Error bars represent standard deviations. The vertical dotted black lines align with the average UMAP value at 3 wpi to indicate that most change in each UMAP occurs before 3 wpi. (n=14 fish) **(E)** Gaussian kernel density estimates for the regions of UMAP space occupied by cruises at each week post-injury for fish that regenerated well. The x-axes are matched between Panels D and E for comparison. (n=14 fish) **(F)** Gait recovery trendlines in UMAP 1, 2, and 3 (left to right) for fish with compromised cellular regeneration. Colored bars indicate the mean trend of each UMAP component. Error bars represent standard deviations. The vertical dotted black lines align with the average UMAP value at 3 wpi to indicate that most change in each UMAP occurs before 3 wpi. (n=4 fish) **(G)** Gaussian kernel density estimates for the regions of UMAP space occupied by cruises at each week post-injury for fish with compromised cellular regeneration. The x-axes are matched between Panels F and G for comparison. (n=4 fish). We restricted data in panels B-G to only include fish that cruised in every assay; hence n-numbers were lower than 30.

Next, we embedded cruise traces using UMAP for three-dimensional visualization. We plotted embedded cruises from fish that regenerated at least 20% glial tissue at the lesion (Figure 4.2B) separately from cruises of fish with relatively poor cellular regeneration (Figure 4.2C). To interpret this embedding, average UMAP values at each time point for decomposed cruise episode exemplars were plotted for highly (Figure 4.2D) and poorly (Figure 4.2F) regenerating fish. For both fish groups, average UMAP values exhibited the most change by 3 wpi. Similarly, for both highly and poorly regenerating fish, reduction of rostral compensation slowed around 3 wpi (Figure 3.9C-D; Figure 3.10C-D) and tail beat frequency returned to normal by 3 wpi (Figure 3.13A-B). To further demonstrate that the embedded space of control cruises was different from all embeddings post-injury, we plotted kernel density estimates (KDE) for three UMAP dimensions at each time point, separated by cellular regeneration outcome (Figure 4.2E,G). Cruises for female fish were embedded in the same space and the results were visually similar (Figure 4.3A-G).

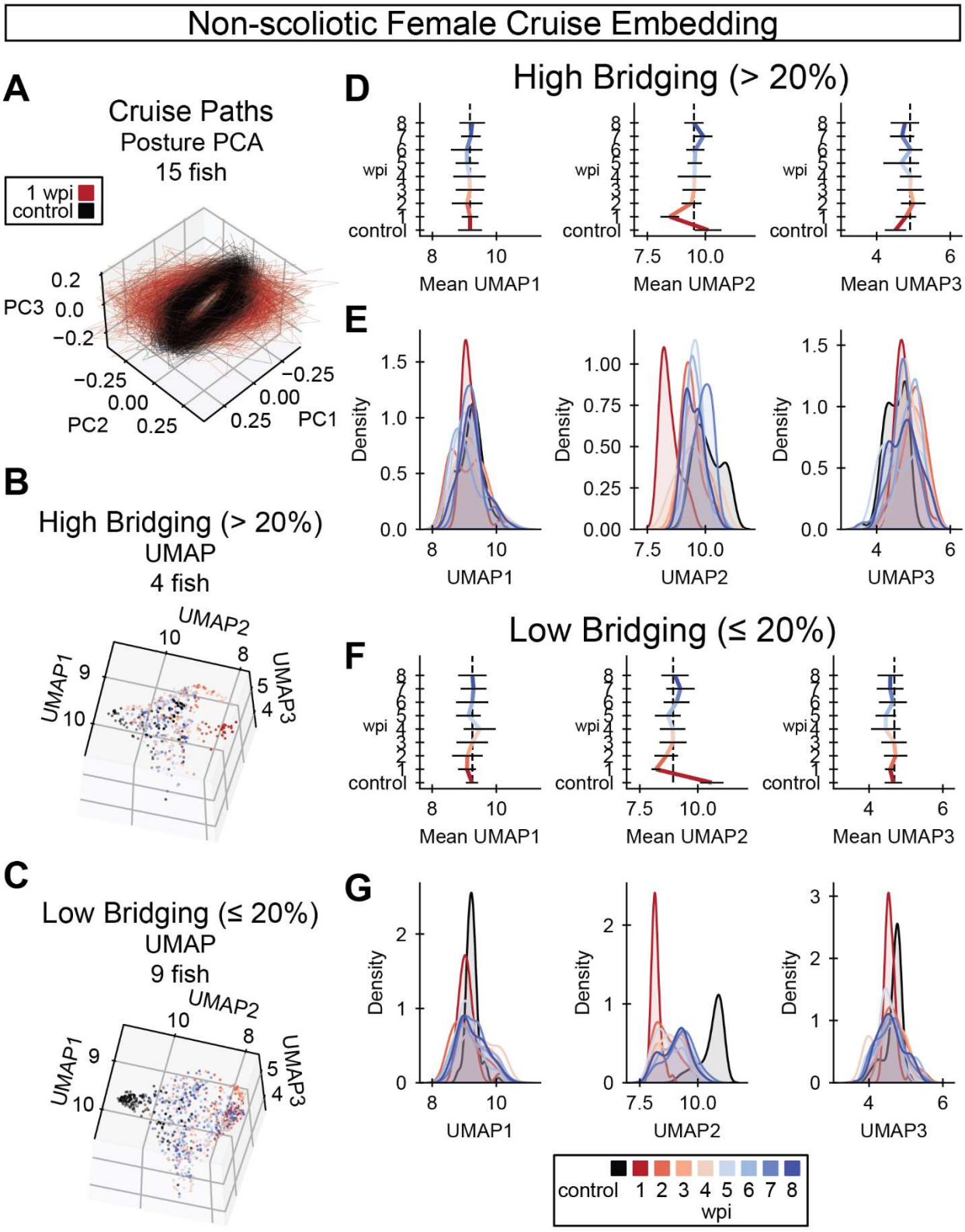

Figure 4.3: UMAP embedding of cruise behaviors for female fish with low scoliosis during SC regeneration.

(A) Cruise poses from control (black) and 1 wpi (red) male zebrafish were decomposed using PCA. Female fish with scoliosis score < 0.35 at 8 wpi are shown. In this posture space, cruise trajectories from acutely injured fish at 1 wpi are markedly distinct from control fish trajectories. (n=15 fish) **(B-C)** Cruise poses were embedded using UMAP with precomputed dynamic time warping (DTW) distances. Cruise poses were analyzed for fish that regenerated well (glial bridging > 20%) in B and for fish with compromised cellular regeneration (glial bridging < 20%) in C. (Panel B: n=4 fish, panel C: n=9 fish) **(D)** Gait recovery trendlines in UMAP 1, 2, and 3 (left to right) for fish that regenerated well. Colored bars indicate the mean trend of each UMAP component. Error bars represent standard deviations. The vertical dotted black lines align with the average UMAP value at 3 wpi to indicate that most change in each UMAP occurs before 3 wpi. (n=4 fish) **(E)** Gaussian kernel density estimates for the regions of UMAP space occupied by cruises at each week post-injury for fish that regenerated well. The x-axes are matched between Panels D and E for comparison. (n=4 fish) **(F)** Gait recovery trendlines in UMAP 1, 2, and 3 (left to right) for fish with compromised cellular regeneration. Colored bars indicate the mean trend of each UMAP component. Error bars represent standard deviations. The vertical dotted black lines align with the average UMAP value at 3 wpi to indicate that most change in each UMAP occurs before 3 wpi. (n=9 fish) **(G)** Gaussian kernel density estimates for the regions of UMAP space occupied by cruises at each week post-injury for fish with compromised cellular regeneration. The x-axes are matched between Panels F and G for comparison. (n=9 fish). We restricted data in panels B-G to only include fish that cruised in every assay; hence n-numbers were lower than 30.

Finally, to test whether the embedded space of control and 8 wpi cruises were significantly different for the four subgroups (male/female, high/low bridging), 2-UMAP KDE overlaps were calculated and compared against a distribution formed from 2-UMAP KDE overlaps with shuffled assay labels (Figure 4.4A-D). All observed overlaps were significantly lower than the shuffled distributions, indicating that 8 wpi cruises were significantly different from control cruises for both male and female fish, high and low bridging.

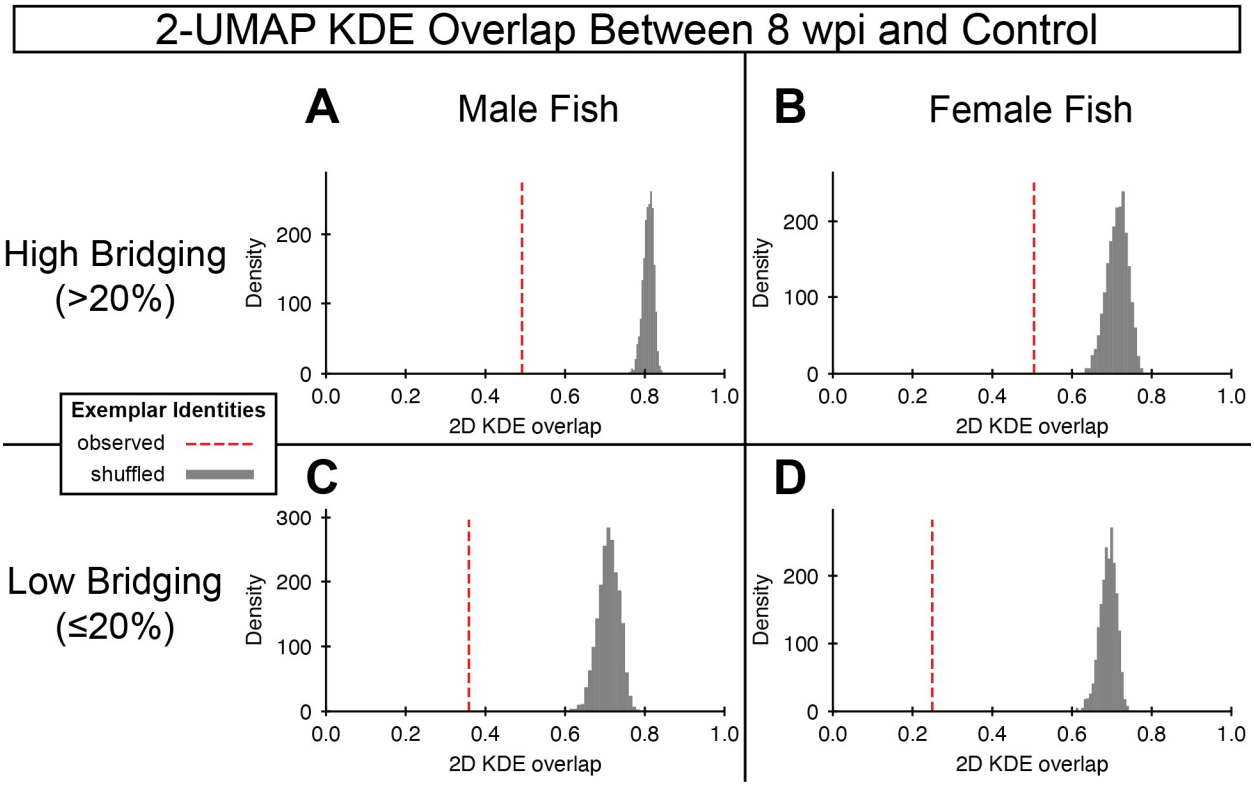

Figure 4.4: Control and 8 wpi cruises are significantly different in the first two UMAP components.
Dotted red lines show the overlapping space of 2-UMAP kernel density estimates (KDEs) for embedded control and 8 wpi cruises. Gray histograms show the distribution of overlapping space of KDEs for the same data with shuffled assay labels, shuffled 2000 times. Although these plots contain data from the embeddings in Figures 4.2 and 4.3, more fish were included in this analysis because fish were only required to have cruised in the control and 8 wpi assays. The final group n-numbers were as follows: (**A**) males with high bridging (n=16), (**B**) females with high bridging (n=5), (**C**) males with low bridging (n=11), (**D**) females with low bridging (n=22). In each grouping, the observed overlap was significantly low according to the corresponding null distribution, so for each group the embedded space of 8 wpi cruises was not identical to the embedded space of control cruises.

This temporal cruise embedding suggested that gait recovers to the greatest extent by 3 wpi and that injury-induced gait changes are incompletely resolved at 8 wpi.

4.2.2 Discussion

To achieve a more comprehensive analysis of cruise gait recovery beyond single gait features, such as rostral compensation, specific fish were explored using cruise sonification, and exemplar cruise episodes from all non-scoliotic fish were embedded with UMAP using dynamic time warping distances. These methods explored successful and unsuccessful gait recovery through visual and audible representations and computational dimension reduction using representative,

exemplar, cruises. For practical reasons, neither method was suited to analyze every annotated cruise. Both methods suggest that well recovered fish recover gait quickly, but that well-recovered gait is still somewhat different from uninjured gait.

In terms of intonation, cruises with the highest measured rostral compensation (1 wpi) sounded jarringly out of tune, and cruises that displayed lower rostral compensation sounded relatively in tune, almost like control cruises. We designed the audio mapping specifically to capture this affect. Unexpectedly, as we listened to the sonification videos, we noticed that note emission timing was irregular after injury, particularly for the poorly recovered fish. Instead of notes emitting in sequence from head to tail, as heard in the control portion of the videos, in some cruises all positions emitted a tone at nearly the same time. In another, the central positions emitted a tone at one time while the endpoints emitted a tone at another time. Uninjured fish gait consists of coordinated wave propagation along the dorsal centerline (57), and the audible rhythm suggested that the severely injured fish had less coordinated wave propagation. We discovered that this was an artifact of the first draft of our sonification method, not a biological result.

Deeper consideration of our methods indicated that this seemingly disrupted propagation of amplitude peaks was a computational anomaly. Whether the tone was emitted on the positive or negative curvature peak depended on which peak was first observed in the frame sequence. Because this decision was made for each position separately, some positions could be emitting on peaks and others on troughs, thus creating artificially irregular rhythm. After patching the code to restrict tone emission to the positive amplitude peak, rostral-to-caudal wave propagation was audibly restored for all cruise segments. The current version of the videos in the repository were generated using this corrected method. This experience taught us that sonification, as a method for data analysis, is subject to the same limitations as classical mathematical analysis despite its unique

advantages. Still, while wave propagation and excessive curvature can be visually perceived, sonification is uniquely suited to present swim gait anomalies to a general audience and to generate hypotheses.

Cruise embedding revealed that recovered gait was not necessarily identical to preinjury gait. Additionally, both healthy and unhealthy recovery trajectories were similar, considering the embedded distributions of both groups changed most dramatically between 1 and 3 wpi. This may reflect changes in tail beat frequency, which was observed to be the same for fish regardless of cellular regeneration (Figure 3.13A-B). Surprisingly, even after selecting for fish that showed elevated regeneration metrics, 8 wpi cruises showed a clearly distinct embedded distribution compared to control cruises before injury. These findings suggest that some injury-induced gait feature persists after an apparently successful recovery. When an abnormal swim gait develops during recovery, it could be due to mistaken axon connections or suboptimal tissue remodeling. Specific SC neurons and regions are known to be associated with aspects of zebrafish locomotion (117,118). After SC transection, as axons reconnect, fast and slow V2a interneurons regrow axons along the rostro-caudal axis, connecting to neurons of the same type and enabling specific features of functional recovery (11). In addition to axon regrowth, it is estimated that as much as one third of SC tissue shows evidence of cell division during SC regeneration (119). Moreover, recent mammalian studies indicate that the neurons required to restore walking after SC injury are not the same as the neurons used for the same behavior before injury (120). Together, these various modes of cellular regeneration may explain why, given the natural variation in recovery outcomes, the kernel density estimates of UMAP-embedded cruises did not completely overlap with those of uninjured control cruises. We propose that differential swim gait development during the recovery process could be due to misguided axon regrowth or suboptimal tissue remodeling, and that further

cellular and behavioral regeneration studies are needed to better understand the cellular basis of swim recovery in zebrafish.

4.3 Tensor Decomposition

4.3.1 Results

Tensor decomposition of all assay measurements corresponds with outcomes at 8 weeks post-injury

Because the tracking experiment produced longitudinal recovery data for individual fish, we applied tensor component analysis (TCA) to explore recovery trajectories. To prepare the data, we concatenated functional measurements from all 9 assays of all 60 fish into a rank-3 tensor. As we did in the correlative analysis, values for each measured attribute were multiplied by -1 if that measurement's average was increased at 1 wpi compared to controls (scoliosis, posture novelty, rostral compensation, tail beat frequency), and we normalized values. The software that we used for TCA did not allow missing values, and we decided not to use interpolation, so 16 fish (6 male, 10 female) had to be removed from the tensor for this analysis. We selected parameters for the model by optimizing for low model error while requiring high model similarity (>0.8; Figure 2.6A-B). After selecting parameters for the model, we obtained 7 tensor components each of which included factors for each axis: fish, assay, and functional measurement (Figure 4.5). To visualize factors, we sorted fish factors by glial bridge size at 8 wpi and sorted assays temporally. Values for many fish factors showed a directional trend, implying that the factor values captured a functional trajectory related to neurological recovery.

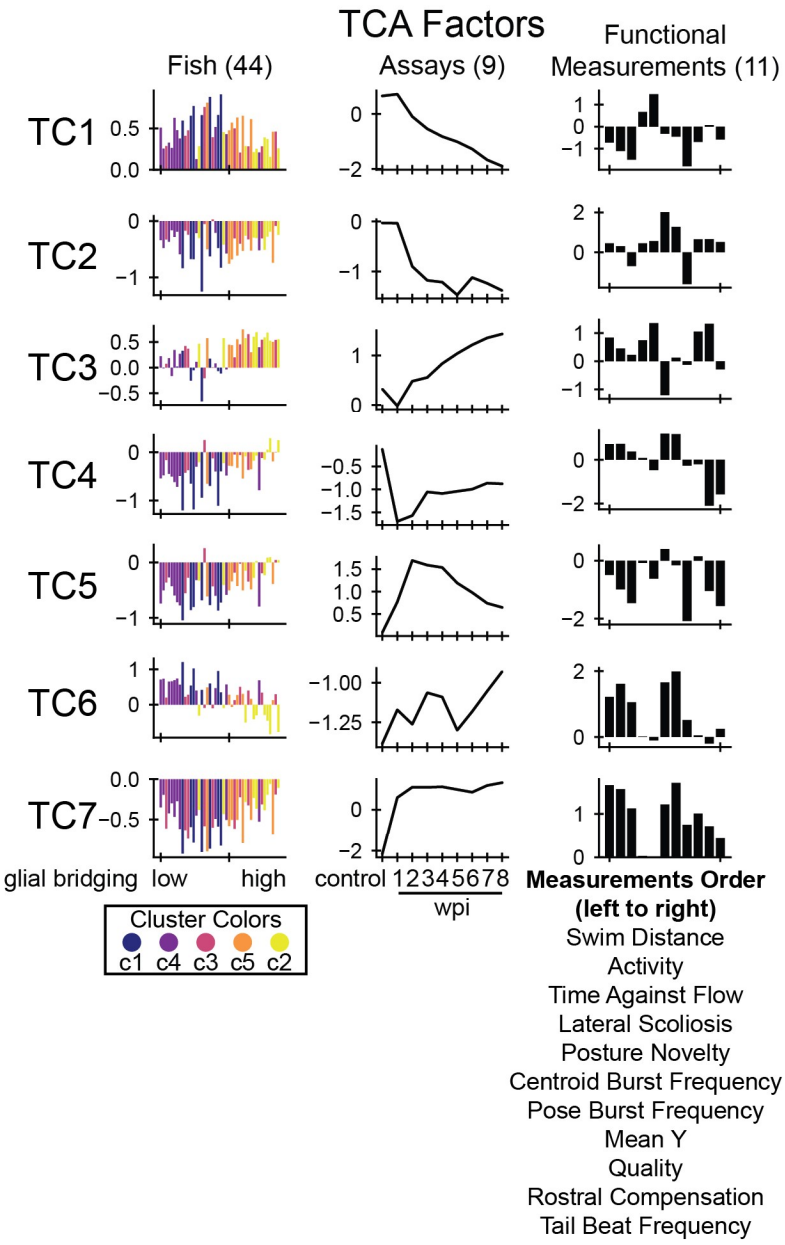

Figure 4.5: Rank-7 tensor component analysis of swim behavior for all tracked fish during SC regeneration. Factors from a rank-7 tensor decomposition corresponding to each axis of the full data tensor: fish, assays (wpi), and functional measurements. Fish are sorted on the x-axis by their percent glial bridging measured at 8 wpi and colored according to the rank of the cluster with respect to average glial bridging. Assays are sorted temporally. Measurements (left to right) are listed below the plots in descending order. 44 out of 60 total fish were analyzed. 16 fish were omitted either due to early death (6 fish) or because cruise waveform measurements were missing due to low activity for at least one assay (10 fish).

We explored this relationship further by clustering fish according to their factor values. We selected a distance threshold parameter that yielded the most clusters, given a high minimum

allowed cluster size (Figure 2.6C). The five resulting clusters of fish were roughly the same size, 7–11 fish per cluster. Cluster averages for measurements taken at 8 wpi were plotted in a heatmap, with clusters sorted by average glial bridging (Figure 4.6). When ordered by average glial bridging in the cluster, clusters also sorted according to posture novelty, perceived quality, and rostral compensation. In the same ordering but omitting cluster 1, clusters 2–5 also sorted according to average measurements of axon regrowth (proximal and distal), swim distance, activity, time against flow, posture burst frequency, and mean y (but in the opposite direction than expected). Lateral scoliosis was sorted decreasing except for clusters c3 and c4. The only measurement averages that clearly were not sorted in this ordering were centroid burst frequency and tail beat frequency. Fish factor values in Figure 4.5 were colored by cluster according to the cluster's average glial bridging.

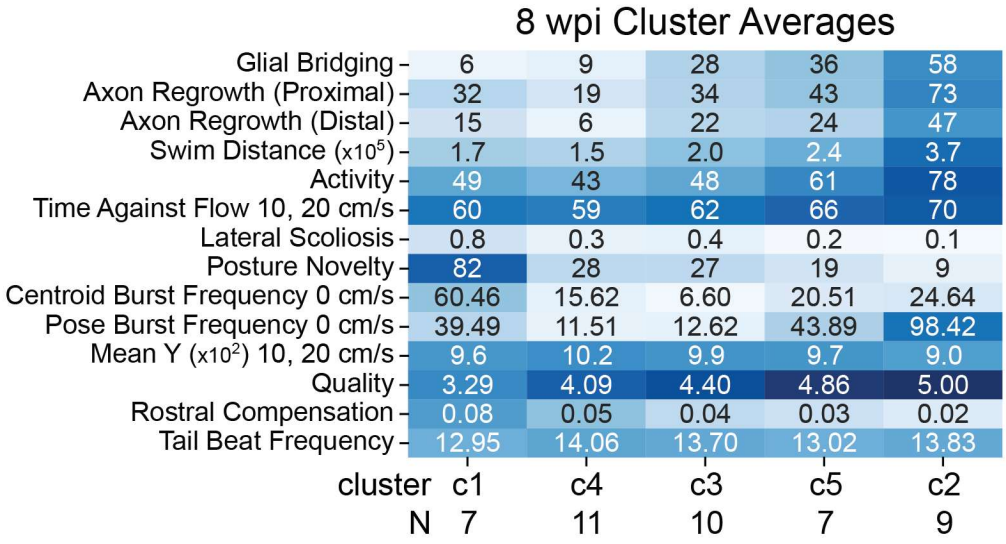

Figure 4.6: Average functional and cellular regeneration outcomes for five clusters of fish identified through tensor decomposition.
Recovery outcomes for the five identified fish clusters, sorted by average glial bridging, low to high, from left to right. Each row's color is normalized such that the darkest blue corresponds to the maximum observation among all fish for that measurement. 44 out of 60 total fish were analyzed. 16 fish were omitted either due to early death (6 fish) or because cruise waveform measurements were missing due to low activity for at least one assay (10 fish).

We expected that assay factors would exhibit a displacement-to-recovery trend from 1–8 wpi, mimicking the recovery trend of most functional metrics (swim capacity: Figure 3.1A-F, rostral compensation: Figure 3.9C-D, tail beat frequency: Figure 3.13A-B). Although some assay factors did capture this trend, many diverged away from control through recovery, and the values of TC1 and TC2 did not change dramatically from control until 2 wpi, capturing a trend more similar to the scoliosis score or posture novelty (Figure 3.7). We interpret the diversity of assay factor trendlines to represent complexities in the differing biological signals of the functional measurements and longitudinal support for non-uniformity of 8 wpi metric correlation signals shown in Figure 3.14A.

We plotted the factors of a rank-1 TCA to determine whether one rank is sufficient to capture the general recovery patterns of classical and novel measurements (Figure 4.7). Indeed, fish factor values correlated well with 8 wpi glial bridging (Spearman $r_s = -0.63$). As expected, assay factors spiked sharply away from control at 1 wpi then trended toward control until about 6 wpi, mimicking many of the classical metrics. Finally, the most highly weighted metrics included pose burst frequency, activity, and swim distance. The least weighted metrics included mean y, scoliosis, and posture novelty, each of which showed trends unlike those presented by other measurements (Figure 3.3D, Figure 3.7A-B). Model error for this rank-1 decomposition was 2.7 times as high as the rank-7 model described above (model errors: rank-1 = 0.528; rank-7 = 0.198). Because the rank-1 factors matched our expectations in terms of fish and assay factors, we conclude that this suite of measurements are collectively well-suited to assess swim function for recovering fish. Overall, rank-1 and rank-7 tensor component analysis and fish factor clustering indicate that recovery trajectories correspond strongly with 8 wpi cellular regeneration measurements.

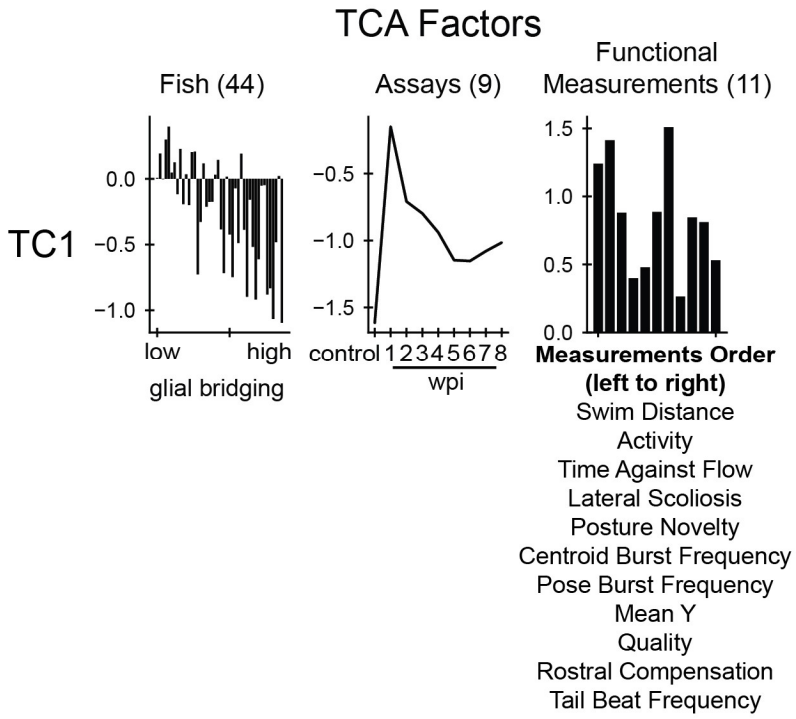

Figure 4.7: Rank-1 tensor component analysis reflects stereotypical recovery trends.
Factors from a rank-1 tensor decomposition corresponding to each axis of the full data tensor: fish, assays (wpi), and functional measurements. Fish are sorted on the x-axis by percent glial bridging measured at 8 wpi. Assays are sorted temporally. Measurements (left to right) are listed below the plots in descending order. 44 out of 60 total fish were analyzed. 16 fish were omitted either due to early death (6 fish) or because cruise waveform measurements were missing due to low activity for at least one assay (10 fish).

4.3.2 Discussion

Both the carefully trained rank-7 model and the naïve rank-1 model contained fish factor values that correlated with 8 wpi glial bridging of the corresponding fish. This result supports the model that swim function is associated with cellular regeneration throughout recovery. To be clear, this association does not imply that swim function causes cellular regeneration. Using current methods, cellular regeneration cannot be measured directly and non-invasively in the spinal cords of living fish. No cellular measurements were included in the input tensor. Given that fish factors in the tensor components correspond to final neurological outcomes suggests that longitudinal measurements of functional ability are a reliable non-invasive proxy for neurological regeneration. Future work may seek to describe, with demonstrable precision, the

degree of cellular regeneration in terms of swim function for accurate non-invasive monitoring of SC regeneration.

We embarked on this study hypothesizing that swim gait quality correlates most strongly with cellular regeneration, compared to classical functional measurements. Based on this hypothesis, we expected to find poorly regenerated fish swimming at moderate capacity, albeit with an abnormal gait. Cluster c1 partially identified a group of fish with this attribute. Fish in c1 presented, on average, the lowest glial bridging, lowest perceived quality, and highest rostral compensation (Figure 4.6). They also swam with high burst frequency at 0 cm/s, moderate activity, and swam further than the cluster with the next lowest glial bridging, c4. Cluster c1's moderate swim capacity may be explained by higher axon regrowth compared to c4. In addition, c1 was measured to have the highest postoperative scoliosis on average, which likely lowered their perceived swim quality and increased measured rostral compensation score. This is because scoliosis was included in our criteria for perceived quality. Additionally, scoliotic bends are stiff points on the fish's body that dramatically lower the cruise curvature profile at that point. So, the absolute difference between a scoliotic fish's cruise curvature profile and the control profile could be higher due to abnormally low, not high, curvature amplitude while cruising. By affecting the rostral compensation score in this manner, scoliosis challenges our definition of rostral compensation on one hand, but adds strength to the score on the other hand, since scoliosis is itself moderately correlated with cellular regeneration (Figure 3.14A). Although fish in cluster c1 had the lowest glial regeneration and swam with the most unusual gait and posture, they did not swim with the least capacity, which defies the classic model. Similar to the pairwise correlation analysis of 8 wpi functional and cellular measurements, TCA provides evidence that cellular regeneration is reflected more strongly through gait and posture than swim capacity.

4.4 Predicting 8 wpi Regeneration from 2 wpi Function

4.4.1 Results

Swim function at 2 weeks post-injury is predictive of cellular regeneration at 8 weeks

Swim distance and rostral compensation were two of the most correlated functional measurements with SC regeneration at 8 wpi. Swim distance and rostral compensation measure different functional classes: swim capacity and gait quality, respectively. They also clustered separately in the pairwise metric analysis (Figure 3.14A) and recovered at different rates: swim distance plateaued by 6 wpi (Figure 3.2A) and rostral compensation by 3 wpi (Figure 3.9C-D). Thus, as distinct functional outputs that correlate well with cellular regeneration, we hypothesized that a combination of swim distance and rostral compensation assessed during early stages of SC regeneration could predict injury outcomes at 8 wpi. To test this hypothesis, we averaged 1 and 2 wpi distance and rostral compensation measurements and plotted them against one another colored by 8 wpi glial bridging (Figure 4.8A). As expected from the correlation analysis, fish with eventual high glial bridging generally swam longer distances and with lower rostral compensation in these early assays. We ranked the fish according to swim distance and negative rostral compensation, then added the two ranks to create a wellness score for early recovery. We divided male and female data separately into two equally sized groups across each sex's wellness score median: a highly regenerative prediction group and a poorly regenerative one. At 8 wpi, both percent glial bridging and proximal axon regrowth were significantly higher in the highly regenerative group compared to the poorly regenerative group (Figure 4.8B).

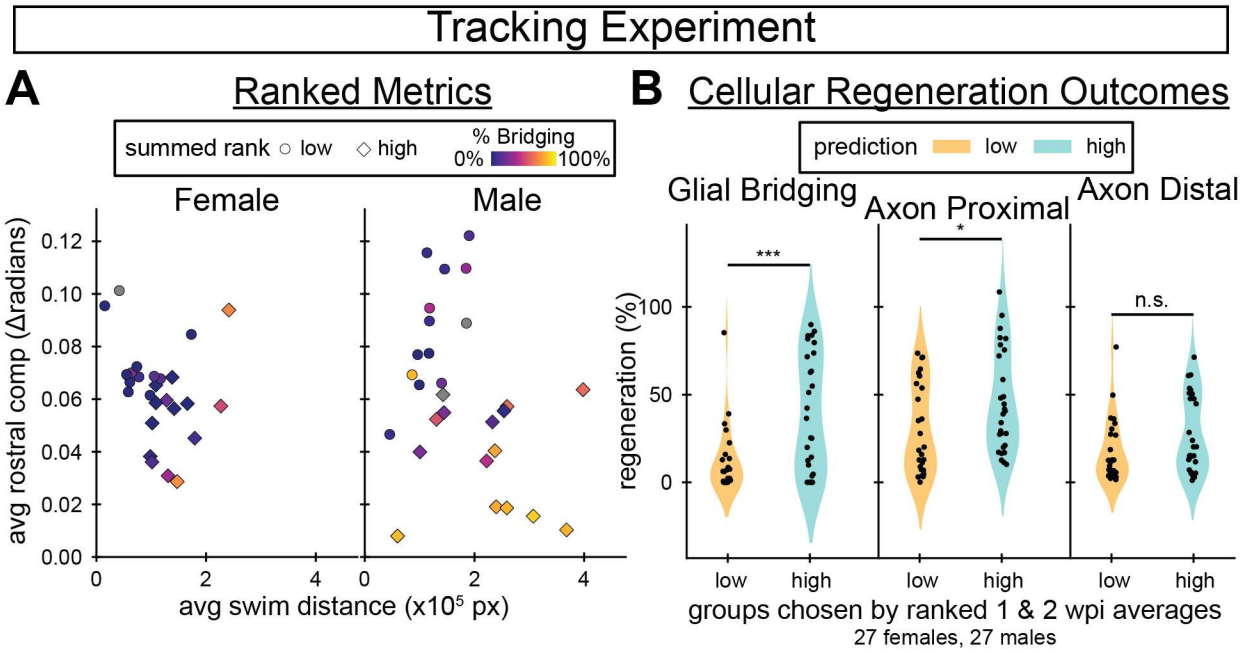

Figure 4.8: Predicting 8 wpi regeneration outcomes in the tracking experiment using measurements taken by 2 wpi.

(A) Swim distance versus rostral compensation was averaged between 1 and 2 wpi. Dots represent individual fish and were colored based on the extent of glial bridging measured at 8 wpi for each fish. Fish that would develop larger glial bridges tended to swim further and exhibit less rostral compensation, in lower right side of each graph. Each fish was assigned a prediction score by adding its rank according to average swim distance to its rank according to average negative rostral compensation, relative to its sex group. (Predicted poorly n=30; predicted well n=28). **(B)** 8 wpi glial bridging and axon regrowth outcomes for groups ranked high in swim distance and low in rostral compensation between 1 and 2 wpi ("high") compared to those ranked low in swim distance and high in rostral compensation ("low"). (Predicted poorly n=27; predicted well n=27). Statistical significance was determined by Student's t-test. p-values represent comparisons between prediction groups. ***P<0.001; **P<0.01; *P<0.05; ns, P>0.05.

Since this analysis was performed after our tracking experiment was completed and final outcomes were measured, a new experiment was performed to validate the prediction method (Figure 4.9A). In the validation experiment, we predicted regeneration outcomes for sixty (30 male, 30 female) fish using the same wellness score described above. Swim behavior was assayed before injury and at 1, 2, and 8 wpi. Unlike the tracking experiment where we separated fish using physical dividers, in the validation experiment fish were housed in male-female pairs to track their identities from the control assay until predictions were calculated after the 2 wpi assay. Predictions were made separately for males and females (Figure 4.9B) like we did for data in the tracking experiment. Predictions for the validation experiment were performed using median wellness scores calculated

in the validation experiment. Once predicted, fish of both sexes were mixed randomly between tanks within the prediction groups, with 5–7 fish per tank. By the end of the experiment, four fish (1 male and 3 females) died in the group predicted to regenerate well, and there were no deaths in the group predicted to regenerate poorly, providing a final comparison of 26 fish to 30 fish. At 8 wpi, glial bridging was significantly elevated in the group that was predicted to recover well compared to the group predicted to recover poorly (Figure 4.9C). The results of this outcome prediction validation experiment indicated that it is possible to predict 8 wpi cellular regeneration outcomes from a subset of 2 wpi measurements.

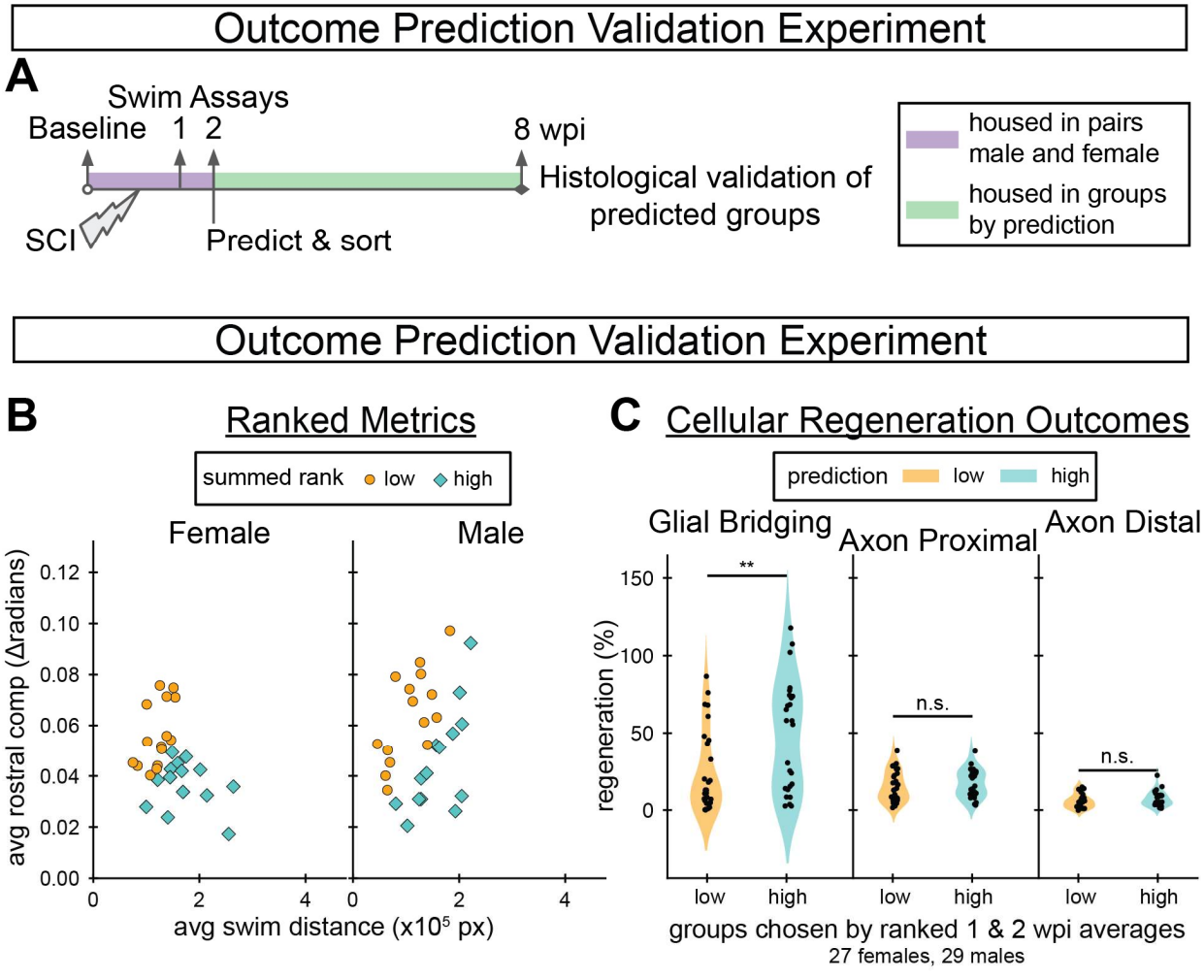

Figure 4.9: Experimental validation for 8wpi outcome prediction.

(A) Schematic overview of the outcome prediction experiment. A total of 60 adult fish (30 males and 30 females) were housed in male-female pairs temporarily to track their identities until low/high regeneration predictions were assigned, then they were housed in prediction groups with 5-7 fish per tank. At 8 wpi, individuals were separated again to correlate final measurements from the endurance and behavior assays with cellular regeneration. Behavior was assayed before injury, 1 wpi, 2 wpi, and 8 wpi. Predictions were made, as described, after the 2 wpi behavior assay. **(B)** Swim distance versus rostral compensation was averaged between 1 and 2 wpi. Dots represent individual fish and were colored based on the predicted outcome. (Predicted poorly n=30; predicted well n=28). **(C)** 8 wpi glial bridging and axon regrowth outcomes for each prediction group. (Predicted poorly n=30; predicted well n=26). Statistical significance was determined by Student's t-test. p-values represent comparisons between prediction groups. ***P<0.001; **P<0.01; *P<0.05; ns, P>0.05.

Recalling that female fish in the tracking experiment regenerated relatively poorly, we explored cellular regeneration in the validation experiment separated by sex. In the validation experiment, axon regrowth was measured lower than expected for both sexes (Figure 4.10B-C). Surprisingly, female fish in the validation experiment regenerated glial tissue more successfully than the male fish (Figure 4.10D). This difference was not driven by outliers (Figure 4.10A), nor were outliers observed for axon regrowth measurements (Figure 4.10B-C).

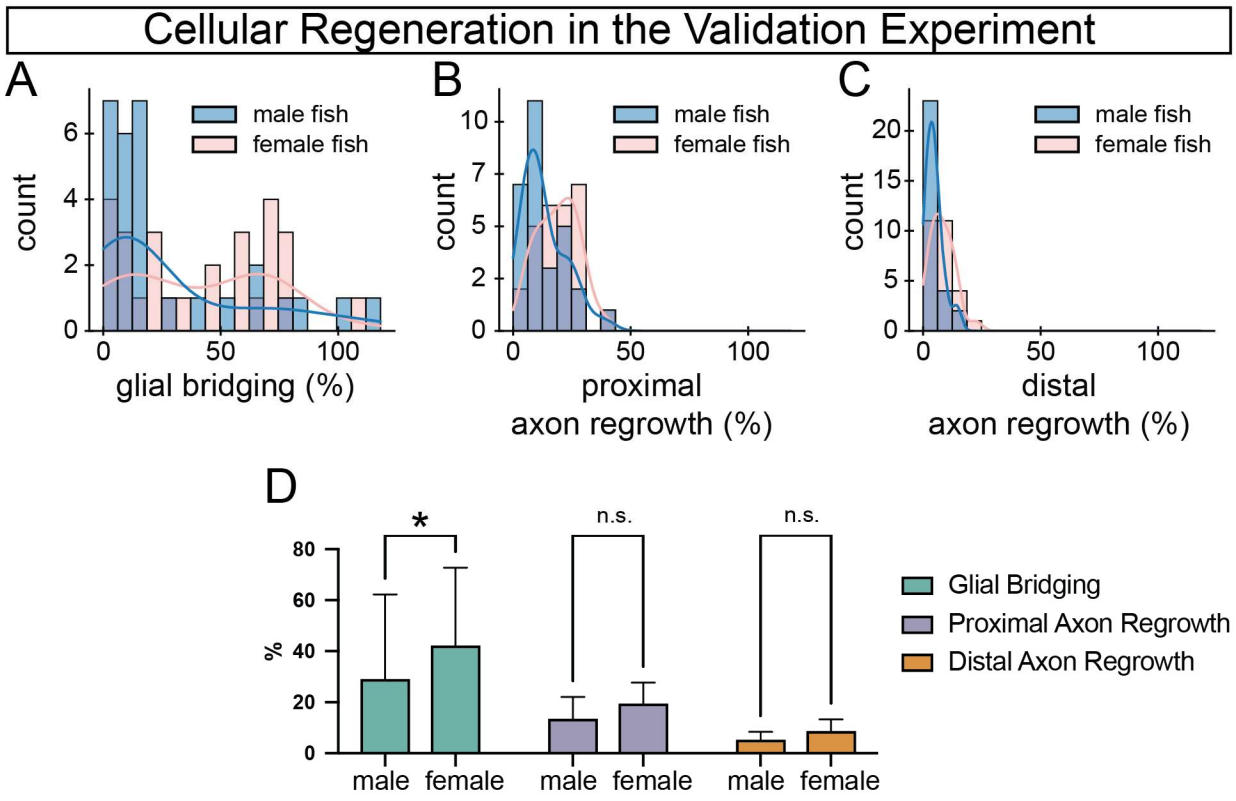

Figure 4.10: Cellular regeneration measured in the validation experiment separated by sex.

n=27 female, 29 male. **(A-C)** Unlike the tracking experiment, female fish in the validation experiment appeared to regenerate more successfully that male fish in terms of glial bridging, proximal axon regeneration, and distal axon regrowth. Measurements for each sex are presented as histograms with kernel density estimates. **(D)** Two-way ANOVA with Šídák's multiple comparisons test indicated that female fish regenerated significantly more glial tissue at the lesion. *P<0.05; ns, P>0.05.

Furthermore, these results prompted us to check whether outcomes were significantly predicted within sexes in the validation experiment. For the tracking experiment, male fish that were predicted to recover well regenerated significantly more glial tissue and axons, proximal and distal to the lesion (Figure 4.11A). In the validation experiment, female fish predicted to recover well regenerated significantly more glial tissue and axons proximal to the lesion (Figure 4.11B). These results indicate that a single experiment is insufficient to conclude that one sex is more capable of regenerating than the other.

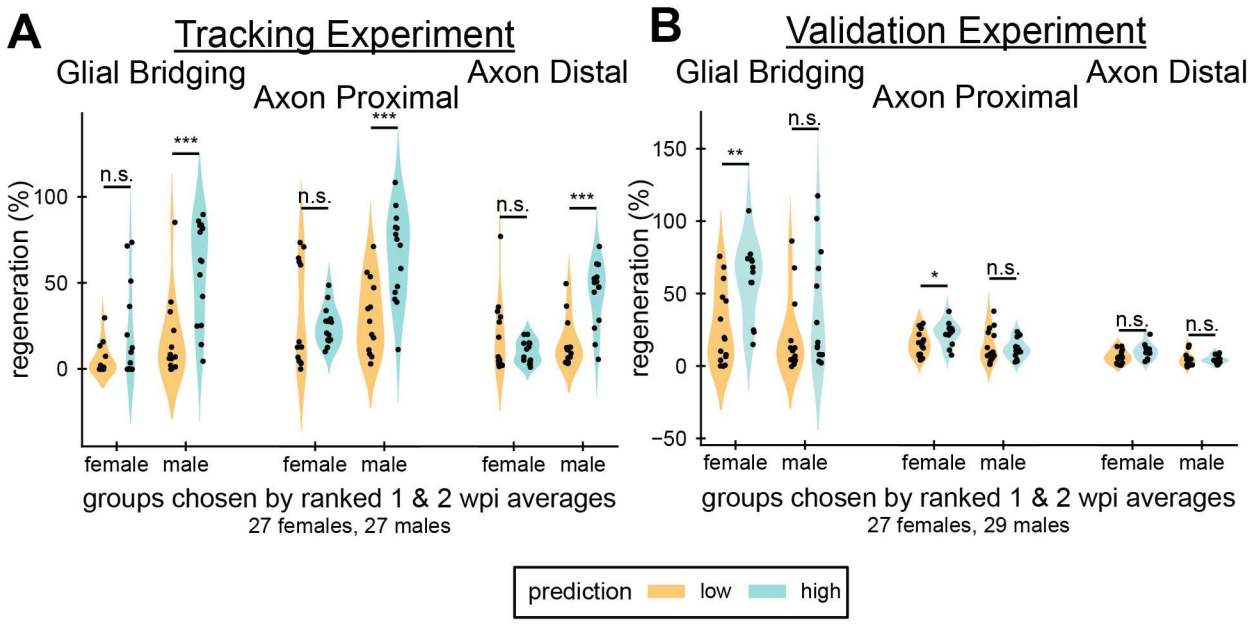

Figure 4.11: Regeneration outcomes for prediction groups in the tracking and validation experiments separated by sex.
Glial bridging and axon regrowth outcomes for each prediction group at 8 wpi. For each measurement type, results for female fish are presented on the left, male fish on the right. (A) Outcomes in the tracking experiment indicate that predictions were significant for male fish. (Females predicted well: 13, poor: 14. Males predicted well: 14, poor: 13). (B) Outcomes in the validation experiment indicate that predictions were significant for female fish, but not in terms of distal axon regrowth. (Females predicted well: 12, poor: 15. Males predicted well: 14, poor: 15). Statistical significance was determined by Student's t-test. p-values represent comparisons between prediction groups. ***P<0.001; **P<0.01; *P<0.05; ns, P>0.05.

Because the validation experiment provided functional and cellular data at 8wpi for individual fish, we clustered the 8 wpi functional and regeneration measurements in the same way that we did for the tracking experiment to validate those results as well. In doing so, we discovered that endurance, a measure of swim capacity that was not evaluated at any other timepoint or in the tracking experiment, was a member of the neural health-associated cluster, cluster 1, not the swim capacity cluster (Figure 4.12A). Unlike the tracking experiment, swim distance and pose burst frequency were not associated with bridging to the same extent (Figure 4.12B-C), and axon regeneration was lower than expected for all fish (Figure 4.12E). Rostral compensation, however, still correlated more strongly with glial bridging than any other measurement (Figure 4.12A,D). These findings provided additional evidence that this rostral compensation score is a neurologically-associated gait quality measurement and suggested that results derived from gait quality replicate more reliably than those derived from swim capacity.

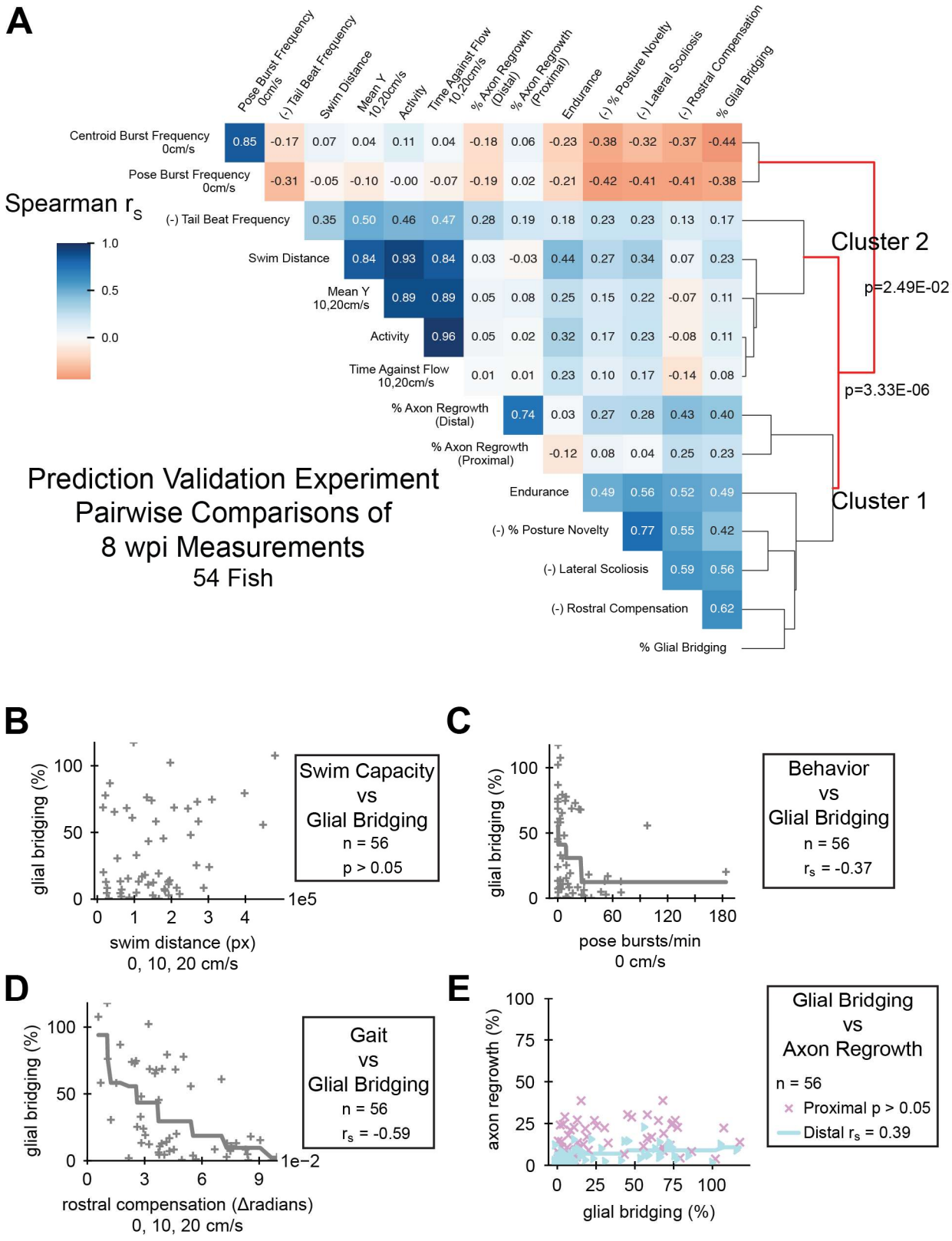

Figure 4.12: Pairwise comparisons of spinal cord regeneration metrics at 8 wpi (male and female fish in the validation experiment).

(A) Heatmap of Spearman's rank correlations (r_s) between cellular and functional measurements. Regeneration metrics include swim capacity, swim quality, structural, and neurological measurements. A dendrogram representing similarities between correlation patterns of measurements is shown. In total, 54 fish at 8 wpi were analyzed. Four fish that did not survive to the end and two fish that could not be measured in all attributes were omitted. Correlations are reported regardless of p-value. For the sake of meaningful clustering, a measured attribute was multiplied by -1 if its average was increased at 1 wpi compared to controls. These attributes are marked with the prefix "(-)" on the label. (n=54) **(B-D)** One metric each of swim capacity (swim distance), behavior (burst frequency), and gait (rostral compensation) were plotted against glial bridging to demonstrate their correlation. Because the Spearman correlation operates on ranked values, we fit monotonic splines to plots where r_s were significant ($p < 0.05$) to visualize possible associations. (n=56) **(E)** Scatter plot showing a weak association between the size of regenerated glial tissue and axon regrowth, proximal and distal. Axon regrowth was measured lower than expected in this experiment. (n=56)

4.4.2 Discussion

In Chapter 2 section 2.4.2, we described two possible ways to quantify rostral compensation, or the difference between cruise curvature profiles: maximum absolute difference and integrated area. We used maximum absolute distance to quantify rostral compensation for all results in this study, but for supplemental comparison after completing all other analyses, we also calculated compensation for all assays using integrated area. In terms of outcome prediction, the two quantifications of rostral compensation yield similar predictions with minimal statistical effect: if we had used integrated area instead, outcome predictions would have been different for four fish (6.9% of 60) in the tracking experiment, and two fish (3.4% of 60) in the validation experiment. We conclude that our chosen strategy, maximum absolute difference, is a satisfactory quantification of rostral compensatory movement.

We performed a validation experiment to explore the hypothesis that rostral compensation and swim distance measurements at 1 and 2 wpi can be used to predict 8 wpi cellular regeneration outcomes. The validation experiment, while not completely successful at predicting significantly different outcomes for both glial bridging and axon regrowth, nonetheless provides a proof of concept for future work. In both the tracking and validation experiments, glial regeneration outcomes were significantly different, which indicates that early functional measurements can be predictive of cellular regeneration measured six weeks later. Moreover, our prediction outcome

validation experiment supports the rostral compensation score as a neurologically meaningful functional metric, and evidence that swim endurance, which was not evaluated in our tracking experiment, may be more associated with neurological health than other swim capacity measurements. Importantly, both the tracking and validation experiments support our conclusion that rostral compensation provides the strongest correlation with cellular regeneration than any other functional measurement that we examined.

Comparing the two experiments, several improvements could be recommended. For one, we likely overestimated swim distance's predictive power. Knowing that gait recovers relatively early, rostral compensation alone may be the best metric for outcome prediction, which remains to be tested. Additionally, the only reason we chose to perform prediction separately for males and females is because in the tracking experiment the female fish swam with reduced capacity and regenerated more poorly. In the validation experiment, however, female fish swam with comparable capacity (Figure 4.9B) and regenerated more successfully (Figure 4.10D). This is surprising not only because the tracking experiment had a different result but also because, unlike the tracking experiment, fish were housed in male-female pairs for nearly three weeks in the validation experiment. It could be hypothesized that in male-female housing conditions the male fish may act more aggressively toward the female fish which could negatively affect the female's early regeneration. Indeed, research has shown that healthy (not SC injury) pair-housed zebrafish tend to have higher levels of cortisol for the first ten days than individually-housed fish, and that fatalities are higher in male-female pairs (121). Future iterations on outcome prediction strategies may prefer not to separate prediction according to sex.

Chapter 5: Conclusions

5.1 Conclusions and Significance

Our study supports standard functional analysis, demonstrating that recovered swim capacity measurements correlate with spinal cord regeneration. We introduce rostral compensation as a gait-driven measurement that correlates with, and likely provides a more accurate functional proxy for spinal cord regeneration than existing functional regeneration metrics. We expect that in future studies rostral compensation will supplement classical swim capacity metrics to greatly improve comprehensive functional assessment. Through posture analysis, we discovered that the fish that would develop injury-induced lateral scoliosis had a set trajectory by two weeks following SC transection. We found that fish in still water swam in a mechanically efficient manner both before and after injury.

We discovered that grouping fish according to their rank in functional attributes two weeks into recovery can divide the fish into groups that have statistically divergent cellular regeneration outcomes at 8 wpi. We propose that developing a gait-driven prediction algorithm could offer powerful benefits to the zebrafish research community. One benefit would be to reduce the time required to complete SC regeneration experiments, most of which currently require 4 to 8 weeks. If outcomes could be forecasted accurately at 2 wpi, experiments could be reduced by as much as 6 weeks. This would save time and money for fish care, vacate housing tanks for other experiments, and may reduce the number of tanks required in circulation, thus reducing water and energy usage. In terms of ethics, it would also reduce the amount of time fish would be required to live with spinal cord injury.

Another benefit of quantitatively associating function with neurological regeneration would be non-invasively tracking neurological wellness. Currently, glial bridging and axon regrowth can only be measured directly after collecting spinal cords. If cellular regeneration had stronger functional correspondences, new types of experiments could be performed. For example, a pharmacological or genetic rescue experiment for regeneration-deficient animals could be performed to test whether regeneration could be reignited after the period of innate wild type regeneration had passed. An experiment of that type would require a strong functional proxy for neurological wellness to know to what extent animals had or had not regenerated before administering a pro-regenerative treatment. We recommend that future efforts to associate swim ability with neuromuscular health should prioritize gait quality analysis over swim capacity, although swim capacity measurements remain relevant for ordinary functional assessment of injured zebrafish.

Importantly, I have taken reasonable steps to make functional calculations of gait, posture, and swim capacity accessible to both the lab and the community. Software written for these studies is publicly available with clear instructions for installation and usage. The repository includes code for classifying behaviors and calculating functional metrics. It also includes code for pose and behavior quality control and video normalization. For the lab, I created a script specific to the lab's computational environment that preprocesses raw videos, obtains DeepLabCut pose annotations, classifies behaviors, performs quality control, and calculates metrics, all in a single invocation. In this way, I have accelerated discovery by providing the means to calculate newly established metrics which are both distinct from previous measurements and demonstrably more associated with glial bridging and axon regrowth after spinal cord transection.

References

1. Center National Spinal Cord Injury Statistical. Traumatic Spinal Cord Injury Facts and Figures at a Glance. Birmingham, AL Available online at: https://msktc org/sites/default/files/SCI-Facts-Figs-2022-Eng-508 pdf. 2022;

2. Silver J. The glial scar is more than just astrocytes. Exp Neurol. 2016 Dec;286:147–9.

3. Sofroniew MV. Dissecting spinal cord regeneration. Nature. 2018 May 16;557(7705):343–50.

4. Becker T, Wullimann MF, Becker CG, Bernhardt RR, Schachner M. Axonal regrowth after spinal cord transection in adult zebrafish. J Comp Neurol. 1997 Jan 27;377(4):577–95.

5. Selzer ME. Mechanisms of functional recovery and regeneration after spinal cord transection in larval sea lamprey. J Physiol (Lond). 1978 Apr;277:395–408.

6. Bernstein JJ. Relation of spinal cord regeneration to age in adult goldfish. Exp Neurol. 1964 Feb;9(2):161–74.

7. Bareyre FM. Neuronal repair and replacement in spinal cord injury. J Neurol Sci. 2008 Feb 15;265(1–2):63–72.

8. Fawcett JW. Overcoming inhibition in the damaged spinal cord. J Neurotrauma. 2006;23(3–4):371–83.

9. Cigliola V, Becker CJ, Poss KD. Building bridges, not walls: spinal cord regeneration in zebrafish. Dis Model Mech. 2020 May 27;13(5).

10. Mokalled MH, Patra C, Dickson AL, Endo T, Stainier DYR, Poss KD. Injury-induced ctgfa directs glial bridging and spinal cord regeneration in zebrafish. Science. 2016 Nov 4;354(6312):630–4.

11. Huang C-X, Wang Z, Cheng J, Zhu Z, Guan NN, Song J. De novo establishment of circuit modules restores locomotion after spinal cord injury in adult zebrafish. Cell Rep. 2022 Oct 25;41(4):111535.

12. van Raamsdonk W, Maslam S, de Jong DH, Smit-Onel MJ, Velzing E. Long term effects of spinal cord transection in Zebrafish: swimming performances, and metabolic properties of the neuromuscular system. Acta Histochem. 1998 Apr;100(2):117–31.

13. Reimer MM, Kuscha V, Wyatt C, Sörensen I, Frank RE, Knüwer M, et al. Sonic hedgehog is a polarized signal for motor neuron regeneration in adult zebrafish. J Neurosci. 2009 Dec 2;29(48):15073–82.

14. Kuscha V, Barreiro-Iglesias A, Becker CG, Becker T. Plasticity of tyrosine hydroxylase and serotonergic systems in the regenerating spinal cord of adult zebrafish. J Comp Neurol. 2012 Apr 1;520(5):933–51.

15. Dias TB, Yang Y-J, Ogai K, Becker T, Becker CG. Notch signaling controls generation of motor neurons in the lesioned spinal cord of adult zebrafish. J Neurosci. 2012 Feb 29;32(9):3245–52.

16. Klatt Shaw D, Mokalled MH. Efficient CRISPR/Cas9 mutagenesis for neurobehavioral screening in adult zebrafish. G3 (Bethesda). 2021 Aug 7;11(8).

17. Burris B, Jensen N, Mokalled MH. Assessment of swim endurance and swim behavior in adult zebrafish. J Vis Exp. 2021 Nov 12;(177).

18. Klatt Shaw D, Saraswathy VM, Zhou L, McAdow AR, Burris B, Butka E, et al. Localized EMT reprograms glial progenitors to promote spinal cord repair. Dev Cell. 2021 Mar 8;56(5):613-626.e7.

19. Saraswathy VM, Zhou L, McAdow AR, Burris B, Dogra D, Reischauer S, et al. Myostatin is a negative regulator of adult neurogenesis after spinal cord injury in zebrafish. Cell Rep. 2022 Nov 22;41(8):111705.

20. Zhou L, McAdow R, Yamada H, Burris B, Shaw DK, Oonk K, et al. Progenitor derived glia are required for spinal cord regeneration in zebrafish. BioRxiv. 2022 Aug 26;

21. Becker CG, Lieberoth BC, Morellini F, Feldner J, Becker T, Schachner M. L1.1 is involved in spinal cord regeneration in adult zebrafish. J Neurosci. 2004 Sep 8;24(36):7837–42.

22. Hui SP, Dutta A, Ghosh S. Cellular response after crush injury in adult zebrafish spinal cord. Dev Dyn. 2010 Nov;239(11):2962–79.

23. Guo Y, Ma L, Cristofanilli M, Hart RP, Hao A, Schachner M. Transcription factor Sox11b is involved in spinal cord regeneration in adult zebrafish. Neuroscience. 2011 Jan 13;172:329–41.

24. Yu Y-M, Gibbs KM, Davila J, Campbell N, Sung S, Todorova TI, et al. MicroRNA miR-133b is essential for functional recovery after spinal cord injury in adult zebrafish. Eur J Neurosci. 2011 May;33(9):1587–97.

25. Yu YM, Cristofanilli M, Valiveti A, Ma L, Yoo M, Morellini F, et al. The extracellular matrix glycoprotein tenascin-C promotes locomotor recovery after spinal cord injury in adult zebrafish. Neuroscience. 2011 Jun 2;183:238–50.

26. Lin J-F, Pan H-C, Ma L-P, Shen Y-Q, Schachner M. The cell neural adhesion molecule contactin-2 (TAG-1) is beneficial for functional recovery after spinal cord injury in adult zebrafish. PLoS ONE. 2012 Dec 21;7(12):e52376.

27. Fang P, Lin J-F, Pan H-C, Shen Y-Q, Schachner M. A surgery protocol for adult zebrafish spinal cord injury. J Genet Genomics. 2012 Sep 20;39(9):481–7.

28. Pan H-C, Lin J-F, Ma L-P, Shen Y-Q, Schachner M. Major vault protein promotes locomotor recovery and regeneration after spinal cord injury in adult zebrafish. Eur J Neurosci. 2013 Jan;37(2):203–11.

29. Ma L, Yu Y-M, Guo Y, Hart RP, Schachner M. Cysteine- and glycine-rich protein 1a is involved in spinal cord regeneration in adult zebrafish. Eur J Neurosci. 2012 Feb;35(3):353–65.

30. Yu Y, Schachner M. Syntenin-a promotes spinal cord regeneration following injury in adult zebrafish. Eur J Neurosci. 2013 Jul;38(2):2280–9.

31. Ma L, Shen Y-Q, Khatri HP, Schachner M. The asparaginyl endopeptidase legumain is essential for functional recovery after spinal cord injury in adult zebrafish. PLoS ONE. 2014 Apr 18;9(4):e95098.

32. Fang P, Pan H-C, Lin SL, Zhang W-Q, Rauvala H, Schachner M, et al. HMGB1 contributes to regeneration after spinal cord injury in adult zebrafish. Mol Neurobiol. 2014 Feb;49(1):472–83.

33. Vajn K, Suler D, Plunkett JA, Oudega M. Temporal profile of endogenous anatomical repair and functional recovery following spinal cord injury in adult zebrafish. PLoS ONE. 2014 Aug 26;9(8):e105857.

34. Liu D, Yu Y, Schachner M. Ptena, but not Ptenb, reduces regeneration after spinal cord injury in adult zebrafish. Exp Neurol. 2014 Nov;261:196–205.

35. Strand NS, Hoi KK, Phan TMT, Ray CA, Berndt JD, Moon RT. Wnt/β-catenin signaling promotes regeneration after adult zebrafish spinal cord injury. Biochem Biophys Res Commun. 2016 Sep 2;477(4):952–6.

36. Wang L-F, Huang S-B, Zhao H-D, Liu C-J, Yao L, Shen Y-Q. Activating transcription factor 3 promotes spinal cord regeneration of adult zebrafish. Biochem Biophys Res Commun. 2017 Jul 1;488(3):522–7.

37. Ma L, Shen H-F, Shen Y-Q, Schachner M. The Adhesion Molecule-Characteristic HNK-1 Carbohydrate Contributes to Functional Recovery After Spinal Cord Injury in Adult Zebrafish. Mol Neurobiol. 2017 Jul;54(5):3253–63.

38. Zeng C-W, Sheu J-C, Tsai H-J. The neuronal regeneration of adult zebrafish after spinal cord injury is enhanced by transplanting optimized number of neural progenitor cells. Cell Transplant. 2020;29:963689720903679.

39. Ji Z, Zhou Z-L, Hao Q, Zhao L, Cui C, Huang S-B, et al. Activating transcription factor 6 contributes to functional recovery after spinal cord injury in adult zebrafish. J Mol Neurosci. 2021 Apr;71(4):734–45.

40. Cui C, Wang L-F, Huang S-B, Zhao P, Chen Y-Q, Wu Y-B, et al. Adequate expression of neuropeptide Y is essential for the recovery of zebrafish motor function following spinal cord injury. Exp Neurol. 2021 Nov;345:113831.

41. Shen W-Y, Fu X-H, Cai J, Li W-C, Fan B-Y, Pang Y-L, et al. Identification of key genes involved in recovery from spinal cord injury in adult zebrafish. Neural Regen Res. 2022 Jun;17(6):1334–42.

42. Hosseini P, Mirsadeghi S, Rahmani S, Izadi A, Rezaei M, Ghodsi Z, et al. Dopamine receptors gene expression pattern and locomotor improvement differ between female and male zebrafish during spinal cord auto repair. Zebrafish. 2022 Aug;19(4):137–47.

43. Ogai K, Hisano S, Mawatari K, Sugitani K, Koriyama Y, Nakashima H, et al. Upregulation of anti-apoptotic factors in upper motor neurons after spinal cord injury in adult zebrafish. Neurochem Int. 2012 Dec;61(7):1202–11.

44. Goldshmit Y, Sztal TE, Jusuf PR, Hall TE, Nguyen-Chi M, Currie PD. Fgf-dependent glial cell bridges facilitate spinal cord regeneration in zebrafish. J Neurosci. 2012 May 30;32(22):7477–92.

45. Briona LK, Dorsky RI. Radial glial progenitors repair the zebrafish spinal cord following transection. Exp Neurol. 2014 Jun;256:81–92.

46. Ohnmacht J, Yang Y, Maurer GW, Barreiro-Iglesias A, Tsarouchas TM, Wehner D, et al. Spinal motor neurons are regenerated after mechanical lesion and genetic ablation in larval zebrafish. Development. 2016 May 1;143(9):1464–74.

47. Wehner D, Tsarouchas TM, Michael A, Haase C, Weidinger G, Reimer MM, et al. Wnt signaling controls pro-regenerative Collagen XII in functional spinal cord regeneration in zebrafish. Nat Commun. 2017 Jul 25;8(1):126.

48. Tsarouchas TM, Wehner D, Cavone L, Munir T, Keatinge M, Lambertus M, et al. Dynamic control of proinflammatory cytokines Il-1β and Tnf-α by macrophages in zebrafish spinal cord regeneration. Nat Commun. 2018 Nov 7;9(1):4670.

49. Zeng C-W, Kamei Y, Shigenobu S, Sheu J-C, Tsai H-J. Injury-induced Cavl-expressing cells at lesion rostral side play major roles in spinal cord regeneration. Open Biol. 2021 Feb 24;11(2):200304.

50. Tsata V, Kroehne V, Wehner D, Rost F, Lange C, Hoppe C, et al. Reactive oligodendrocyte progenitor cells (re-)myelinate the regenerating zebrafish spinal cord. Development. 2020 Dec 16;147(24).

51. Chang W, Pedroni A, Bertuzzi M, Kizil C, Simon A, Ampatzis K. Locomotion dependent neuron-glia interactions control neurogenesis and regeneration in the adult zebrafish spinal cord. Nat Commun. 2021 Aug 11;12(1):4857.

52. Huang C-X, Zhao Y, Mao J, Wang Z, Xu L, Cheng J, et al. An injury-induced serotonergic neuron subpopulation contributes to axon regrowth and function restoration after spinal cord injury in zebrafish. Nat Commun. 2021 Dec 7;12(1):7093.

53. Vasudevan D, Liu Y-C, Barrios JP, Wheeler MK, Douglass AD, Dorsky RI. Regenerated interneurons integrate into locomotor circuitry following spinal cord injury. Exp Neurol. 2021 Aug;342:113737.

54. Hossainian D, Shao E, Jiao B, Ilin VA, Parris RS, Zhou Y, et al. Quantification of functional recovery in a larval zebrafish model of spinal cord injury. J Neurosci Res. 2022 Aug 20;

55. Doyle LMF, Roberts BL. Exercise enhances axonal growth and functional recovery in the regenerating spinal cord. Neuroscience. 2006 Aug 11;141(1):321–7.

56. Ljunggren EE, Haupt S, Ausborn J, Ampatzis K, El Manira A. Optogenetic activation of excitatory premotor interneurons is sufficient to generate coordinated locomotor activity in larval zebrafish. J Neurosci. 2014 Jan 1;34(1):134–9.

57. Girdhar K, Gruebele M, Chemla YR. The behavioral space of zebrafish locomotion and its neural network analog. PLoS ONE. 2015 Jul 1;10(7):e0128668.

58. Mearns DS, Donovan JC, Fernandes AM, Semmelhack JL, Baier H. Deconstructing Hunting Behavior Reveals a Tightly Coupled Stimulus-Response Loop. Curr Biol. 2020 Jan 6;30(1):54-69.e9.

59. Fontaine E, Lentink D, Kranenbarg S, Müller UK, van Leeuwen JL, Barr AH, et al. Automated visual tracking for studying the ontogeny of zebrafish swimming. J Exp Biol. 2008 Apr;211(Pt 8):1305–16.

60. Thomas LSV, Gehrig J. Multi-template matching: a versatile tool for object-localization in microscopy images. BMC Bioinformatics. 2020 Feb 5;21(1):44.

61. Mathis A, Mamidanna P, Cury KM, Abe T, Murthy VN, Mathis MW, et al. DeepLabCut: markerless pose estimation of user-defined body parts with deep learning. Nat Neurosci. 2018 Sep;21(9):1281–9.

62. Graving JM, Chae D, Naik H, Li L, Koger B, Costelloe BR, et al. DeepPoseKit, a software toolkit for fast and robust animal pose estimation using deep learning. eLife. 2019 Oct 1;8.

63. Liu X, Yu S-Y, Flierman NA, Loyola S, Kamermans M, Hoogland TM, et al. OptiFlex: Multi-Frame Animal Pose Estimation Combining Deep Learning With Optical Flow. Front Cell Neurosci. 2021 May 28;15:621252.

64. Pereira TD, Tabris N, Matsliah A, Turner DM, Li J, Ravindranath S, et al. SLEAP: A deep learning system for multi-animal pose tracking. Nat Methods. 2022 Apr 4;19(4):486–95.

65. Mwaffo V, Zhang P, Romero Cruz S, Porfiri M. Zebrafish swimming in the flow: a particle image velocimetry study. PeerJ. 2017 Nov 14;5:e4041.

66. McCullough MH, Goodhill GJ. Unsupervised quantification of naturalistic animal behaviors for gaining insight into the brain. Curr Opin Neurobiol. 2021 Oct;70:89–100.

67. Hsu AI, Yttri EA. B-SOiD: An Open Source Unsupervised Algorithm for Discovery of Spontaneous Behaviors. BioRxiv. 2019 Sep 16;

68. Sun G, Lyu C, Cai R, Yu C, Sun H, Schriver KE, et al. Deepbhvtracking: A novel behavior tracking method for laboratory animals based on deep learning. Front Behav Neurosci. 2021 Oct 28;15:750894.

69. Bohnslav JP, Wimalasena NK, Clausing KJ, Dai YY, Yarmolinsky DA, Cruz T, et al. DeepEthogram, a machine learning pipeline for supervised behavior classification from raw pixels. eLife. 2021 Sep 2;10.

70. Xu J, Hu C, Jiang Q, Pan H, Shen H, Schachner M. Trimebutine, a small molecule mimetic agonist of adhesion molecule L1, contributes to functional recovery after spinal cord injury in mice. Dis Model Mech. 2017 Sep 1;10(9):1117–28.

71. Vrinten DH, Hamers FFT. "CatWalk" automated quantitative gait analysis as a novel method to assess mechanical allodynia in the rat; a comparison with von Frey testing. Pain. 2003 Mar;102(1–2):203–9.

72. Barbeau H, Ladouceur M, Norman KE, Pépin A, Leroux A. Walking after spinal cord injury: evaluation, treatment, and functional recovery. Arch Phys Med Rehabil. 1999 Feb;80(2):225–35.

73. Maynard FM, Bracken MB, Creasey G, Jr JFD, Donovan WH, Ducker TB, et al. International standards for neurological and functional classification of spinal cord injury. Spinal Cord. 1997 Dec 18;35(5):266–74.

74. Basso DM, Beattie MS, Bresnahan JC. A sensitive and reliable locomotor rating scale for open field testing in rats. J Neurotrauma. 1995 Feb;12(1):1–21.

75. Basso DM, Beattie MS, Bresnahan JC. Graded histological and locomotor outcomes after spinal cord contusion using the NYU weight-drop device versus transection. Exp Neurol. 1996 Jun;139(2):244–56.

76. Basso DM, Fisher LC, Anderson AJ, Jakeman LB, McTigue DM, Popovich PG. Basso Mouse Scale for locomotion detects differences in recovery after spinal cord injury in five common mouse strains. J Neurotrauma. 2006 May;23(5):635–59.

77. Hamers FP, Lankhorst AJ, van Laar TJ, Veldhuis WB, Gispen WH. Automated quantitative gait analysis during overground locomotion in the rat: its application to spinal cord contusion and transection injuries. J Neurotrauma. 2001 Feb;18(2):187–201.

78. Beare JE, Morehouse JR, DeVries WH, Enzmann GU, Burke DA, Magnuson DSK, et al. Gait analysis in normal and spinal contused mice using the TreadScan system. J Neurotrauma. 2009 Nov;26(11):2045–56.

79. Nessler JA, De Leon RD, Sharp K, Kwak E, Minakata K, Reinkensmeyer DJ. Robotic gait analysis of bipedal treadmill stepping by spinal contused rats: characterization of intrinsic recovery and comparison with BBB. J Neurotrauma. 2006 Jun;23(6):882–96.

80. Shi D, Zhang W, Zhang W, Ding X. A review on lower limb rehabilitation exoskeleton robots. CJME. 2019 Dec;32(1):74.

81. Vamsikrishna KM, Dogra DP, Desarkar MS. Computer-Vision-Assisted Palm Rehabilitation With Supervised Learning. IEEE Trans Biomed Eng. 2016;63(5):991–1001.

82. Lee S-J, Jung S-K. Posture Symmetry based Motion Capture System for Analysis of Lower -limbs Rehabilitation Training. Journal of Korea Multimedia Society. 2011 Dec 31;14(12):1517–27.

83. Schindelin J, Arganda-Carreras I, Frise E, Kaynig V, Longair M, Pietzsch T, et al. Fiji: an open-source platform for biological-image analysis. Nat Methods. 2012 Jun 28;9(7):676–82.

84. Nath T, Mathis A, Chen AC, Patel A, Bethge M, Mathis MW. Using DeepLabCut for 3D markerless pose estimation across species and behaviors. Nat Protoc. 2019 Jul;14(7):2152–76.

85. Lemaître G, Nogueira F, Aridas CK. Imbalanced-learn: A python toolbox to tackle the curse of imbalanced datasets in machine learning. The Journal of Machine Learning Research. 2017;18(1):559–63.

86. McInnes L, Healy J, Saul N, Großberger L. UMAP: uniform manifold approximation and projection. JOSS. 2018 Sep 2;3(29):861.

87. Pedregosa F, Varoquaux G, Gramfort A, Michel V, Thirion B, Grisel O, et al. Scikit-learn: Machine learning in Python. the Journal of machine Learning research. 2011;12:2825–30.

88. Virtanen P, Gommers R, Oliphant TE, Haberland M, Reddy T, Cournapeau D, et al. SciPy 1.0: fundamental algorithms for scientific computing in Python. Nat Methods. 2020 Mar;17(3):261–72.

89. Team RC. R: A Language and Environment for Statistical Computing. 2021;

90. Kimes P. sigclust2: sigclust2: Statistical Significance of Clustering. 2018;

91. Kimes PK, Liu Y, Neil Hayes D, Marron JS. Statistical significance for hierarchical clustering. Biometrics. 2017 Jan 18;73(3):811–21.

92. Hunter JD. Matplotlib: A 2D Graphics Environment. Comput Sci Eng. 2007;9(3):90–5.

93. Waskom M. seaborn: statistical data visualization. JOSS. 2021 Apr 6;6(60):3021.

94. Harris CR, Millman KJ, van der Walt SJ, Gommers R, Virtanen P, Cournapeau D, et al. Array programming with NumPy. Nature. 2020 Sep 16;585(7825):357–62.

95. The pandas development team. pandas-dev/pandas: Pandas 1.0.3. Zenodo. 2020;

96. McKinney W. Data structures for statistical computing in python. Proceedings of the 9th Python in Science Conference. SciPy; 2010. p. 56–61.

97. Williams AH, Kim TH, Wang F, Vyas S, Ryu SI, Shenoy KV, et al. Unsupervised Discovery of Demixed, Low-Dimensional Neural Dynamics across Multiple Timescales through Tensor Component Analysis. Neuron. 2018 Jun 27;98(6):1099-1115.e8.

98. Giorgino T. Computing and Visualizing Dynamic Time Warping Alignments in*R* : Thedtw Package. J Stat Softw. 2009;31(7).

99. Delcourt J, Ovidio M, Denoël M, Muller M, Pendeville H, Deneubourg J-L, et al. Individual identification and marking techniques for zebrafish. Rev Fish Biol Fish. 2018 Dec;28(4):839–64.

100. McHenry MJ, Lauder GV. The mechanical scaling of coasting in zebrafish (Danio rerio). J Exp Biol. 2005 Jun;208(Pt 12):2289–301.

101. Wiggin TD, Anderson TM, Eian J, Peck JH, Masino MA. Episodic swimming in the larval zebrafish is generated by a spatially distributed spinal network with modular functional organization. J Neurophysiol. 2012 Aug 1;108(3):925–34.

102. Fero K, Yokogawa T, Burgess HA. The behavioral repertoire of larval zebrafish. In: Kalueff AV, Cachat JM, editors. Zebrafish models in neurobehavioral research. Totowa, NJ: Humana Press; 2011. p. 249–91.

103. Kulshrestha R, Kuiper JH, Masri WE, Chowdhury JR, Kaur S, Kumar N, et al. Scoliosis in paediatric onset spinal cord injuries. Spinal Cord. 2020 Jun;58(6):711–5.

104. Mayfield JK, Erkkila JC, Winter RB. Spine deformity subsequent to acquired childhood spinal cord injury. J Bone Joint Surg Am. 1981 Dec;63(9):1401–11.

105. Veldhuizen AG, Wever DJ, Webb PJ. The aetiology of idiopathic scoliosis: biomechanical and neuromuscular factors. Eur Spine J. 2000 Jun;9(3):178–84.

106. Taylor GK, Nudds RL, Thomas ALR. Flying and swimming animals cruise at a Strouhal number tuned for high power efficiency. Nature. 2003 Oct 16;425(6959):707–11.

107. Beal DN, Hover FS, Triantafyllou MS, Liao JC, Lauder GV. Passive propulsion in vortex wakes. J Fluid Mech. 2006 Feb 8;549(1):385.

108. Dubińska-Magiera M, Daczewska M, Lewicka A, Migocka-Patrzałek M, Niedbalska-Tarnowska J, Jagla K. Zebrafish: A model for the study of toxicants affecting muscle development and function. Int J Mol Sci. 2016 Nov 19;17(11).

109. Yaksi E, Jamali A, Diaz Verdugo C, Jurisch-Yaksi N. Past, present and future of zebrafish in epilepsy research. FEBS J. 2021 Dec;288(24):7243–55.

110. Sheets L, Holmgren M, Kindt KS. How Zebrafish Can Drive the Future of Genetic-based Hearing and Balance Research. J Assoc Res Otolaryngol. 2021 Jun;22(3):215–35.

111. Dogra D, Ahuja S, Kim H-T, Rasouli SJ, Stainier DYR, Reischauer S. Opposite effects of Activin type 2 receptor ligands on cardiomyocyte proliferation during development and repair. Nat Commun. 2017 Dec 1;8(1):1902.

112. Whittemore L-A, Song K, Li X, Aghajanian J, Davies M, Girgenrath S, et al. Inhibition of myostatin in adult mice increases skeletal muscle mass and strength. Biochem Biophys Res Commun. 2003 Jan 24;300(4):965–71.

113. Park HC, Hong SK, Kim HS, Kim SH, Yoon EJ, Kim CH, et al. Structural comparison of zebrafish Elav/Hu and their differential expressions during neurogenesis. Neurosci Lett. 2000 Jan 28;279(2):81–4.

114. Curado S, Anderson RM, Jungblut B, Mumm J, Schroeter E, Stainier DYR. Conditional targeted cell ablation in zebrafish: a new tool for regeneration studies. Dev Dyn. 2007 Apr;236(4):1025–35.

115. Horn JL. A RATIONALE AND TEST FOR THE NUMBER OF FACTORS IN FACTOR ANALYSIS. Psychometrika. 1965 Jun;30:179–85.

116. Zanella A, Harrison CM, Lenzi S, Cooke J, Damsma P, Fleming SW. Sonification and sound design for astronomy research, education and public engagement. Nat astron. 2022 Aug 15;6(11):1241–8.

117. Barrios JP, Wang W-C, England R, Reifenberg E, Douglass AD. Hypothalamic dopamine neurons control sensorimotor behavior by modulating brainstem premotor nuclei in zebrafish. Curr Biol. 2020 Dec 7;30(23):4606-4618.e4.

118. Bagnall MW, McLean DL. Modular organization of axial microcircuits in zebrafish. Science. 2014 Jan 10;343(6167):197–200.

119. Reimer MM, Sörensen I, Kuscha V, Frank RE, Liu C, Becker CG, et al. Motor neuron regeneration in adult zebrafish. J Neurosci. 2008 Aug 20;28(34):8510–6.

120. Kathe C, Skinnider MA, Hutson TH, Regazzi N, Gautier M, Demesmaeker R, et al. The neurons that restore walking after paralysis. Nature. 2022 Nov 9;611(7936):540–7.

121. Keck VA, Edgerton DS, Hajizadeh S, Swift LL, Dupont WD, Lawrence C, et al. Effects of Habitat Complexity on Pair-Housed Zebrafish. J Am Assoc Lab Anim Sci. 2015 Jul;54(4):378–83.